



UNIVERSITAT  
POLITÈCNICA  
DE VALÈNCIA



UNIVERSITAT POLITÈCNICA DE VALÈNCIA

Escuela Técnica Superior de Ingeniería del Diseño

Análisis y Optimización de Estructuras Espaciales  
Desplegables Inspiradas en Origami

Trabajo Fin de Máster

Máster Universitario en Ingeniería Aeronáutica

AUTOR/A: Velázquez Navarro, Ester

Tutor/a: Lázaro Navarro, Mario

CURSO ACADÉMICO: 2022/2023



UNIVERSITAT POLITÈCNICA DE VALÈNCIA  
Escuela Técnica Superior de Ingeniería del Diseño

---

ANALYSIS AND OPTIMIZATION OF ORIGAMI INSPIRED  
DEPLOYABLE SPACE STRUCTURES

---

TRABAJO DE FIN DE MÁSTER  
**Master en Ingeniería Aeronáutica**

**Autora:**

Ester Velázquez Navarro

**Tutor:**

Mario Lázaro Navarro

**Tutor externo:**

Pablo Solano López

**Curso académico:**

2022/2023

July 17, 2023



---

*A mis abuelos, a mis padres  
y a mi hermana*



---

*Science progresses best when observations  
force us to alter our preconceptions.*

– Vera Rubin



---

## Agradecimientos

Gracias a todos los que han formado parte de esta aventura que han sido los últimos seis años de mi vida, tanto en Madrid como en Valencia. Todo lo que he vivido y crecido ha sido gracias a cada una de las personas que me han acompañado y han estado ahí.

Gracias en especial a Sara, Saúl y Fer por estar cada mañana (algunos más que otros) y por hacerme sentir como en casa estando tan lejos de la mía. Gracias a todas las personas con las que me he cruzado en la UPV, profesores y alumnado, por hacerme crecer como persona y como profesional. Gracias a Mario Lázaro por aceptar tutorizarme a pesar de no ser su área de conocimiento, ha sido un placer tenerte como profesor.

Gracias a todas las personas que me han soportado durante este proceso; a Sara, Mario, Alondra, Aurora, Pablo, Raúl, Sergio y Raquel. Gracias por acogerme, apoyarme y acompañarme cada día. Gracias sobretodo a Adri por ser mi sustento constante y por estar ahí desde el principio.

Gracias enormes a Pablo Solano, por querer que trabajase a su lado durante los pasados meses y seguramente durante los futuros. Gracias por confiar en mi desde el principio y por tutorizarme en esta gran aventura, que sé que no ha sido sencillo. Gracias a Inés por su motivación y apoyo durante los últimos años, aunque fuese en la distancia. Thank you so much Joshika for the work have done, as well as the help you have given me. Agradecer también a Marta y a Javi, por dedicarme su tiempo y conocimiento siempre que lo he necesitado. Y cómo no, agradecer a Hodei, por haberme acompañado y apoyado durante estos meses.

Por último, agradecer a quienes realmente han hecho esto posible, a mis abuelos, a mis padres, a mi hermana, a mis tíos, a Boli y a Nico. Gracias por apoyarme de manera incondicional y por siempre haberme dejado volar todo lo alto que he querido.

Gracias.





---

## Resumen

A medida que la industria espacial aumenta, existe una creciente demanda de grandes estructuras espaciales presurizadas como pueden ser hábitats o tanques de combustible. Hoy en día, los vehículos lanzadores ofrecen un volumen y unas restricciones bastante limitadas para la carga de pago. Por ello, el uso de estructuras flexibles o desplegadas resulta una solución factible a esta problemática. Entre ellas, las estructuras inspiradas en origami surgen proporcionando una solución de compromiso: requieren una configuración que sea lo suficientemente flexible y rígida para ser almacenado y soportar las cargas estructurales durante el lanzamiento, a pesar de presentar un alto ratio de empaquetamiento.

Las estructuras basadas en origami ofrecen grandes ventajas como: un alto ratio de volumen de pliegue y despliegue o la habilidad para mantener sus propiedades estructurales tras desplegarlo reiteradas veces. Este trabajo busca el diseño y optimización de un demostrador desplegable para una misión de un Cubesat de 12U. Por ello, este diseño requiere un estudio paramétrico con el fin de obtener una estructura que muestre el mejor comportamiento bajo los requisitos establecidos.

Entre los posibles patrones de Origami, basándose en la bibliografía, se ha seleccionado el Kresling dado que permite la construcción de una estructura cilíndrica a modo de demostrador. Se ha implementado un uso novedoso de materiales con una configuración dual de manera que, se obtiene un patrón más flexible sin ser necesario el uso de bisagras o elementos similares. La elaboración del estudio se ha realizado mediante el solver de elementos finitos Abaqus, comandado externamente mediante código elaborado en Python. Finalmente, tras obtener las configuraciones factibles y deseadas, se ha aplicado un método de optimización con el fin de generar la mejor solución al problema propuesto.

El demostrador de origami bajo estudio servirá como una prueba de concepto en órbita de la viabilidad de la tecnología desplegable de una manera económica. Comprobando, a su vez, el uso innovador de materiales y su configuración final ofreciendo un nuevo camino a seguir en la fabricación de estructuras espaciales más grandes de las que a día de hoy son posibles.

**Palabras clave:** Demostrador, Origami, kresling, diseño, optimización.

---

## Abstract

As the space industry is growing, there is an increasing demand for pressurized, large structures in space, such as habitats or fuel deposits. This demand faces a non-negligible challenge: the limited payload volume of launch vehicles, with a highly constrained shape. Therefore new engineering solutions are on need, being the most promising the bendable/deployable ones. And among them, Origami inspired, deployable structures arise providing a solution of compromise: while they present high packaging ratios (i.e., foldability) they require for a material and structural configuration flexible enough to be stowed during launch but stiff enough to withstand structural loads.

Origami-inspired structures offer advantages as a high deployed-to-stowed volume ratio or the ability to retain its structural properties after repeated deployment. This work aims to design and optimize an origami inspired deployable structure that will be used as a technology demonstrator of fitting into a 12U CubeSat. Consequently, a parametric study of the possible configurations will be performed in order to derive the one that shows the best static and dynamic behaviour under the requirements of such a mission.

Among the many Origami patterns, based on previous work available on the literature, the chosen one has been the Kresling ori, building a cylindrical shape for the final technological demonstrator. A novel use of materials is proposed combining two different kinds of printable materials, obtaining a more flexible pattern without requiring mechanical hinges or similar. The whole study, involving deployment and un-deployment behaviour has been studied under Python scripting and Abaqus FEM solver. Finally, once all the feasible and desired configurations are computed an optimization process is applied in order to obtain the most suitable under pre-defined requirements.

The origami demonstrator under study will serve as an economical in-orbit proof-of-concept for a viable deployment technology. While testing an innovative use of materials and configuration, offering a new way for much larger structures in space than the currently possible.

**Key words:** Demonstrator, Origami, Kresling, design, optimization.

---

## Resum

A mesura que la indústria espacial augmenta, hi ha una creixent demanda de grans estructures espacials pressuritzades, així com hàbitats o tancs de combustible. Hui, els vehicles llançadors ofereixen un volum limitat per a la càrrega de pagament, així com grans restriccions de forma. Per això, noves solucions com a estructures flexibles o desplegable resulten necessàries. I entre elles, les estructures inspirades en origami, sorgeixen proporcionant una solució de compromís: si bé presenten una alta ràtio d'empaquetament, requereixen una configuració que siga prou flexible per a ser emmagatzemat durant el llançament i prou rígid per a suportar les càrregues estructurals .

Les estructures basades en origami ofereixen avantatges com una gran ràtio de volum de plec i desplegament o l'habilitat per mantindre les seues propietats estructurals després de desplegar-lo reiterades vegades. Aquest treball cerca el disseny i l'optimització d'un demostrador desplegable per a una missió d'un Cubesat de 12U. Per això, aquest disseny requereix un estudi paramètric per obtindre una estructura que mostre el millor comportament sota els requisits establits.

Entre els possibles patrons d'Origami, basant-se en la bibliografia, s'ha seleccionat el Kresling, permetent la construcció d'una estructura cilíndrica com a demostrador. S'ha implementat un ús nou de materials amb una configuració dual, de manera que s'aconsegueix un patró més flexible sense ser necessari l'ús de frontisses o elements similars. Tot l'estudi, incloent-hi el comportament durant el plegat i desplegat, ha estat estudiat mitjançant el salvar d'elements finits: Abaqus, comandat externament mitjançant codi elaborat a Python. Finalment, un cop es tenen les configuracions factibles i desitjades, s'ha aplicat un mètode d'optimització seleccionat per obtindre la millor solució al problema proposat.

El demostrador d'origami sota estudi servirà com a prova de concepte en òrbita de la viabilitat de la tecnologia desplegable d'una manera econòmica. Comprovar alhora l'ús innovatiu de materials i la seua configuració final, oferint un nou camí a seguir per a estructures espacials més grans de les ara possibles.

**Paraules clau:** Demostrador, Origami, Kresling, disseny, optimització.

---

## Contents

<b>List of Figures</b>	<b>xiv</b>
<b>List of Tables</b>	<b>xvi</b>
<b>List of Abbreviations and Nomenclature</b>	<b>xvii</b>
<b>I REPORT</b>	<b>1</b>
<b>1 Introduction</b>	<b>3</b>
1.1 Project aims and overview . . . . .	3
1.2 Framework . . . . .	3
1.3 Project organization . . . . .	4
1.4 Report disposition . . . . .	5
1.5 Used tools . . . . .	6
<b>2 State-of-the-art</b>	<b>8</b>
2.1 Origami patterns and geometry . . . . .	9
2.1.1 Miura . . . . .	9
2.1.2 Yoshimura . . . . .	10
2.1.3 Kresling . . . . .	11
2.2 Modeling and simulation of deployable mechanism . . . . .	12
2.3 Multi-objective optimization . . . . .	14
<b>3 Statement of the problem</b>	<b>16</b>
3.1 Origami geometry . . . . .	17
3.2 Folding and deployment process . . . . .	19
3.3 Materials . . . . .	21
3.4 Optimization procedure . . . . .	22
3.5 Simulation parameters . . . . .	25
3.6 Workflow . . . . .	26
<b>4 Structural model</b>	<b>28</b>
4.1 Geometry definition . . . . .	28
4.2 Simulation environment . . . . .	31
4.2.1 Material assignment . . . . .	31
4.2.2 Boundary conditions . . . . .	32

---

4.2.3	Analysis procedures . . . . .	36
4.3	Model validation . . . . .	38
4.3.1	Independence mesh analysis . . . . .	38
4.3.2	Energy balance . . . . .	44
4.3.3	Packaging ratio . . . . .	45
<b>5</b>	<b>Optimization</b>	<b>49</b>
5.1	Sampling methodology . . . . .	49
5.2	Design variables and model description . . . . .	51
5.3	Surrogate models . . . . .	51
5.4	Optimum cases analysis . . . . .	56
5.4.1	Results for optimum cases . . . . .	59
5.4.2	N rings results . . . . .	63
<b>6</b>	<b>Conclusion and future works</b>	<b>65</b>
6.1	Conclusions . . . . .	65
6.2	Future works . . . . .	66
<b>A</b>	<b>Sampled design variables</b>	<b>67</b>
<b>II</b>	<b>SPECIFICATION SHEET</b>	<b>71</b>
	<b>Specification Sheet</b>	<b>73</b>
<b>1</b>	<b>Software Conditions</b>	<b>73</b>
1.1	Python 3.11 . . . . .	73
1.2	Abaqus CAE 2022 . . . . .	73
1.3	Dakota Sandia . . . . .	74
1.4	Adobe Illustrator and Adobe Photoshop 2023 . . . . .	74
<b>2</b>	<b>Tools Conditions</b>	<b>74</b>
2.1	abqpy Library . . . . .	74
2.2	SMT Library . . . . .	74
<b>3</b>	<b>Hardware Requirements</b>	<b>75</b>
<b>III</b>	<b>Sustainable Development Goals (SDG)</b>	<b>77</b>
	<b>Sustainable Development Goals</b>	<b>79</b>

---

---

<b>1 Project contribution</b>	<b>79</b>
<b>2 Each goal compliance explanation</b>	<b>80</b>
2.1 Gender equality . . . . .	80
2.2 Industry, innovation and infrastructure . . . . .	80
<b>IV BUDGET</b>	<b>81</b>
<b>Project budget</b>	<b>83</b>
<b>1 Time distribution</b>	<b>83</b>
<b>2 Budget breakdown</b>	<b>85</b>
2.1 Salary cost . . . . .	85
2.2 Software cost . . . . .	86
2.3 Hardware cost . . . . .	87
2.4 Budget summary . . . . .	87
<b>References</b>	<b>89</b>

---

**List of Figures**

1	Gantt chart of the thesis. . . . .	5
2	Scheme of the deployment sequence. (Adapted from [1]) . . . . .	8
3	Miura pattern. [Own elaboration] . . . . .	10
4	Yoshimura pattern. [Own elaboration] . . . . .	11
5	Kresling pattern. [Own elaboration] . . . . .	11
6	Kresling origami at different stages of deployment. [2] . . . . .	12
7	Experimental set-up for single fold stiffness. (Adapted from [3]) . . . . .	13
8	Experimental deployment sequence of elastic hinges. (Adapted from [4]) . . . . .	13
9	Sheet examples with crease folds (a) and smooth folds (b). (Adapted from [5]) . . . . .	14
10	Representation of a Pareto front. (Adapted from [6]) . . . . .	15
11	Sketch of the 12U prototype with the origami structure. [7] . . . . .	16
12	Flat pattern parameters. [Own elaboration] . . . . .	17
13	3D representation. [Own elaboration] . . . . .	18
14	Height of design according to the bi-stable behaviour. (Adapted from [8]) . . . . .	18
15	Inner and outer volumes illustration. [Own elaboration] . . . . .	19
16	Folding process. [Own elaboration] . . . . .	19
17	First deployment process. [Own elaboration] . . . . .	20
18	Second deployment process. [Own elaboration] . . . . .	20
19	Example of composite material implementation. [Own elaboration] . . . . .	21
20	Example of printable material implementation. [Own elaboration] . . . . .	22
21	Illustrative examples of three sampling strategies for a two-dimensional problem. (Adapted from [9]) . . . . .	25
22	Workflow. . . . .	27
23	Coding workflow. . . . .	27
24	Structural model flow chart. [Own elaboration] . . . . .	28
25	First sketch appearance in Abaqus interface . . . . .	29
26	Final sketch appearance in Abaqus interface . . . . .	29
27	Assembly process in Abaqus interface. . . . .	30
28	Assembly process in Abaqus interface. . . . .	30
29	Flat pattern view and material assignment. . . . .	31
30	Material assignment in 3D model. . . . .	31
31	Tie constraint between triangles. [Own elaboration] . . . . .	32
32	Tie constraint for top surface. [Own elaboration] . . . . .	33
33	Coupling constraint for top and bottom flexible material. [Own elaboration] . . . . .	33
34	Pinned boundary condition. [Own elaboration] . . . . .	34



35	Displacement boundary condition. [Own elaboration] . . . . .	34
36	Pressure condition. [Own elaboration] . . . . .	35
37	Tabular (left) and smooth-step (right) amplitudes representation. [Own elaboration] . . . . .	37
38	Von Mises stress evolution during the three stage defined: folding, deployment thanks to bi-stability and inflation deployment. . . . .	38
39	Approximated Von Misses Stress in front of the number of sides. . . . .	39
40	Contour of Von Mises Stress [MPa] on deformed shape for different values of $n$ . . . . .	39
41	Visualization of the node under study. . . . .	40
42	Von Mises evolution for different mesh sizes ( $n = 4$ ). From bigger size (5 elements per side) at upper left, to smaller size (30 elements per side) right below). . . . .	40
43	Von Mises evolution for different mesh sizes ( $n = 5$ ). From bigger size (10 elements per side) at upper left, to smaller size (30 elements per side) right below). . . . .	41
44	Von Mises evolution for different mesh sizes ( $n = 5$ ). From bigger size (40 elements per side) at upper left, to smaller size (100 elements per side) below). . . . .	41
45	Von Mises evolution for different mesh sizes ( $n = 5$ ), with 6 mesh elements rows in flexible material region. From bigger size (100 elements per side) above, to smaller size (130 elements per side) below). . . . .	42
46	Illustration for three mesh types: <i>quad</i> , <i>quad-tri</i> and <i>tri</i> . . . . .	42
47	Final sketch implemented for the mesh distribution. . . . .	43
48	Von Mises evolution for distributed meshes ( $n = 5$ ). Mesh with 130 elements per side (—), distributed mesh Version 1 in blue (- -) and Version 2 in green (- -). . . . .	43
49	Energy evolution for <i>130 elements</i> mesh (—) and <i>Version 2</i> mesh (- -). . . . .	44
50	Total energy evolution for <i>130 elements</i> mesh (—) and <i>Version 2</i> mesh (- -). . . . .	45
51	Total energy evolution for $n = 5$ . . . . .	46
52	Deformation evolution for completed folding. . . . .	47
53	Total energy evolution comparison for $n = 5$ , $n = 6$ , $n = 12$ and $n = 20$ . . . . .	48
54	Maximum and minimum $h$ values limits for feasible Kresling geometries. . . . .	49
55	Sampling result with values out of bounds. . . . .	50
56	Corrected sampling results. . . . .	50
57	Surrogate model for $n = 6$ . . . . .	52
58	Surrogate model for $n = 7$ . . . . .	52
59	Surrogate model for $n = 8$ . . . . .	53
60	Surrogate model for $n = 9$ . . . . .	53
61	Surrogate model for $n = 10$ . . . . .	54
62	Surrogate model for $n = 11$ . . . . .	54
63	Surrogate model for $n = 12$ . . . . .	55

64	Optimum results evolution for the seven cases under study. Von Mises stress (left) and Inner volume (right). . . . .	56
65	Zoom of optimum results evolution for the seven cases under study. . . . .	57
66	Optimum results represented for stress versus volume. . . . .	57
67	Pareto front. Von Mises stress in front of Inner volume for each $n$ value. . . . .	58
68	Von Mises stress for obtained results. . . . .	59
69	Total energy for obtained results. . . . .	60
70	Total energy for obtained results at folding, free deployment and inflation. . . . .	61
71	Total energy for obtained results zooming in second deployment. With resulting time values in seconds. . . . .	61
72	Illustration about structure evolution during the whole process. . . . .	62
73	Folding evolution for $N = 10$ . . . . .	63
74	Deployment evolution (first and second) for $N = 10$ . . . . .	64

## List of Tables

1	Used tool divided by implementation. . . . .	7
2	Material properties for rigid (PLA) and flexible (TPU) materials. [10] . . . . .	22
3	Resulting mesh comparison. . . . .	44
4	Packaging ratio values for each number of sides. . . . .	48
5	Surrogate model determination coefficient comparison. . . . .	55
6	Summarized optimization results per number of sides. . . . .	58
7	Design variables from LHS. . . . .	67
8	Hardware requirements for the project development. . . . .	75
9	Hardware requirements (without post-processing) for the project development. . . . .	75
10	Degree of compliance with the sustainable development goals. . . . .	79
11	Project time distribution in hours. . . . .	85
12	Budget summary. . . . .	87

## List of Abbreviations and Nomenclature

### General concepts

BC	Boundary Condition
DOF	Degrees Of Freedom
FEM	Finite Elements Method
GA	Genetic Algorithm
GUI	Graphic User Interface
LHS	Latin Hypercube Sampling
MOGA	Multi-objective Genetic Algorithm
PLA	Polylactic Acid
RMS	Response Surface Method
SOGA	Single-objective Genetic Algorithm
TPU	Thermoplastic Polyurethane

### Origami geometry

$a$	Side of the regular polygon of the base
$b$	Kresling triangle hypotenuse
$c$	Kresling triangle leg (which is not $a$ )
$h$	Height of the flat pattern
$h_3$	Height of the 3D pattern
$h_{3,2}$	Height of the 3D pattern for bi-stable states
$N$	Number of rings of the pattern
$n$	Number of sides of the polygon circumscribed
$R$	Radius of the inscribed base circumference



---

**Part I**  
**REPORT**



# 1 Introduction

## 1.1 Project aims and overview

Within space industry evolution, large pressurized structures have become demanded ones. These structures might be used as fuel deposits or habitats being its first disadvantage launching restriction. Payload volume is the most limiting parameter for a launch; therefore, a minimum volume is required for optimizing the payload distribution.

In order to accomplish aforementioned disadvantage, origami structures came to offer large structures that can be folded during launch. This thesis aims to analyse and optimize origami inspired structure with tubular shape for providing a solution for a CubeSat demonstrator. However, there are more objectives within general one, being there explained as follows:

- 1. Provide a code which generates an input file to be simulated**, i.e. automatize the model for parameter analysis. Requiring parameterization of the geometry, boundary conditions and interactions in the model.
- 2. Model and simulate an innovative material use** for providing a feasible solution for technology under develop. Solution shall provide manufacturing material configuration, in order to be consequently validated.
- 3. Validate the model** with expected results. It means to assure that the model accomplished behaviour established by the pattern selected.
- 4. Find packaging ratio of the implemented structure**, which means to find how many times can the pattern be folded. Therefore, the suitability inside of desired CubeSat can be analysed.
- 5. Find the optimal configuration** of selected pattern by simulating the parameterized model. The optimization shall analyse the structure stress and the volume inside it.

Once thesis aims are described, it is required to define framework under which the project has been developed, organization scheduling, an explanation of the report disposition, implemented tools and finally the personal growth during the last months.

## 1.2 Framework

The present work is based on the analysis and optimization of a deployable prototype designed with the Universidad Rey Juan Carlos (URJC) in Madrid and the Technical University of Delft (TU Delft). The prototype is expected to fit into a 12U CubeSat, developing a proto-flight model for the desired mission.

Pre-design and prototyping is made in TU Delft by Joshika Sachithanandan and Inés Uriol Balbin, while the analysing and optimizing work is developed in parallel in the URJC, being this thesis part of a collaborative project.

Therefore, in the timeline of this thesis, another one was on progress developing the prototype expected (Sachithanandan's thesis, supervised by Uriol Balbin). Both works are clearly separated, but in the present one, some of the results obtained by TU Delft are going to be cited as "TU Delft elaboration".

### 1.3 Project organization

From the beginning of this project, it has been planned to be divided in the following work packages, in order to achieve a coherent and structured work. Although present report is divided into different sections, the work made by the author has been planned as it is illustrated in the Figure 1.

Work packages have been divided into six different ones, listed and described as follows:

- **WP 1 - State-of-the-art.** First work package was focused on obtaining and organizing all the information available at the moment of technology under development or similar studies previously made.
- **WP 2 - Requirement analysis.** Once technology available is under knowledge for the author and the final aim is to analyse a demonstrator satellite, requirements seem to be necessary. It means to analyse the satellite capabilities and discover what can be applied or not.
- **WP 3 - Parametric study.** This package aims with defining the pattern parameter to be analysed and optimized. In this work package starts working on **first and second aims** with coding and modelling the geometry.
- **WP 4 - Mesh study.** Starting with simulating different mesh configurations in order to obtain a feasible one. This work package is clearly linked to the next one, due to required iterative process during modelling and meshing. Here is highlighted the model validation aim, which follows the **third aim** of the expected.
- **WP 5 - Deployment and folding modelling.** Simulating the deployment and folding requires an accurate analysis looking for a realistic and converged solution. This WP aims to generate the **fourth goal**, by searching with simulations the packaging ratio of the structure.
- **WP 6 - Optimization model.** Finally, this work package aims with the **fifth and final objective**, involving the optimum configuration for the desired mission. Being involved also the study of viability of results compared with the expected origami pattern behaviour.



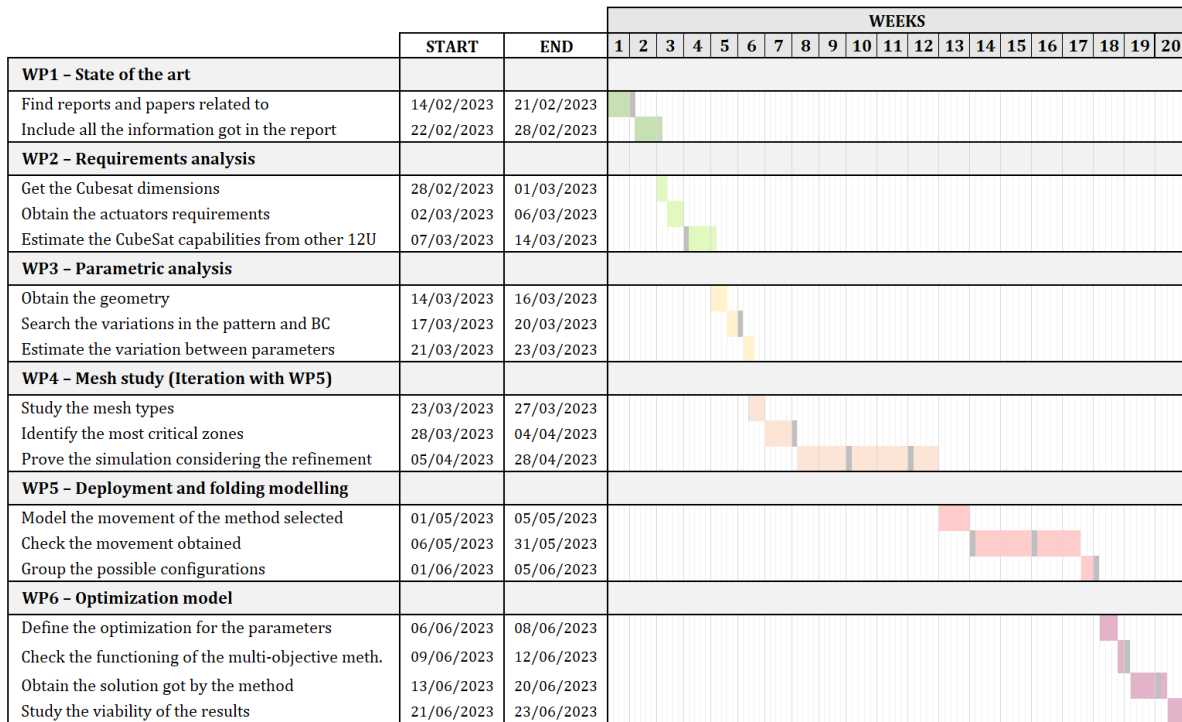


Figure 1: Gantt chart of the thesis.

As can be seen, each work-package is represented with a different color in order to clarify the reader comprehension. Moreover, *grey* shading days are referred to biweekly meeting with TU Delft.

## 1.4 Report disposition

Aside from the work-packages previously mentioned, project development has been divided into the six following described chapters.

- **Chapter 1 - Introduction.** The present one, which introduce the thesis by describing its aims, the framework behind, the project organization, this explanation of the report disposition and the used tools.
- **Chapter 2 - State-of-the-art.** Summary of current state of the art of the origami inspired space structures, its deployable mechanism and multi-objective optimization.
- **Chapter 3 - Statement of the problem.** Explanation about the problem to be solve, which includes the origami geometry obtained theory, a description about the folding and deployment processes implemented in this thesis, materials under study and a brief explanation about the optimization procedure selected. With all this information, this chapter ends introducing the simulation parameters to be used and the workflow implemented.

- **Chapter 4 - Structural model.** Once the statement of the problem is completed, the structural model to be introduced in FEM solver shall be defined. In this chapter are illustrated the geometry, the assignation of the materials, the boundary conditions and the analysis procedure used. Finally, validation of the model is shown by the independence mesh analysis and the study about the energy balance.
- **Chapter 5 - Optimization.** From structural model, optimization process by sampling and surrogate generation is made. In this section, the process made and result obtained are described and discussed. From this section, thesis results arise.
- **Chapter 6 - Conclusion and future works.** Finally, from result obtained and all the process made, conclusions and future work are listed and summarized. In this section are analyzed the future work in function of the one made and the conclusions obtained.

## 1.5 Used tools

As this thesis looks towards analysis and optimization of a space structure, the main software implemented has been FEM solver **Abaqus CAE**. Being this one the most used for the mentioned application. This solver can be used from the GUI or by Python scripting. Commonly it is used to generate the inputs files and the launch them in the Abaqus Kernel.

Nevertheless, in this thesis the use of Abaqus is made by an external Python library which launch directly the solver. Therefore, the calculus required to define the geometry, generate and submit the Abaqus files, are made without opening the solver. This FEM solver works with the following type of files [11]:

- **CAE.** Model database file, which reflects all the interactions made in the application. Here is the whole definition of the model, with the interface readable format. When the CAE is generated, a *jnl* (journal-file) is as well produced. The *jnl* includes all the information generated by the CAE in a text file format. Both files depends on the version of Abaqus used.
- **INP.** The *INP* or *Input* file is the generic for all the Abaqus version. It contains a complete description of the numerical model. The input file is a text file that has an intuitive, keyword-based format, being it easy to modify using a text editor if necessary.
- **ODB.** Output database file, which includes the results obtaining after submit the model in the solver. This output can be just read by Abaqus and interpreted by C++ or Python.

In the present work, the version used has been the 2022 one, being facilitated by TU Delft. Moreover, the library used was the **AbqPy** [12] one, adapted for this Abaqus version. All the project was developed using **Visual Studio Code**, for running the python codes generated. Being both of them license free.

On the other hand, the optimization tool implemented was **Dakota Sandia**, from National Technology and Engineering Solutions of Sandia, LLC. As it is indicated in its website [13], Dakota delivers both state-of-the-art research and robust, being an usable software for optimization and UQ.

Apart from the numerical section of this thesis, this report has been developed by the online tool Overleaf, by latex coding. And all the figures generated by own elaboration has been made or post-processed with **Adobe Photoshop 2022** and **Adobe Illustrator 2022**, with the licenses given by the ETSID.

All in all, used tools can be divided and summarized as they are in the following table.

Table 1: Used tool divided by implementation.

<b>Implementation</b>	<b>Tool</b>
<b>FEM solver</b>	Abaqus CAE 2022
<b>Scripting method</b>	Python 3.11, AbqPy, Visual Studio Code
<b>Optimization method</b>	Dakota Sandia
<b>Post-processing</b>	Adobe Illustrator 2022, Adobe Photoshop 2022

## 2 State-of-the-art

Origami pattern creases for rigid structures have been widely studied in order to build useful origami structures. They are based in the ancient art of paperfolding providing them its qualities. Being essentially, its key aspects, deployability, scalability, possibility of self-actuation and the easiness in manufacturing [14]. Thus, these qualities make them suitable for space structures.

From around the 70's decade, several designs of rigid origami structures have been proposed for space structures. Rigid origami or rigid-foldable origami is referred to an origami surface where the facets are substituted with rigid panels and the foldlines with hinges or a similar mechanism [15]. The first proposal for origami in space structures was the Miura-ori [16, 17], used in the packaging of deployable solar panels. This method is based in the deployability quality of the origami, making possible to suit in a rocket a huge size surface, in a folded way. Thus, it makes feasible to fit space vehicles into the launch vehicle requirements, becoming a lightweight structure with a small size during transportation.

An example of the method mentioned can be seen in the Figure 2. There, the Ikaros Solar Sail turns from a relatively small and rigid cylinder to a huge and flat solar sail thanks to the deployability of the origami.

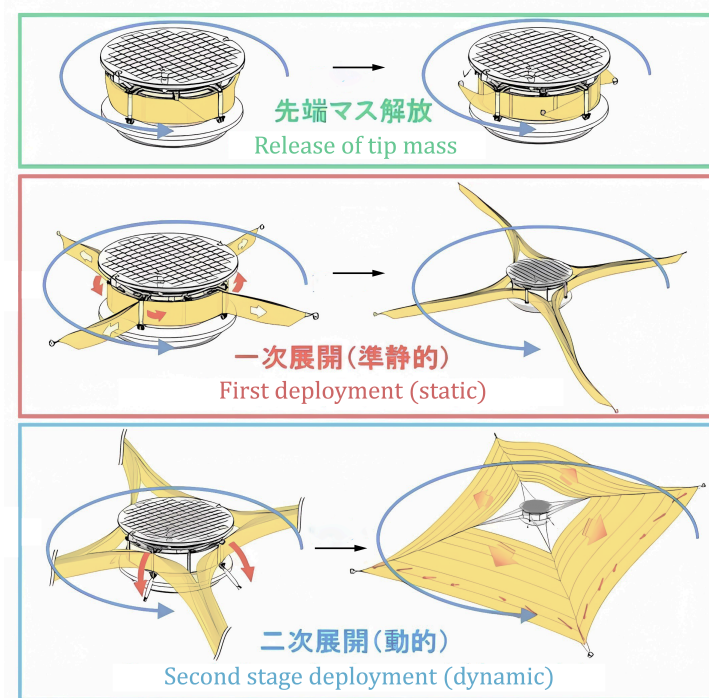


Figure 2: Scheme of the deployment sequence. (Adapted from [1])

Due to the possibilities given by origami, it has been studied going into different roots of knowledge. They can be easily divided in four big ones as follows [14].

- **Deployability** The capacity of the structure to be packaged has been widely analysed in order to get an optimal packaged factor. Therefore, folded compact systems can efficiently fit into the dimensions of launch vehicle.
- **Geometry optimization.** An optimization of the pattern in order to get the most suitable packaged and unpackaged structure. This study allows to get better geometry in function of required mission. Therefore, pattern selection and optimized parameters gives an optimal final shape (depending on the volume, length, surface, etc).
- **Material composition.** The materials used in the structure will define its stiffness and deployability. The hinges or similar method used as foldlines is critical in the structure design.
- **Actuation system.** It may be one of the most investigated items of origami space structures. The desired geometry limits the mechanism used. It has been studied ones as could be: the self-deployable, the scissor mechanism, materials with self-memory, inflation or motor-driven actuators.

Nevertheless, once the bases for generic studies are known, they should be applied on cylindrical structures. Therefore, the pattern selected generates a cylinder with the maximum volume inside and the most efficient method in order to keep the properties of the structure. The most common origami patterns used for this type of structures are the Miura-Ori (previously mentioned), the Yoshimura and the Kresling [7].

In order to get a overall comprehension of this thesis, the state-of-the-art can be divided into the origami patterns and geometry, modeling and simulation of deployable mechanism, and finally, the multi-objective optimization, being it the final aim of the project.

## 2.1 Origami patterns and geometry

The expected geometry of the desired structure is a cylinder. Thus, the pattern used shall be constrained to deploy as a tubular structure. The three mentioned patterns can achieve this constraint, therefore they are described in the following sections.

They are represented thanks to two diagrams in order to give to the reader a better comprehension. They are a unit cell (2D to be assembled) and a 3-dimension (3D) diagram of the origami cylinder. In the 2D diagram the ridges and valleys foldlines, are represented by solid and dotted lines, respectively.

### 2.1.1 Miura

Most of the design for space structures are based on miura-ori pattern, becoming the most used one. [14] The suitability of this pattern for the application mentioned is due to its high degree of symmetry. Thus, it involves advantages in: rigidly folded, number of degrees of freedom (DOF), its Poisson's ratio and flat-foldable.

Thus, about the *rigidly folded*, it can be continuously deformed and then turns from folded into unfolded state keeping the stiffness of the structure. [18] This could be the expected result taking the Figure 3 as reference, because of the evident symmetry of the pattern. As can be seen, the unit cell in this pattern is comprised by parallelograms or obtuse trapezoids in function of the desirable behaviour of the structure.

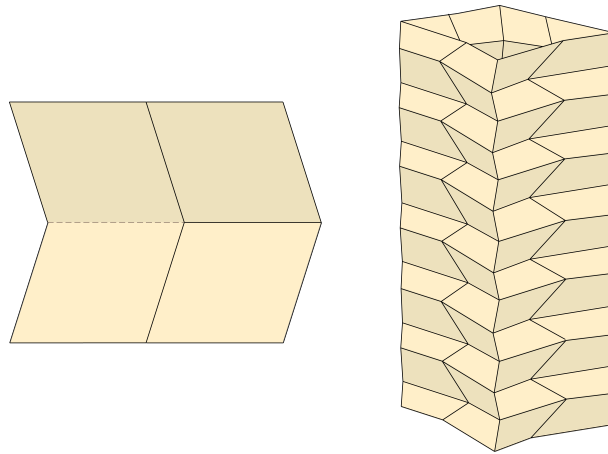


Figure 3: Miura pattern. [Own elaboration]

On the other hand, it is 1 *DOF* mechanism, instead of the common 6 rigid *DOF*. Thus, it is enough to lock this single *DOF* to get a structure. Being able to get the pattern deployable with a single gesture. [19] Finally, it exhibits negative *Poisson's ratio*, which means that unfold the pattern decrease the projected area in both planar directions. Implying because of the nature of the pattern that it can be completely folded, getting a structure where all the faces are almost coplanar. [18]

### 2.1.2 Yoshimura

The Yoshimura pattern is one of the *ori*-patterns which came arise from natural phenomena. [7] Comprised of adjacent triangles that form the diamond shape, as can be seen in the unit cell and in the 3D representation (see Figure 4). This type of pattern and derivatives has been studied for many structures, in order to obtain its mechanical response and energy absorption characteristics.

In comparison with the Miura-ori, this pattern offers as well *rigid foldability*, 1 *DOF* and *flat foldability*, making it easier to study and manufacture. Nevertheless, instead of Miura, it exhibits positive *Poisson's ratio*.

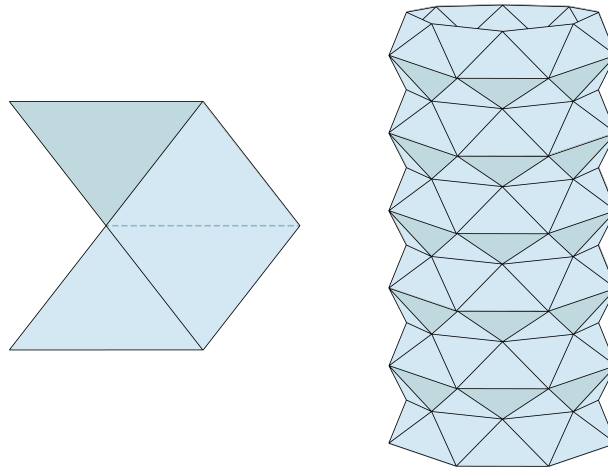


Figure 4: Yoshimura pattern. [Own elaboration]

### 2.1.3 Kresling

Kresling pattern arises from the twist buckling of a thin cylinder. Being able to transform instability into a multi-stability behaviour. Thus, this pattern exhibits a great potential for tubular applications. As can be seen in the Figure 5, this model is characterized by alternating mountain and valley creases angled along the direction of twist. Thanks to its geometry, it may be bistable, thus it requires moderate panel deformations to compress to a compact state. [2]

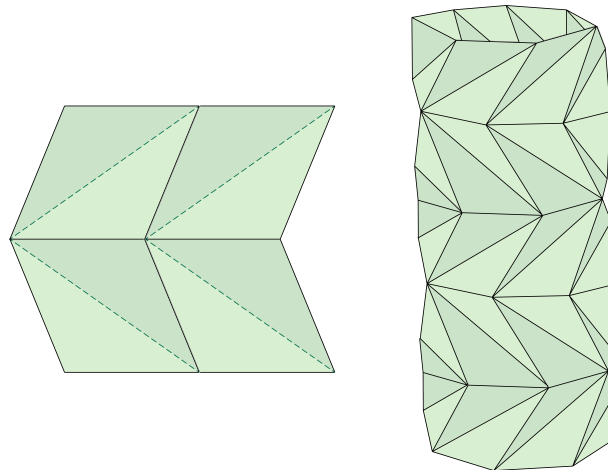


Figure 5: Kresling pattern. [Own elaboration]

The most remarkable advantage of this pattern is the independence of its modules or ring cells. It appears thanks to its configuration making each module independently deployed to its extended or compressed state. [2] The behaviour described can be easily understood seen the Figure 6.

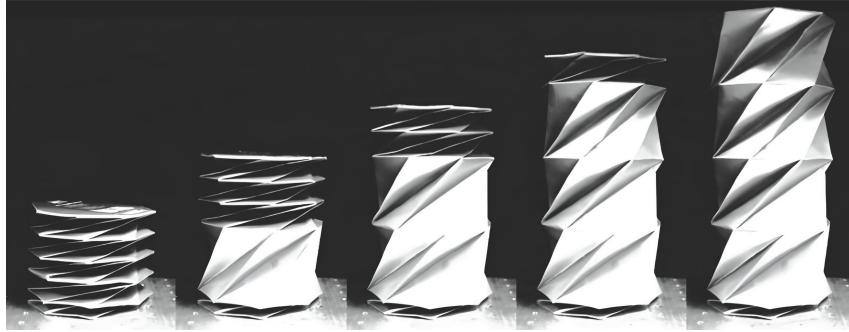


Figure 6: Kresling origami at different stages of deployment. [2]

Kresling tubular structures can be therefore composed of multiple ring cells serially connected, generating a single multi-stable structure. Thus, each state of the one represented in the previous figure, is completely stable.

Finally, as it is mentioned by Meloni et al. [14], this pattern exhibits, as the Yoshimura one, *flat foldability* and positive *Poisson ratio*. Nevertheless, the structure can be model as a 6-DOF system, which may add complexity to the model, but it has been seen that this pattern may reveal robust and effective deployable structures. [2]

## 2.2 Modeling and simulation of deployable mechanism

As origami has been used in several structural applications, it has been widely simulated in several conditions. For this reason, there are many types of hinges or similar mechanisms in order to obtain the best suitable behaviour of the structure. The common way to model the creases is by torsional springs, changing its properties in function of the real mechanism.

First of all, the paper has been the obvious first option to model origami structures. As it is described by Grey [3], the paper is *a useful material as it is cheap, freely available, and easy to work with*. Therefore its stiffness matrix was characterized experimentally by a prototype described in the Figure 7.

This modelling showed a significant hysteresis and non-linearity in the fold response. It may suggest a near plastic deformation in the crease due to the damage induced within the paper. This phenomenon exhibits a natural rest angle of the fold. Configuration which comprised as well with the minimum energy state of the structure.

On the other hand, another deployable mechanism studied is the use of elastic hinges. One of the most significant studies is the provided by the MARSIS (Mars Advanced Radar for Subsurface and Ionosphere Sounding) antenna, that was flown and deployed in 2005 on the ESA's Mars Express. [4] Nonetheless, in the study made by Fulton et al. [4] elastic hinges have been tested in an experimental and the hinge method used is tape spring hinge embedded in the structure (see Figure 8). Therefore, it was determined



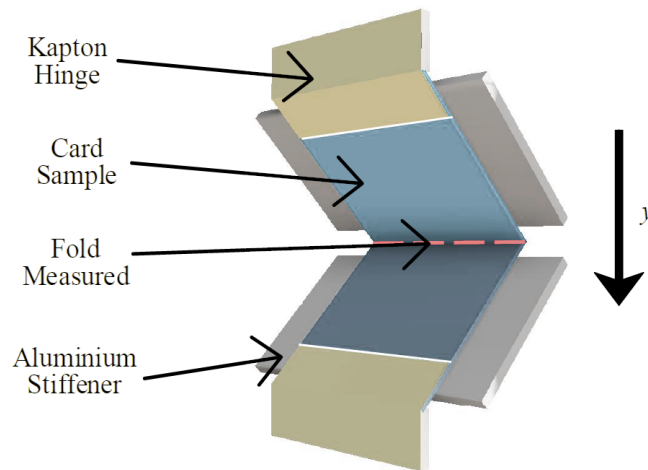


Figure 7: Experimental set-up for single fold stiffness. (Adapted from [3])

that the simulations done of 1-DOF and 4-DOF hinge models showed good prediction of the deployment in time. Nevertheless, the deployment of both models was not correctly achieved: its behaviour past the peak deployment and it is not well predicted due to constraint violations and the damping in the model, being consequently of the lack of contact.

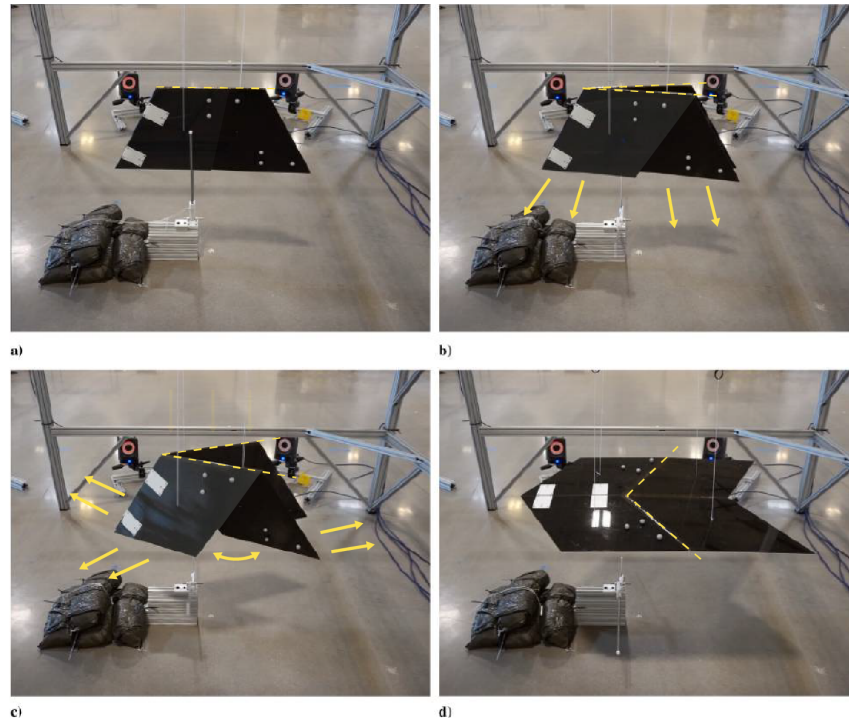


Figure 8: Experimental deployment sequence of elastic hinges. (Adapted from [4])

Guided by these application, it is useful to highly the origami folds modelling is the one defined by Peraza et al. [5]. They propose to change the assumption of creased folds into smooth folds based in its dynamic's behaviour. The folds as straight-line segments which divide the sheet into faces, just keeping the zeroth order geometric continuity ( $G^0$ ). Therefore, the smooth folds seem like a better approach when thickness and curvature is considered. This proposal can be easily seen in the figure 9.

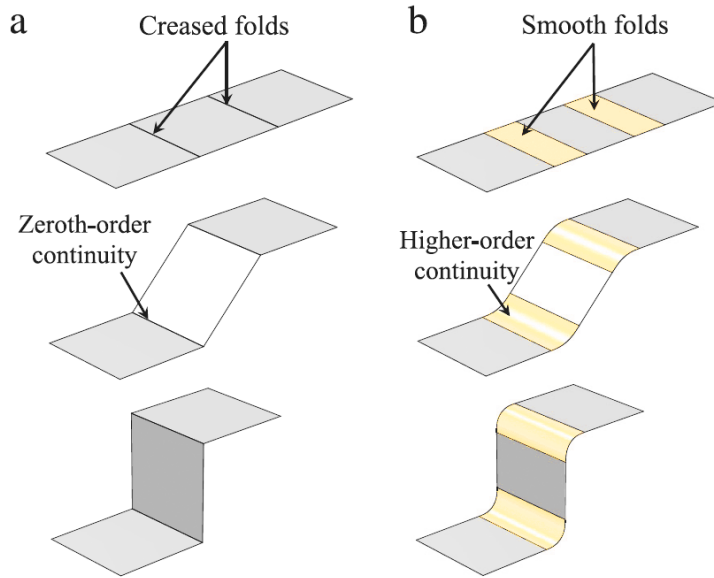


Figure 9: Sheet examples with crease folds (a) and smooth folds (b). (Adapted from [5])

It has been modelled by applying the principle of minimum potential energy and kinematically admissible displacement that satisfy the mechanical equilibrium under determined loads. As it occurs in the studied mentioned before, this method has been tested by experiment and simulation. Thus, this studied demonstrate that this method can be useful for origami structures.

The three both studies implement experimental and simulation process, where all the simulations were done with Abaqus. Abaqus is a Dassault System software developed for FEA (Finite Element Analysis) and its functionalities will be developed in the simulation section of this thesis.

### 2.3 Multi-objective optimization

Multi-objective optimization for any structure has been intensely studied for the last decade. In the case of origami structures, it is required to highlight the only study with a similar purpose of this thesis, the one described by Yang et al. [20]. As its title said, they studied the "*Multi-objective optimization of multi-cell tubes with origami patterns for energy absorption*". The aim of this paper was to find the optimal designs with low initial peak force, high specific energy absorption and small fluctuation of the

crushing force. Thus, the method used was the RMS (Response Surface Method) in order to formulate the objective functions. RMS was introduced by Box and Wilson [21] and it is described as a collection of mathematical and statistical techniques in order to analyse problems by an empirical model.

As results, they obtain Pareto frontiers by different constrained reduction of specific energy absorption (SEA). [20] Being the Pareto front is defined as the set of non-dominated solutions, where each objective is considered as equally good (see figure 67). [22] And it is, as well, compared FEM result with theoretical values.

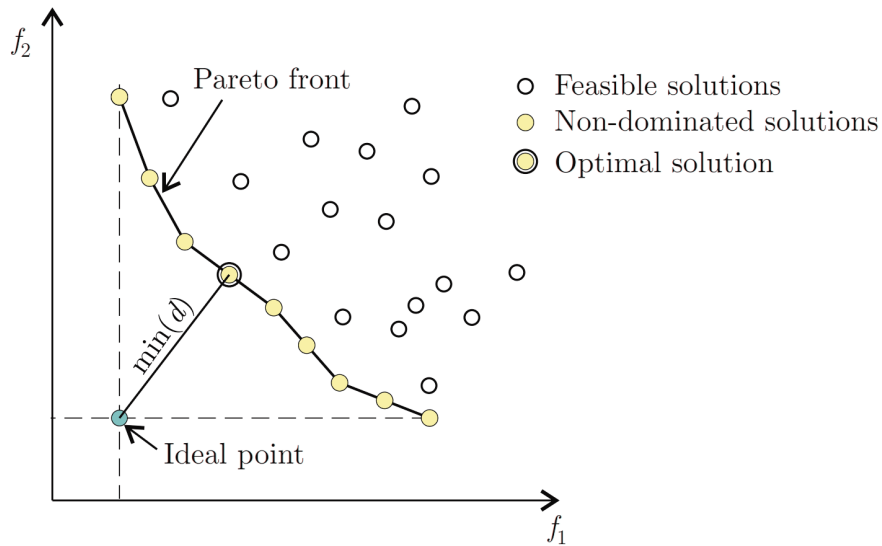


Figure 10: Representation of a Pareto front. (Adapted from [6])

On the other hand, another common way to solve multi-objective optimization is using optimization libraries or frameworks. An example of this method is the DAKOTA framework, which offers the algorithms required for performing samplings, meta-model construction and robust genetic optimization algorithms. It is used inside of Python, as can be seen in J. Paz doctoral thesis [9]. In this thesis, the optimization is made for crashworthiness analysis and design, with an application to aircraft structures.

### 3 Statement of the problem

As it was previously mentioned, this project shall follow the guidelines given by Uriol and Solano [7]. The prototype of a 12U satellite constraints the dimensions of the origami structure in order to fit in the usable part of the satellite (see Figure 11).

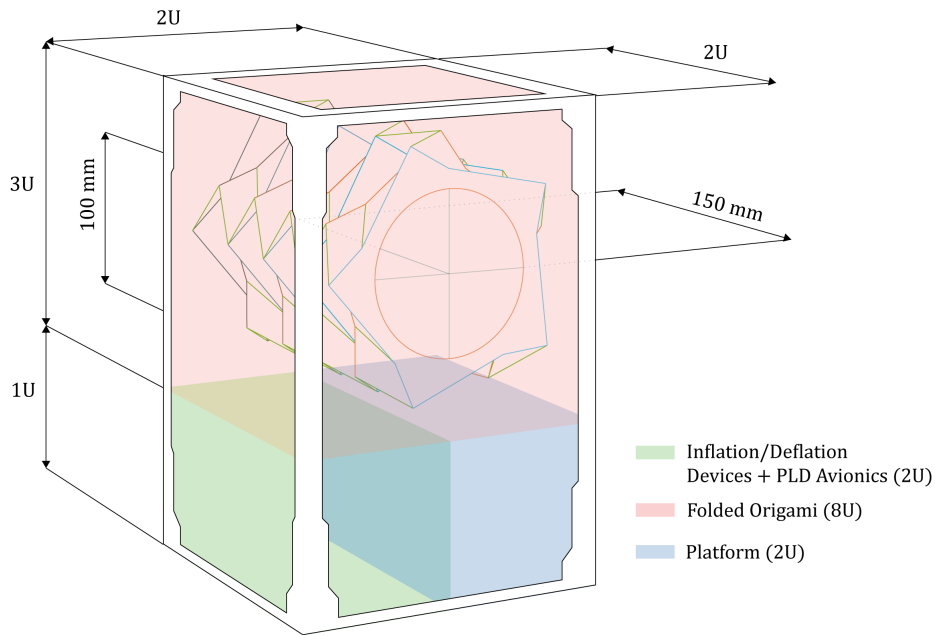


Figure 11: Sketch of the 12U prototype with the origami structure. [7]

On the other hand, because of the behaviour of the Kresling pattern it will be the more suitable pattern, compared with the Yoshimura and the Miura [7]. Therefore, the whole project will be based on this pattern, developing an optimal design for the expected application.

Overall, this project is defined by the following constraints.

- **Radius** The radius of the pattern shall be less or equal to 50 mm.
- **Folded height** The completely folded height, in order to fit inside of the 12U satellite, shall be less or equal to 150 mm.
- **Pattern** The pattern used shall be the Kresling one.

Once these constraints are defined it is required to define the possible states of the origami structure, in order to improve the reader comprehension. As it was introduced in the state-of-the-art (see section 2), **the origami can be described in three different configurations**. Here, they are described as:

- **Flat configuration.** Based on the flat pattern, which is a 2D geometry.

- **Deployed or unpacked configuration.** The one it occurs when the pattern is mount, i.e., it is not under any type of stress, is just the material folded. It gets a 3D geometry.
- **Un-deployed, stowed or completely folded configuration.** Referred to the configuration that happens when the deployed one get folded. Finally, it is an almost flat but 3D geometry.

Being the constraints and possible configurations defined, the problem shall be defined by its geometry, the folding and deployment processes defined, the material implemented and the optimization procedure. With all those ingredients, simulation parameters can be defined and the workflow planned.

### 3.1 Origami geometry

The kresling pattern closure has been defined as a geometric problem to be solved [23]. Due to the bases of the geometry, this pattern is defined by triangles located around a circumference making up a cylinder-shaped geometry.

Then, the pattern could be defined by it number of sides  $n$ , the radius of the cylinder  $R$  and the height of the flat pattern  $h_2$ . According to Hunt [23], in order to form the 3D geometry, the pattern should accomplish the following equations (see figure 12).

$$a \cdot h_2 = d \left( \frac{d}{\tan(\varphi/2)} + \sqrt{a^2 + d^2} \right) \quad (1)$$

where  $a$  is given by the cylinder constraints (see figure 13) as

$$a = 2R \cdot \sin(\varphi/2) \quad (2)$$

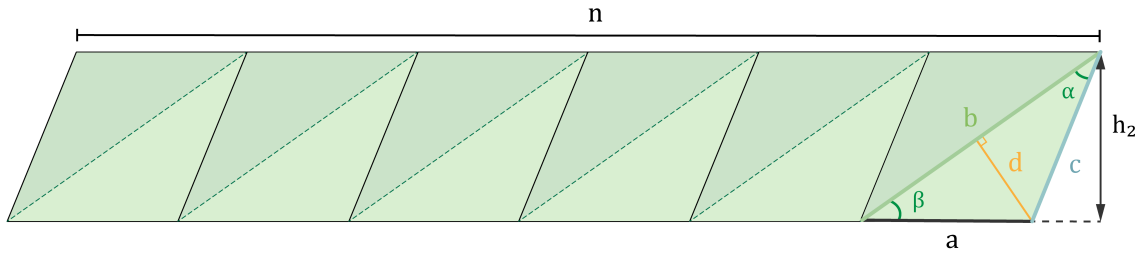


Figure 12: Flat pattern parameters. [Own elaboration]

Folding the flat pattern represented in the figure 12 it will make up the 3D geometry shown in the figure 13. The geometry obtained is a cylinder shape one, with the sides imposed by the flat pattern configuration.

As it is described by Berre et al. [8], the folding performance has a bi-stable response by accomplishing

$$G(h_3, \mu) = \arcsin \left( \frac{\sqrt{b^2 - h_3^2}}{2R} \right) - \arcsin \left( \frac{\sqrt{c^2 - h_3^2}}{2R} \right) - \frac{\pi}{n} = 0 \quad (3)$$

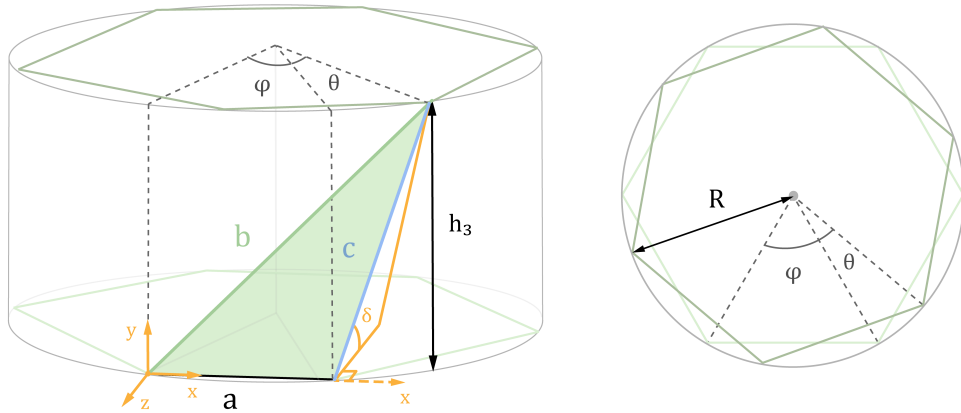


Figure 13: 3D representation. [Own elaboration]

where  $\mu = (b, c, n, R)$ . Therefore, the design heights could be  $h_{3_1}$  and  $h_{3_2}$  defined as:

$$G(h_{3_1}, \mu) = 0 \tag{4}$$

$$G(h_{3_2}, \mu) = 0 \tag{5}$$

Being the  $h_{3_1}$  the one referred to the flat folded shape and the  $h_{3_2}$  to the one deployed. It can be easily understood in the figure 14.

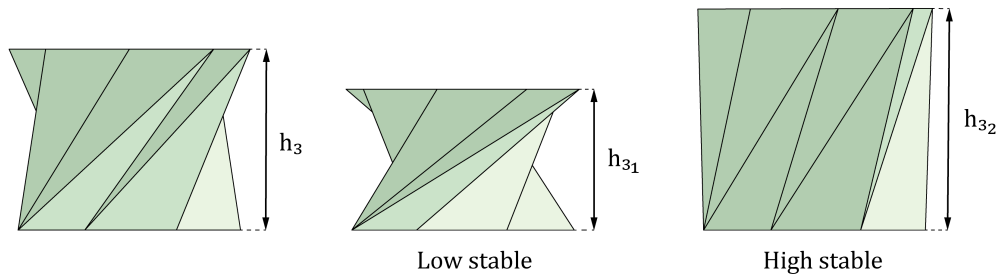


Figure 14: Height of design according to the bi-stable behaviour. (Adapted from [8])

In order to obtain the design, the height used will be the second one, in order to regarding the real thickness and the behaviour of the material used. Thus, with the dimensions of the flat pattern and the height of the 3D ori, the  $\delta$  angle can be obtained. This angle is the one between the horizontal plane and the triangle of the figure 13, i.e., the angle around the x axis to reach the  $h_3$  desired height.

---

From the 3D formed geometry and in order to achieve a prototype for a habitat, the volume inside of the pattern is critical. Therefore, in this thesis two different internal volumes have been considered. First one, the **inner volume**, which is defined as the volume of cylinder which fit inside of the deployed structure. Whereas, the second volume, **outer volume**, is referred to the whole space inside of the structure. Both ones are represented in the following figure by the yellow region.

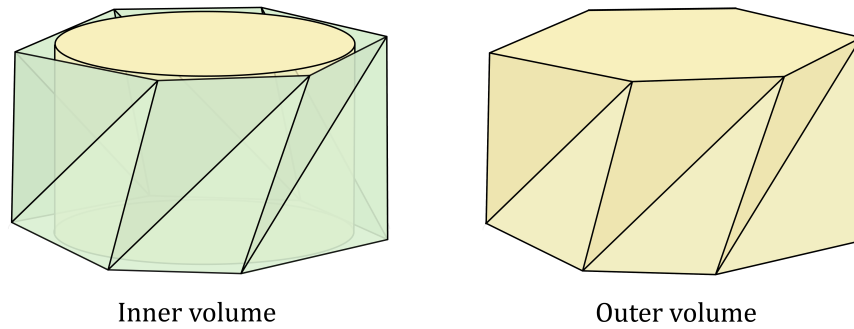


Figure 15: Inner and outer volumes illustration. [Own elaboration]

### 3.2 Folding and deployment process

The simulation used involves the movements of folding and deploying the 3D ori pattern. Thus the movement is divided into two different process, **starting from the second stable state which is the initial state of the origami structure.**

Therefore, the **folding process** is clearly illustrated in the Figure 16. As can be seen, the movement occurs just in the vertical axis and because of the pattern properties it folds twisting. The final configuration is the folded state.

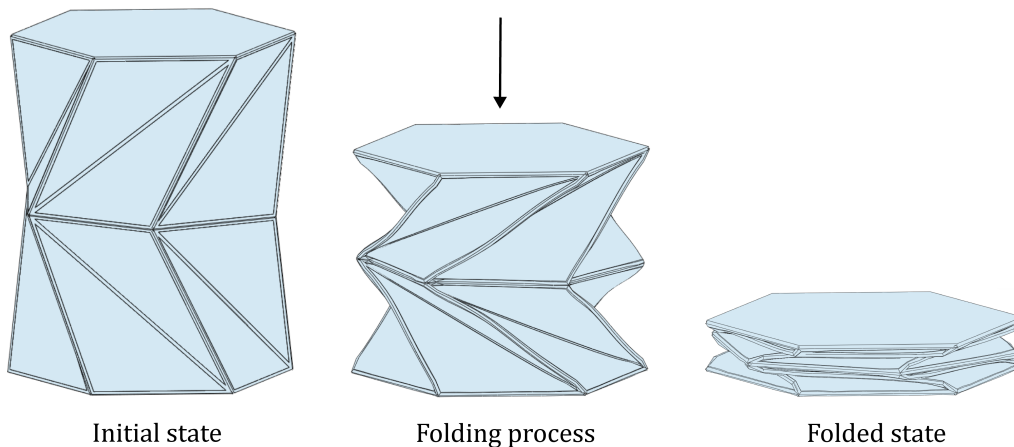


Figure 16: Folding process. [Own elaboration]

Once this folded state is obtained, the **deployment process** starts in order to obtain the mayor inner volume. The deployment is opposite process of folding, going from the folded state to one near the initial, which will be the deployed state.

In this study, the deployment process selected is the inflation method. As it is described by Uriol and Solano [7], the Kresling pattern calls for this one. Thus, taking profit of the bi-stable behaviour, the pattern goes to the second stable state ( $h_{3_2}$ ) and then starts the inflation. First stage of the deployment thereby is a steady transition to a stable state.

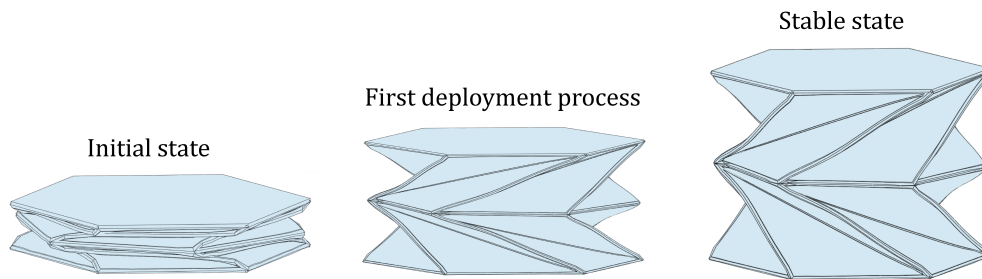


Figure 17: First deployment process. [Own elaboration]

In the second stage, air pressurized is supplied into the inside of the origami cylinder, creating a pressurized volume. This process is described in the Figure 18.

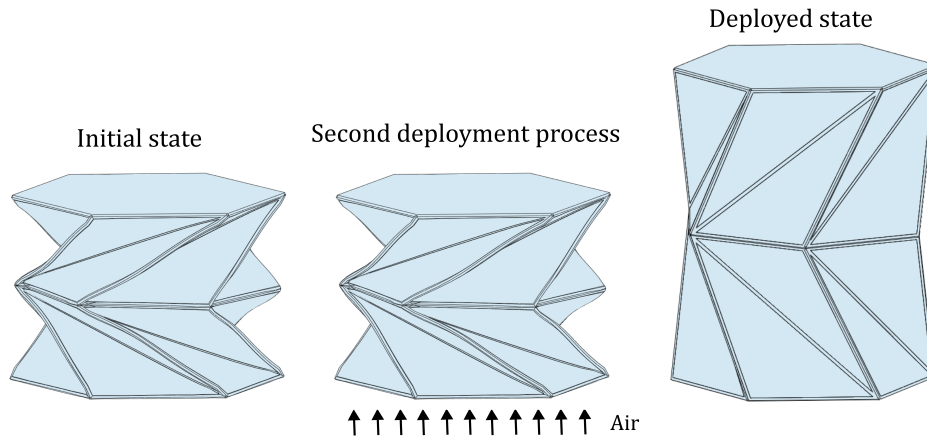


Figure 18: Second deployment process. [Own elaboration]



### 3.3 Materials

One of the most critical problems of origami space structures is the trade-off between the stiffness and bendable properties of the pattern. A solution of compromise can be the use of two different materials, with a bendable and a stiff one. It can be applied by many techniques as:

- **Composite material.** Based on the nature of the composite materials the stiffness of the fibres and the flexibility of the matrix, it can be applied. The idea is to made a pattern with a lower fibre volume contents in the creases, in order to make a rigid material more bendable, Fig. 19.

This type of materials shall be cured to achieve the stiffness pre-defined, and this curing process can be made by novel methods. Some as electric curing using the Joule heating or curing by magnetic induction heating, are feasible methods to develop in a not-atmosphere space environment [24]. Thus, applying them can rigidize the structure when it is completely deployed.

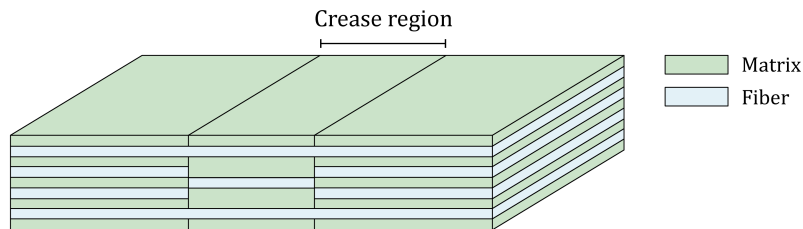


Figure 19: Example of composite material implementation. [Own elaboration]

- **Printable materials.** The most common material used with a 3D printer is the PLA (Polylactic Acid). This material shows a large rigidity when it is printed with a thickness bigger than the filament, making it difficult to fold. Therefore, it seems suitable for stiff structures but not for bendable ones. However, there are flexible printable such as the TPU (Thermoplastic Polyurethane). One of the main characteristics of this material is the capability of being one of the most versatile engineering thermoplastics materials with elastomeric properties [25].

In this case, the proposed technique is to print PLA in the regions where the stiffness is required and TPU in the crease regions. Thus, the flexibility and rigidity of the whole pattern increase. An example of the material definition is represented, Fig. 20.

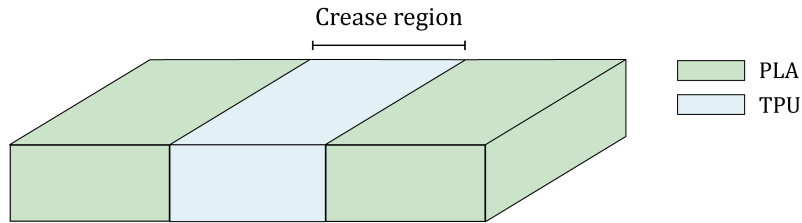


Figure 20: Example of printable material implementation. [Own elaboration]

In the present thesis, the method implemented has been the second one, the use of printable materials. This selection is based on its easier manufacturing process. In order to print the pattern automatically, it is required a 3D printer with dual extruder. As it was introduced, the prototyping part of the project is not part of this thesis, it was developed in TU Delft.

In order to define the material for the simulation as well as check its behaviour, it is required to introduce the material properties. Therefore, they are summarized in the following table.

Table 2: Material properties for rigid (PLA) and flexible (TPU) materials. [10]

	PLA (Polyactic Acid)	TPU (Thermoplastic Polyurethane)
<b>Tensile modulus [MPa]</b>	2346.5	26
<b>Tensile strength [MPa]</b>	49.5	8.6
<b>Poisson module [-]</b>	0.35	0.45
<b>Density [g/cm3]</b>	1.24	1.22

### 3.4 Optimization procedure

As it is defined, optimization procedures are based on minimizing or maximizing a set of objectives functions with chosen input values within an allowed design space. Thus, the set which best the function responses under the defined criteria, becomes the result. [9] The problem includes is therefore defined by three things: an objective function, a constraint set, and a desired outcome. [26]

As it is described by Paz [9], any optimization problem can be defined as a minimizing problem defined by:

$$\text{minimize } (f_1(x), \dots, f_i(x), \dots, f_l(x)) \quad (6)$$

where

$$x = (x_1, \dots, x_d) \quad (7)$$

Needing to be under the conditions:

$$h_j(x) = 0, (j = 1, 2, \dots, J) \quad (8)$$

$$g_k(x) \leq 0, (k = 1, 2, \dots, K) \quad (9)$$

$$(10)$$

Where, the three mentioned parts are identified as follows:

$$\begin{aligned} f_1(x), \dots, f_l(x) &\equiv \text{Objective functions} \\ h_j(x), g_j(x) &\equiv \text{Constraint set (Equality and inequality)} \\ x &\equiv \text{Desired outcome (or design variables)} \end{aligned}$$

In the event of  $l = 1$ , i.e., the problem is defined by a single objective function, the solution results of a single point. Nevertheless, if  $l \geq 2$ , i.e. more than one objective, the problem turns into multi-objective, becoming the result a set of points.

An optimization problem can be solved by several method, due to the extensive research and algorithms available. However, each one is based on the characteristics it may suit for the desired type of problem. All in all, a major division can be made according to the derivative purpose: gradient-based or gradient-free. Although, the first one is often considered as highly efficient, its robustness depends on the expensive derivative calculations, discontinuities, or an intractable noise, resulting of the objective functions. [9]

The optimization procedure can be divided in three different strategies, in this case the most remarkable ones are: meta-heuristic method, surrogate-based method and sampling strategy. Thus, when these three elements are described, the optimization method gets defined.

- **Meta-heuristics**, term coined by Glover, involves all modern nature-inspired algorithms, as could be *Simulated Annealing*, *Genetic Algorithms*, *Artificial Neural Networks* and *Tabu Search*. [27] Based on the literature [9], in this thesis, the strategy used is the **Genetic algorithms**.

Genetic algorithms are considered the most widespread and versatile evolutionary ones. They are based on Darwin's theory of natural selection, which means attaining among a defined population the 'survival of the fittest'. The method encodes solutions as individuals and bits as chromosomes, basing the method on mutation, mating and selection. Therefore, by the adequate adjustment of the method parameter, a global optimum can be rapidly obtained. [9, 27, 28]

- **Surrogate-based** method simplify the optimization by replacing the expensive and complex physical models by another physical or mathematical model with the purpose of reducing evaluating time. These models are called surrogate- or meta- models. Towards this time reduction, the orig-

inal objective functions  $f_i$  are replaced by  $\hat{f}_i$ . Thus, as it is generally built with more manageable functions, the model results faster when computing. [9]

The surrogate model quality shall be ensured. Carrying out this aim, different approaches, which might consist on: sweeping the ranges of design variables in order to find the fitness of the objective functions or scaling the variables to make them be in the same magnitude order, minimizing the malfunction of the surrogate model. [9]

- **Sampling** strategy is the previous step for obtaining the surrogate model. As sampling is reduced to select the number of studied points  $N_s$ , the strategy chosen results crucial due to it will condition the quality of the obtained surrogate model. According to Paz [9], in this thesis the selected strategy is the Latin Hypercube sampling (LHS), developed by McKay et al. [29]. This sampling method will reduce the computing load linked to methods as the Montecarlo available ones.

Illustrations in Figure 56, show the two-dimension representation for different sampling method.

As can be seen in the first illustration, Fig. 21a, random sampling produce regions of parameter space without enough samples and other regions overcrowded. While the full factorial, Fig. 21b, selects a sample for each interval and every possible combination, resulting in an oversized  $N_s$ . Finally, with the LHS, Fig. 21c, a single value is chosen from each parameter interval, Which shows an efficient and adequately sampling for the entered design space. [9]

The whole optimization method implemented in this thesis has been made by free software **Dakota Sandia**. Within this tool, selected method has been the named *Moga*. MOGA means Multi-objective Genetic Algorithm, i.e. a global optimization method that does Pareto optimization for multiple objectives. Meanwhile supporting general constraints as well as a mixture of real and discrete variables. [13]

Following **MOGA** documentation in Dakota Website [13], the algorithm follows these three basic steps:

1. Initialize the population.
2. Evaluate the population, which means calculating for each population member, the objective function and constraint.
3. Loop until converged, or stopping criteria reached. This step includes: 1) performing crossover and mutation, 2) evaluation of the new population, 3) assessing the fitness of each member, 4) replacing the population with the selected ones, 5) applying pressure to the new population and finally 6) testing the convergence.
4. Test for convergence.

Therefore, many parameters can be defined in order to find the fitness solution during the evolution process. However, before deciding the GA definition, the simulation parameters (including objective functions and design variables) shall be defined.

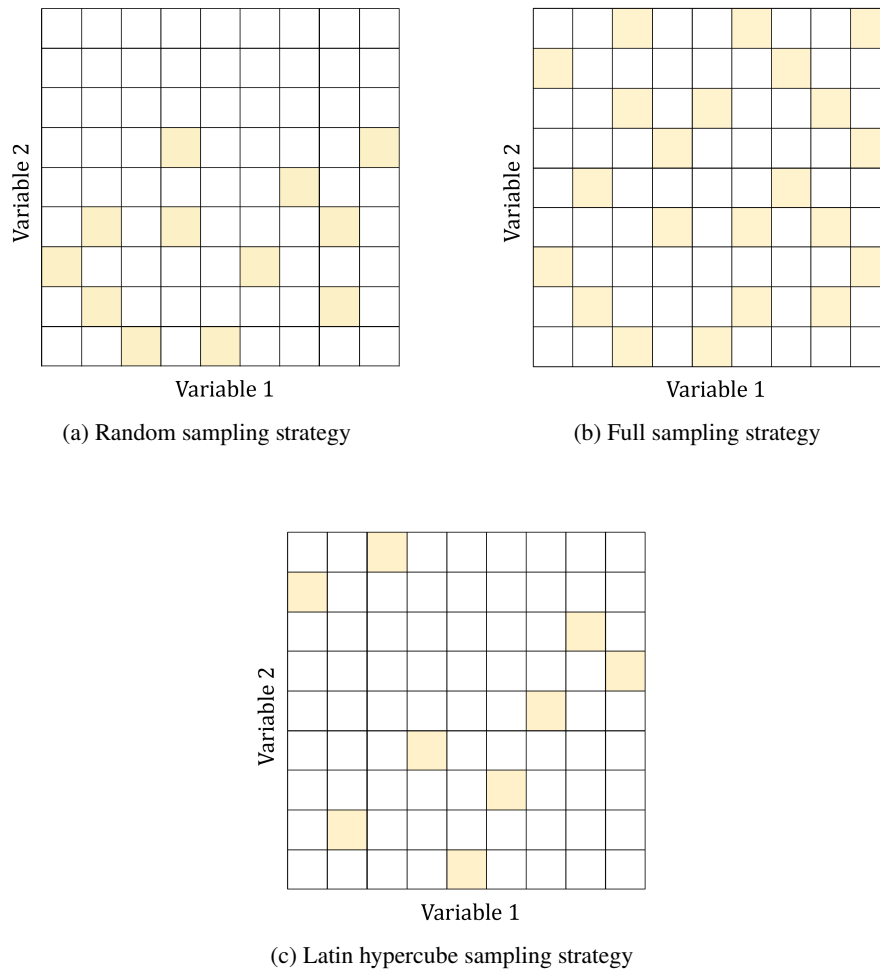


Figure 21: Illustrative examples of three sampling strategies for a two-dimensional problem. (Adapted from [9])

### 3.5 Simulation parameters

Model has been clearly divided into three main approaches: **geometry definition**, **structural simulation** and **optimization process**. Obtaining from each one the parameters required for the next. It means that output given by the geometry definition will define the structural simulation and therefore the simulation outputs will define the optimization process.

Regarding on the parameters defined on the Section 3.1, the parameters used in each section are defined as follows.

- **Geometry definition.**
  - **Inputs.** Radius ( $R$ ) which is constrained to the aforementioned 50 mm, flat pattern height ( $h$ ) and number of sides ( $n$ ).

- **Outputs.** Horizontal flat projection ( $x_h$ ), side length ( $a$ ), deployed height ( $h_3$ ) and projection angle between XY plane and  $h_3$  vector ( $\delta$ ).
- **Structural simulation**
  - **Inputs.** Derived inputs from **geometry definition** and the number of rings ( $N$ ), the thickness of both implemented elements ( $e_1, e_2$ ), material selection, process to performance (folding or deployment), number of output intervals, width of the material used in the crease and maximum mesh size defined by the number of elements per  $a$  side ( $n_e$ ).
  - **Outputs.** Inner volume ( $V_i$ ), Von Mises stress ( $S_M$ ) evolution, kinetic energy ( $E_k$ ), internal energy ( $E_i$ ), artificial strain energy ( $E_{as}$ ), external work ( $W_e$ ) and total energy ( $E_T$ ).
- **Optimization process.**
  - **Inputs.** Inner volume ( $V_i$ ) and maximum Von Mises stress ( $S_{M_{max}}$ ) derived from **structural simulation**.
  - **Outputs.** Optimal number of sides ( $n_{opt}$ ) and optimal flat height ( $h_{opt}$ ).

Thus, it becomes the whole process outputs the same parameters as the initial inputs, achieving a "loop" where the optimal solution for the parameters defined, can be simulated. It means that the optimal geometry can be considered for changes in the additional inputs of the simulations.

### 3.6 Workflow

After having defined the problem statement, the workflow can be defined. Based on the three approaches aforementioned, the results of this thesis shall be based on the optimization results. Therefore, the inputs of the first step, **geometry definition**, shall be obtained from the sampling of the **optimization process**. As well as optimization result can be introduced in **geometry definition** and offer a completed **structural simulation** of the optimized geometry.

On resume, the path followed in the optimization process is described by the following steps:

- **Step 1** - Generate by the Latin Hypercube sampling the  $N_s$  required inputs to implement the **optimization**. Thus, the sampling method shall provide as outputs: the number of sides ( $n$ ) and the flat pattern height ( $h$ ).
- **Step 2** - Yield the  $N_s$  **geometry** configurations.
- **Step 3** - Launch all the generated geometries in Abaqus in order to run the **structural simulation**.

- **Step 4** - Validate the solution generated in the structural simulations and run the optimization method with the results obtained in the **Step 3**.

Looking for a better comprehension of the reader, this workflow, regarding the simulation parameters defined, is illustrated in the following figure.

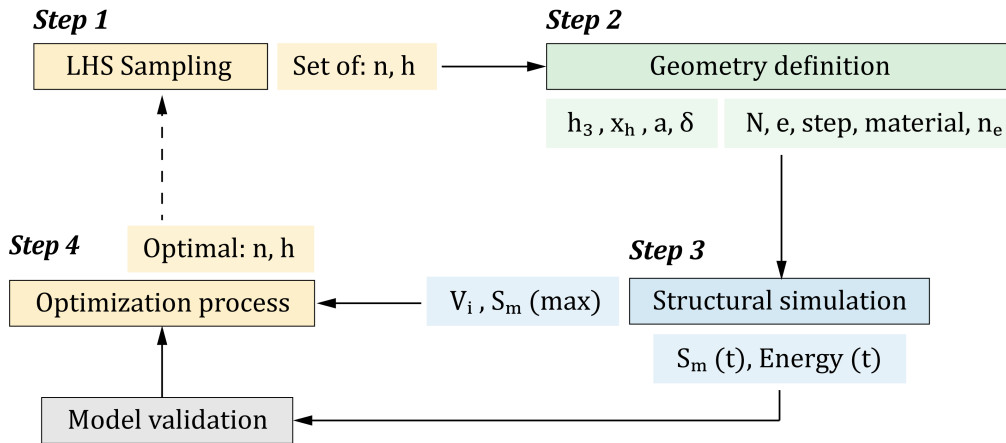


Figure 22: Workflow.

As the whole project has been developed using Python scripting, the workflow above has been replicated indicating the '.py' files used with its outputs files consequently.

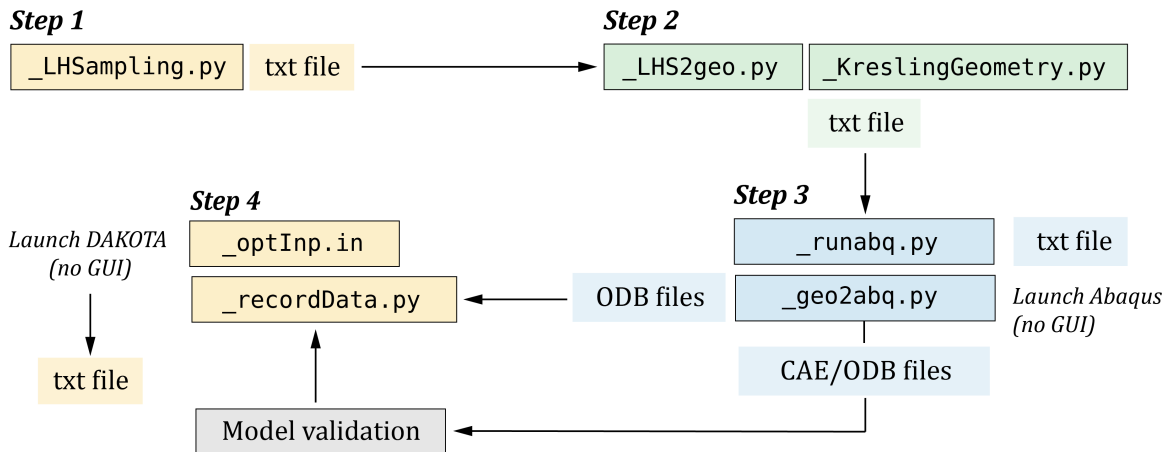


Figure 23: Coding workflow.

Files mentioned can be consulted in the following online repository code: <https://github.com/estervelazqueznavarro/parametric-simulation-kresling-ori>. There, the reader could find the explanation for each file and its dependencies.

## 4 Structural model

The implemented model is developed in an external and automatic Python script. Thus, in the script the order used to define the model follows the modules order used in Abaqus. However, in the present section the structure followed has been changed in order to increase the guidelines comprehension used. The flow chart implemented has been the followed one.

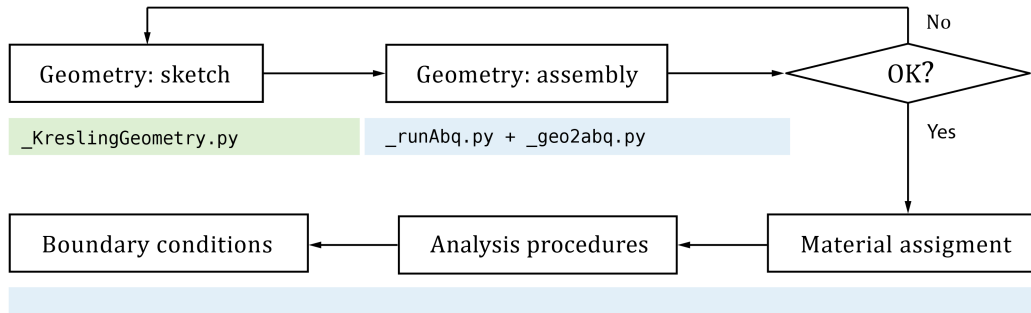


Figure 24: Structural model flow chart. [Own elaboration]

As can be seen, an iterative process has been implemented by checking the assembly part with the geometry previously calculated. If the pattern is correctly assembled, the path followed has been to define the material, the analysis procedure, and the boundary conditions.

In this report the boundary conditions are firstly presented in order to select the procedure which response better to them. Finally, the whole structural model shall be validated by the obtained results.

### 4.1 Geometry definition

Under the knowledge of the kresling geometry defined in the section 3.1, the model has been defined in Abaqus. Therefore, it has been defined in the modules `Part` and `Assembly` as follows.

- 1. Geometry calculation.** Developed in the function `kreslingGeometry`, getting the outputs required to build the model in Abaqus. These outputs are:  $h$ ,  $x_H$ ,  $a$ ,  $h_3$  and  $\rho$  (as they are illustrated in the Figure 12 and 13).
- 2. Sketch definition.** The sketch is defined by the previous parameters by drawing lines in a single sketch, as can be seen in the following figure. Starting here the implementation of the `completeRingFunction` function.

The part has been pre-defined as a shell element, as it is defined in the model developed by Grey [3]. Supported by the statement: shell elements are used to model structures in which one dimension, the thickness, is significantly smaller than the other dimensions [11].



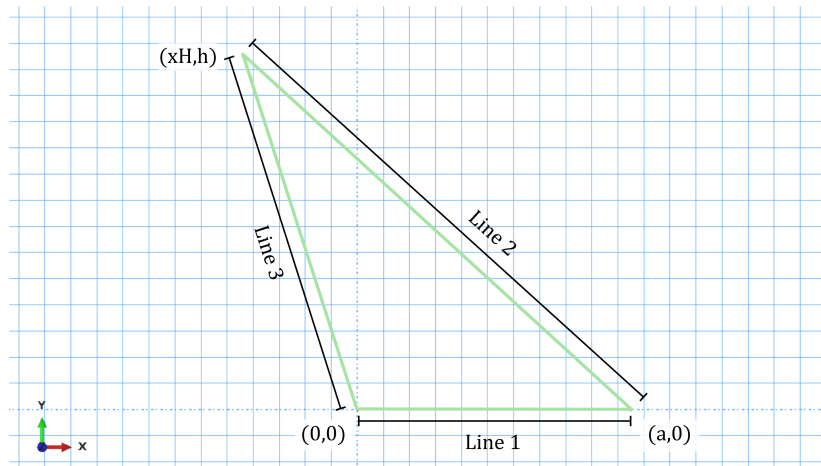


Figure 25: First sketch appearance in Abaqus interface

- 3. Part definition.** Once the sketch is done, the part is defined by its shape (in **Part** module). In this case the solid is generated as a shell, following the example used by Grey [3]. In this part, in order to add the second material, a partition was made with the command named `PartitionFaceBySketch`. Thus, an offset was made in the previously sketch, with a known  $e$  value.

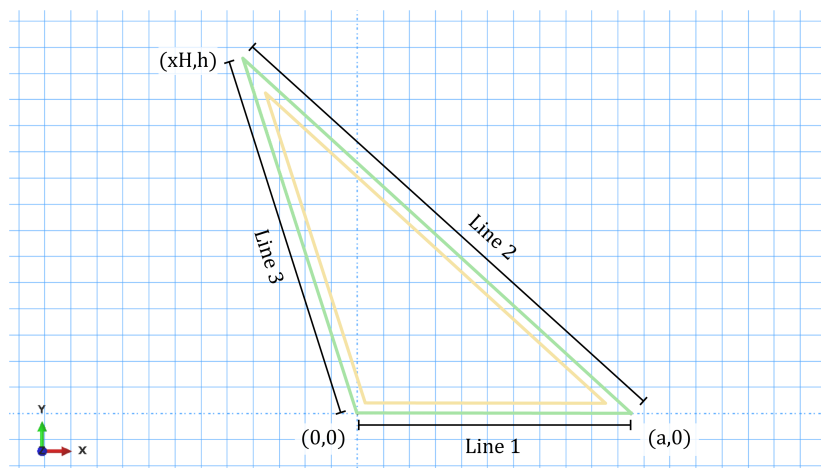


Figure 26: Final sketch appearance in Abaqus interface

In the Figure 26 can be seen the initial sketch (green line) and the offset sketch (yellow line), defining the final geometry used. This partition will be used in the **Property** module, to assign each material to each part (see section 4.2.1).

- 4. Assembly.** The **Assembly** module has been used to suit the part created in the desired position. Thus, this single part was used to create **four different instances** that will form the final pattern, thanks to the command `Rotate`.

Following the steps shown in the Figure 27, the first assembly (number one in the figure) was rotated in the x axis to reach the desired  $\delta$  angle and a circular pattern was applied to it, using the command `RadialInstancePattern`. Then a plane was created (yellow first zone) through the position of the instances around the circle defined. Thanks to this plane, the second instance can be positioned by the command `ParallelFace` and another circular pattern is applied.

Once the first ring is ready, the original part is rotated and translated in order to reach the desired position of the fourth instance. Repeating the process made with the first instance, another plane is created in order to suit the third and final instance.

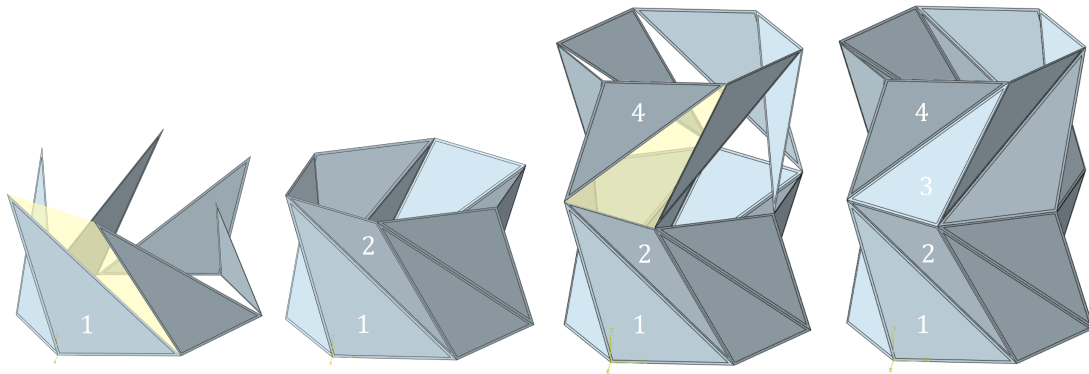


Figure 27: Assembly process in Abaqus interface.

Thus, an ori cell is revolved obtaining the final cell-ring. Applying then a linear pattern, a large structure could be obtained with N number of cell-rings, Fig. 28. There, it can be seen the enumeration used in function of N.

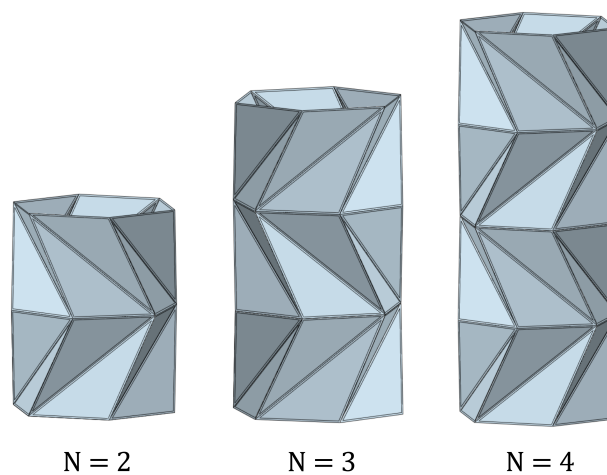


Figure 28: Assembly process in Abaqus interface.

## 4.2 Simulation environment

Once the geometry is obtained and parameterized, simulation environment shall be defined according to the natural behaviour of the origami simulated. This section is the most critical one of the project due to the required simulation accuracy. Which shall be finally validated.

### 4.2.1 Material assignment

As it was described in the section 3.3, the materials implemented in the module **Property** are the PLA and TPU. They are located in the main surface of the triangles and in the creases, respectively. Two sections are assignment to each region defined in sketch (made in section 4.1). In the Figure 29, it is illustrated both materials. There, the rigid material (PLA) is represented with green and the flexible (TPU) with dark blue.

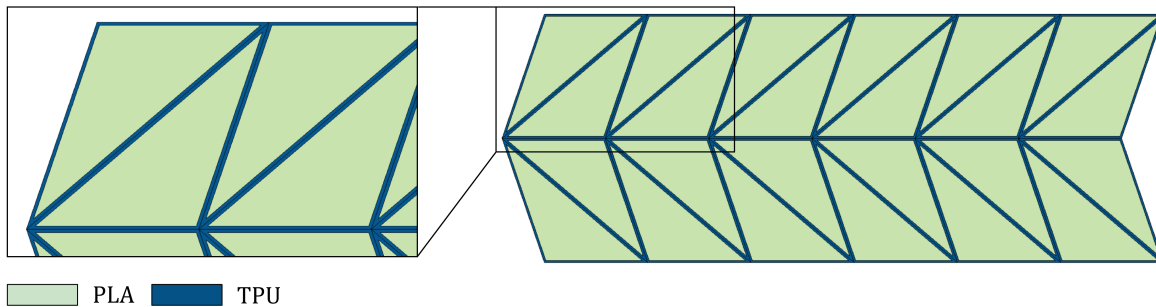


Figure 29: Flat pattern view and material assignment.

Thus, the dual material implementation in the patter turns into the representation in the Figure 30, when the pattern is folded.

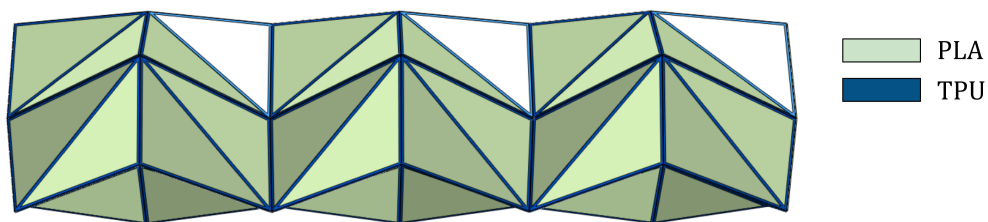


Figure 30: Material assignment in 3D model.

### 4.2.2 Boundary conditions

Under the expected behaviour when the structure gets folded and deployed, the origami shall be well constrained. Constraints applied can be divided into three types: **constraints** and **loads**. Corresponding the denomination used with the one implemented in Abaqus.

The **constraints**, from **Interaction** module, are used in order to fix the movement between the used parts and to tie the parts previously assembled. Therefore, three types of interactions have been used, as it is described as follows.

- **Contact.** By the command named `ContactProperty`, the general contact is modelled. It defines the mechanical surface interaction models that govern the behaviour of surfaces when they are in contact [11]. This interaction is assigned in the whole model because of the nature of origami and the contact produced when it gets folded.

The properties defined has been: friction-less **tangential behaviour** (named by `TangentialBehaviour`) and separation allowed for hard **normal behaviour** (named by `NormalBehaviour`). Property expanded from the Initial step to the end of the simulation.

- **Tie.** Tie constraint (named `Tie`) is used in order to fix the edges between the triangular parts of the pattern. Therefore, they are used in all pair of triangles in contact with a surface-based constraint. It is defined by a main and a secondary surface where the nodes will be restricted. Following the Abaqus Manual [11], it constrains each of the nodes on the slave surface to have the same motion and the same value of temperature, pore pressure, acoustic pressure, or electrical potential as the point on the master surface to which it is closest.

Thus, a master or main and slave or secondary surfaces shall be defined for each pair. The Figure 31 shows a selected tie constraint. Here the master surface is defined as the orange edge from the left triangle and the slave the one from the right triangle. Keeping main-left and secondary-right relations in the whole pattern.

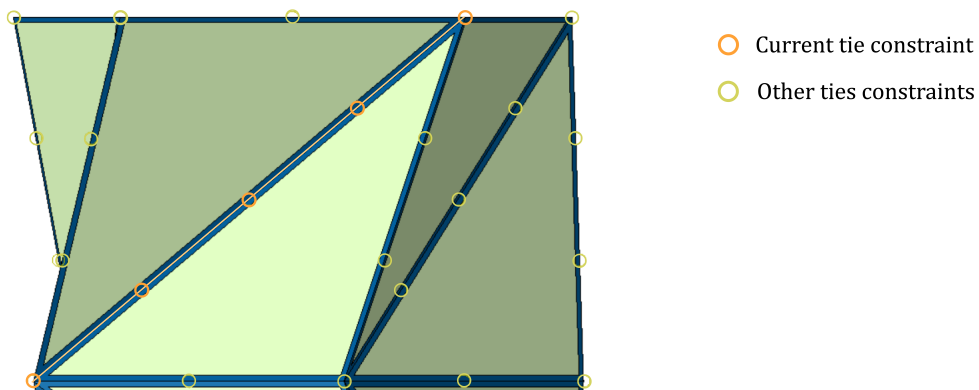


Figure 31: Tie constraint between triangles. [Own elaboration]

Furthermore, this constraint is used in the closure surface of the pattern or top surface. Where the main surface is the plate and the secondary one is the edges in contact (from the triangles), Fig. 32.

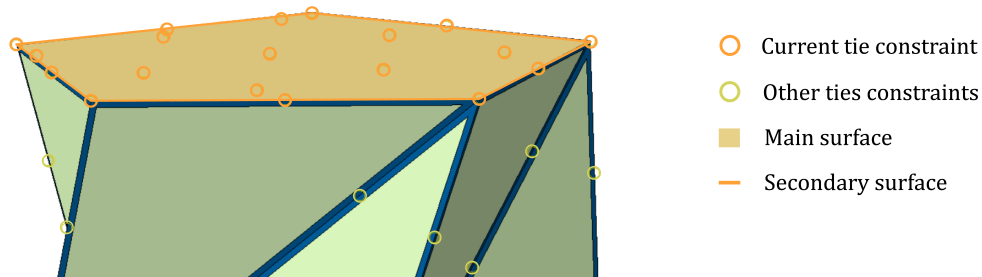


Figure 32: Tie constraint for top surface. [Own elaboration]

- **Coupling.** Surface-based coupling constraint (named `Coupling`) couples the motion of a collection of nodes on a surface to the motion of a reference node [11]. Two regions of coupling are defined in the current model.

Firstly, as the triangle part is defined by two different materials, the flexible one shall be constrained in order to reach a feasible behaviour. Both top and bottom regions of TPU are fixed to the PLA region, Fig 33. Then, the control points are referred to the PLA vertices and the surface to the closed-polygon edges of the flexible material.

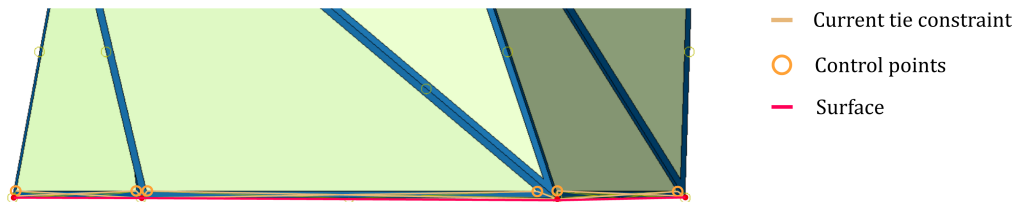


Figure 33: Coupling constraint for top and bottom flexible material. [Own elaboration]

On the other hand, in the `Load` module, three types of loads are defined. Where load cases are defined as sets of loads and boundary conditions used to define a particular loading condition [11]. They are described as follows.

- **Pinned.** Boundary condition applied in the bottom sides-surface in order to pinned it. Thus, translation is equal to zero in the three axes. An orange cone is illustrated in the Figure 34 for each constrained direction. This BC is **propagated in both processes**, folding and deployment.

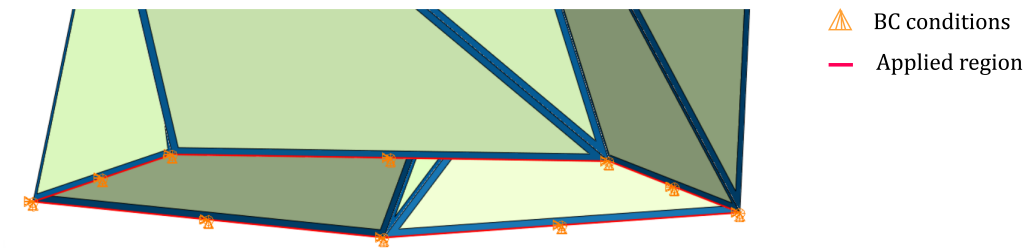


Figure 34: Pinned boundary condition. [Own elaboration]

- **Displacement.** The folding process is defined with displacement boundary condition in order to keep the final state controlled. Thus, it is referred to the top surface defined by the top plate.

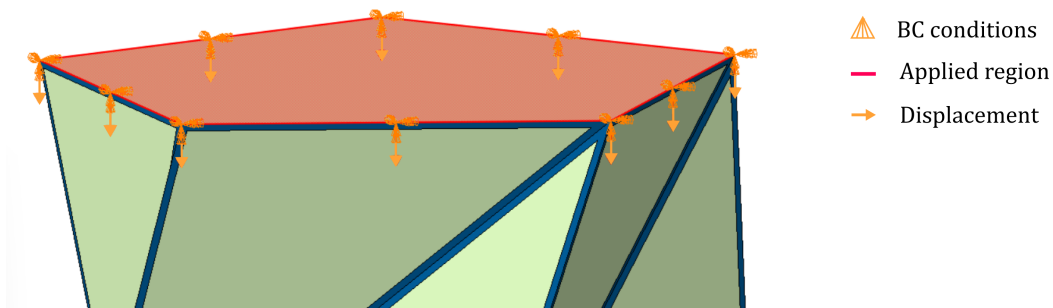


Figure 35: Displacement boundary condition. [Own elaboration]

- **Pressure.** The inflation process is made by applying pressure inside of the tube-shaped pattern when it is in its second stable state. An internal pressure is applied in each surface of the pattern, in order to simulate the inflation state mentioned. Figure 36, shows the condition introduced in Abaqus CAE.

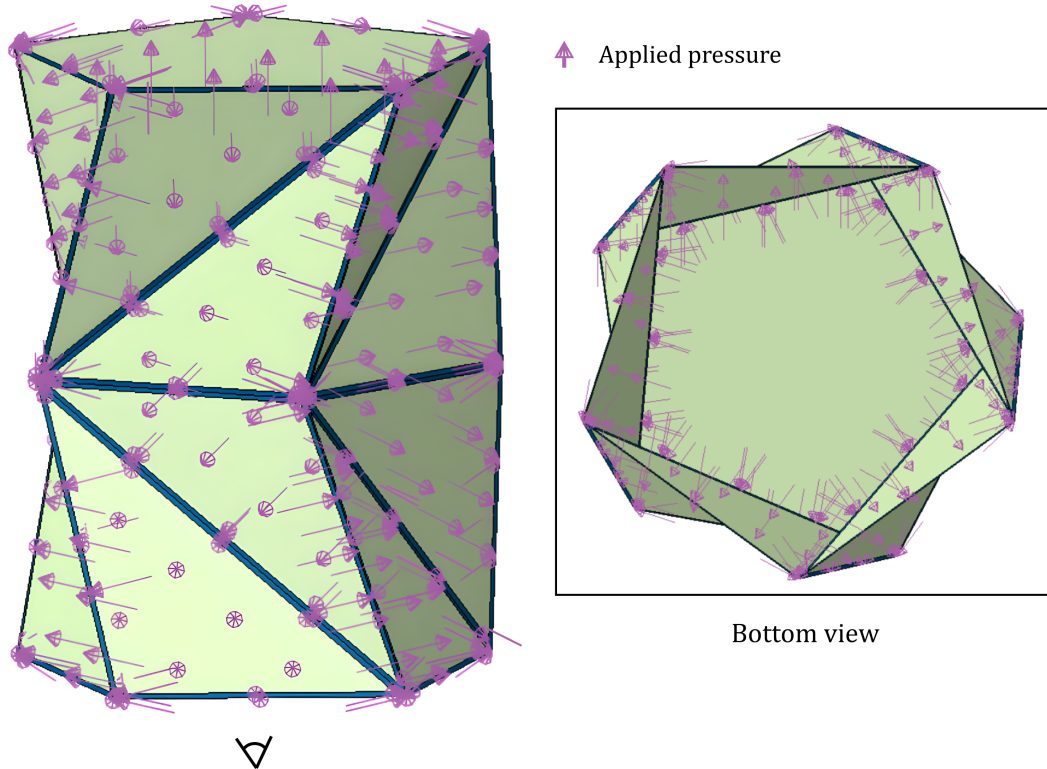


Figure 36: Pressure condition. [Own elaboration]

It can be seen the pressure imposed in all internal faces pointing out. Bottom view is illustrated in order to provide a better view for the reader comprehension.

### 4.2.3 Analysis procedures

Following the folding and deployment processes, the procedure implemented in the analysis shall accomplish the desired conditions. Both processes are based on a large displacement and deformation of at least one of the implemented materials, in order to obtain the completely folded pattern. The model defined, however, is over-constraining some of the nodes because of joining parts and the coupling applied.

As is mentioned in the Abaqus Manual [11], the procedures offered are clearly divided into: **Abaqus/Standard** and **Abaqus/Explicit**. Firstly, the dynamic model has been selected because of the effect of the inertia in the model and its real behaviour. Nevertheless, Abaqus offers an Implicit Dynamics (based on Standard analysis) and Explicit Dynamics. Which ones have been compared as follows [11]:

- In an implicit dynamic analysis the integration operator matrix must be inverted and a set of nonlinear equilibrium equations must be solved at each time increment. Whereas in an explicit dynamics, displacements and velocities are calculated in terms of quantities that are known at the beginning of an increment. Thus, the global mass and stiffness matrices need not be formed and inverted.
- In explicit analysis the cost increases linearly with problem size, whereas the cost of solving nonlinear equations (regarded in implicit analysis) rises faster than linearly with problem size.
- Complicated, very general, three-dimensional contact problems with deformable bodies in ABAQUS/Explicit.

In this case, due to the mentioned contact interactions (see Section 4.2.2 for interaction descriptions), **explicit analysis is required**.

Boundary conditions as the Displacement and pressure are defined by an amplitude during each step or in the total model time. For the present cases of folding and deployment, two amplitude types might suit in the model:

- **Tabular**. Implying a ramp function, which involves a ramp between 0 and the desired time step that grows from 0 to 1. It has been illustrated in figure 37 (left illustration).
- **Smooth step**. Representing an step with smooth growth and end. Its shape turns more similar to a tabular function (previous one), with a smoother evolution. It is as well, illustrated in Figure 37 (right illustration).



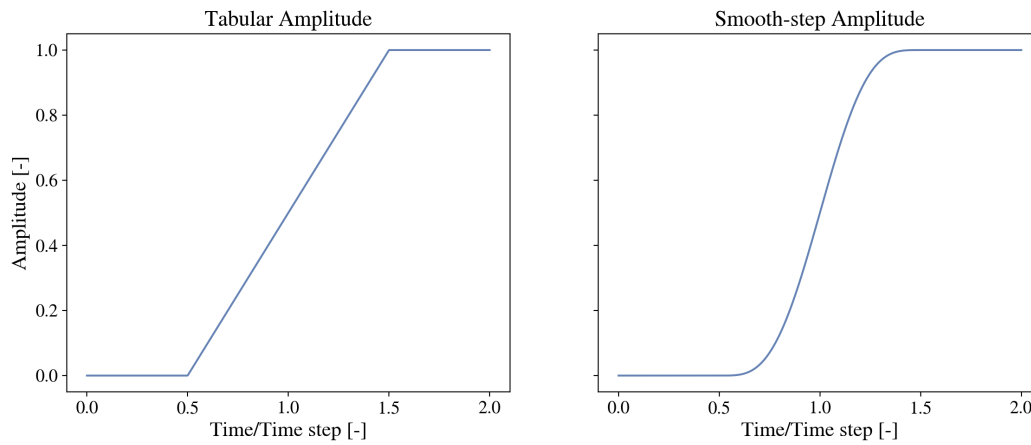


Figure 37: Tabular (left) and smooth-step (right) amplitudes representation. [Own elaboration]

As the model might achieve a quasi-static behaviour, the best result for modeling both amplitudes seemed to be the smooth step. By simulating, the results show a better response for smooth one than for the tabular one. Furthermore, with the smooth step, the simulation gets almost time-independent, becoming possible to reduce the step time (to milliseconds) and consequently the simulation time. [11]

### 4.3 Model validation

Before implementing the optimization method, the model shall be validated. Thus, the model needs to achieve minimum requirements in order to represent the real behaviour. This validation is based on the mesh independence analysis and an energy balance, which should bring a solution to accomplish the pattern behaviour.

#### 4.3.1 Independence mesh analysis

As structural model shall be validated before assuming the results obtained, the mesh shall be independent. Being this analysis firstly based on the Von Mises stress evolution.

In the first instance, the path followed was to obtain the worst case scenario between the possible configurations. Number of sides, described as  $n$ , was seen as the most influenced parameter in the folding process. This first process of the three one described in the *Folding and Deployment process* (see Section 3.2), has been selected as the most limiting one. Following figure shows the evolution of Von Mises stress during these three processes. This plot is used as a reference of the evolution not considered as feasible result.

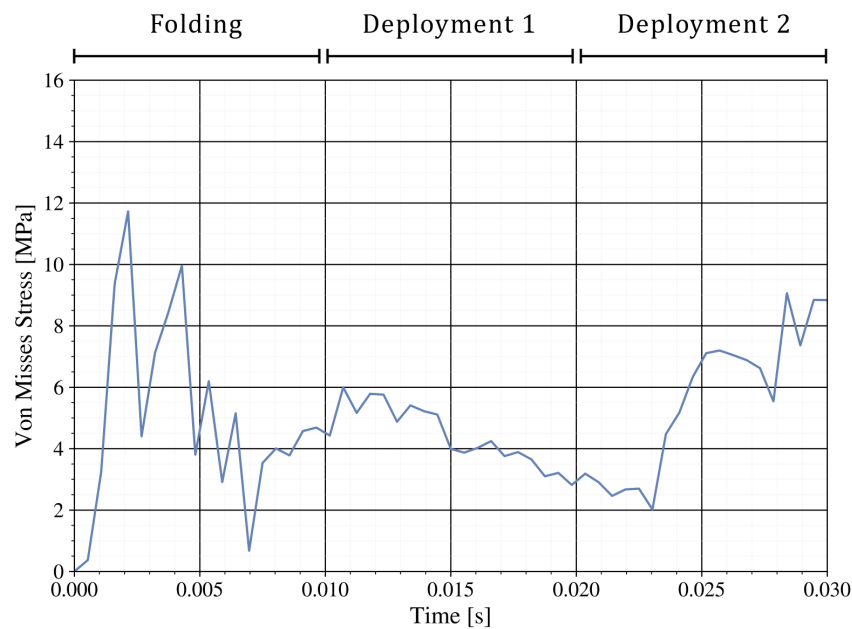


Figure 38: Von Mises stress evolution during the three stage defined: folding, deployment thanks to bi-stability and inflation deployment.

Therefore, a study of the maximum stress value (Von Mises Stress) has been made for each number of sides, Fig 39. The thirteen structural models have been implemented with an equivalent mesh, considering the same number of elements for each side. Results shown are not the model results, due to the limited

mesh size implemented, it just brings an approximated evolution of the stress.

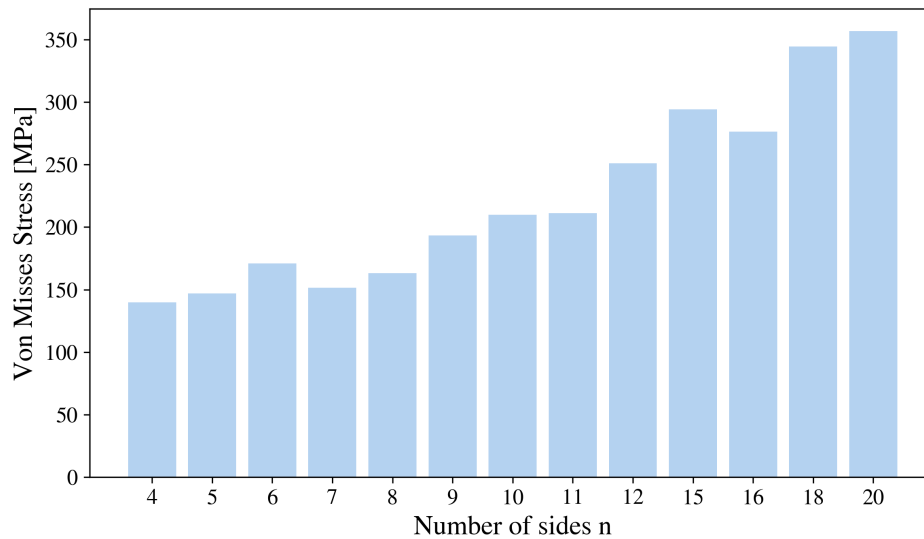


Figure 39: Approximated Von Mises Stress in front of the number of sides.

As result, most limiting case seems to be the one with the bigger number of sides,  $n = 20$ . Contour plots, otherwise, show a better distribution of stress when  $n$  grows. In the Figure 40 are represented the Von Mises stress over three configurations of the pattern (with different  $n$  values), at same frame. As it can be seen the response of the pattern is to focus the stress on the corners, showing a better behaviour with larger values of  $n$ .

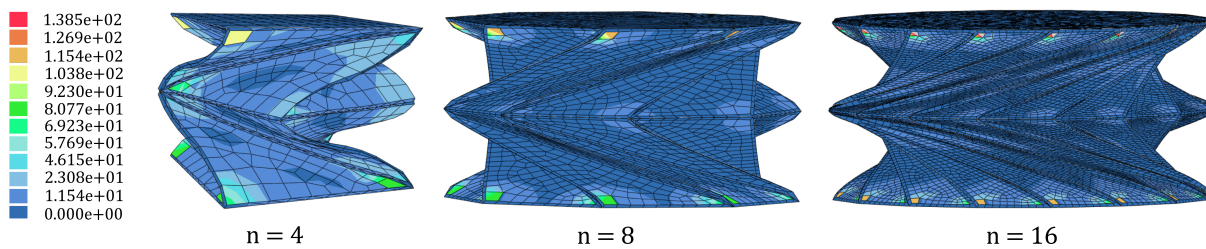


Figure 40: Contour of Von Mises Stress [MPa] on deformed shape for different values of  $n$ .

Thus, the origami pattern with  $n$  value equal to four, i.e. a pattern with a square base, was chosen as the worst case scenario. The analysis of this pattern was made with different mesh size in order to find the independent one.

This study has been made in the expected critical point of the structure, the one where eight of the triangles are in contact. Mentioned node is represented in Figure 41, and all the results presented are related to it.

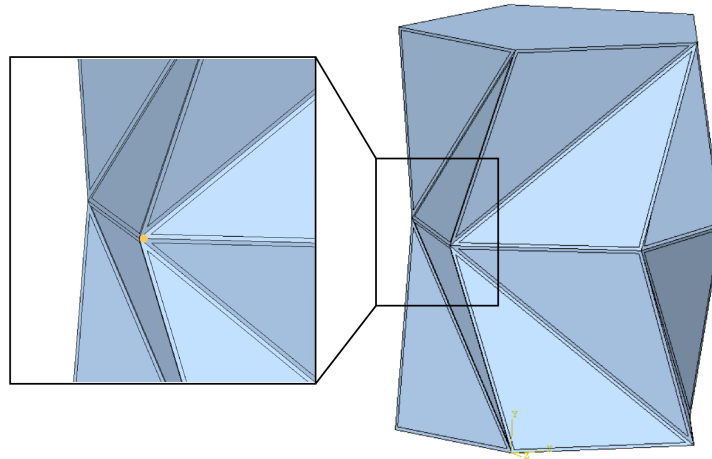


Figure 41: Visualization of the node under study.

#### 4.3.1.1 Element size

All meshes were defined by number of elements in the side of the regular polygon base (previously named *a*). As results, curves illustrated in Figure 42, were obtained.

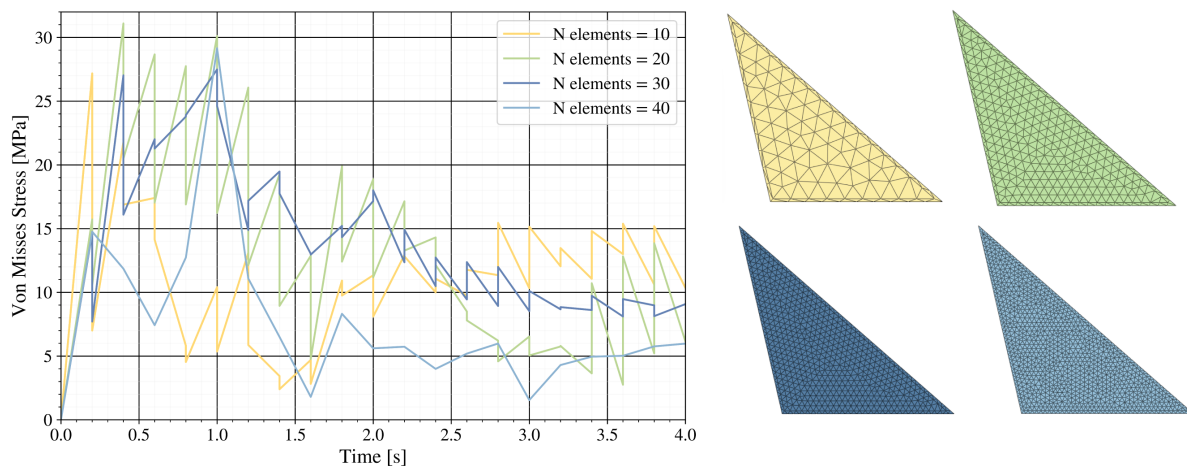


Figure 42: Von Mises evolution for different mesh sizes ( $n = 4$ ). From bigger size (5 elements per side) at upper left, to smaller size (30 elements per side) right below).

Above figure shows the evolution of the Von Mises Stress over the time simulated for each mesh size, next to each representation by colours. Here can be seen the evolution between the number of elements and the progress of the results. As result, a bigger the number of elements produces a minor number of oscillations, i.e. the error decrease.

Although a better result is shown with the mesh of 40 elements, the simulation shows a discontinuity in the flexible material creases. Therefore, as more homogeneous folding results are obtained while

increasing the number of sides, the mesh independence turn to be made with five sides (pentagonal base). Becoming then the worst (but feasible) case scenario.

Same procedure made for square polygon, was implemented for the five sides case. Thus, an evolution of the Von Mises Stress depending on the element size was obtained. In Figure 43, are represented four cases with different mesh size, where can be seen similar results to the ones obtained for the square pattern. Here, however, the simulation results seem to be much better.

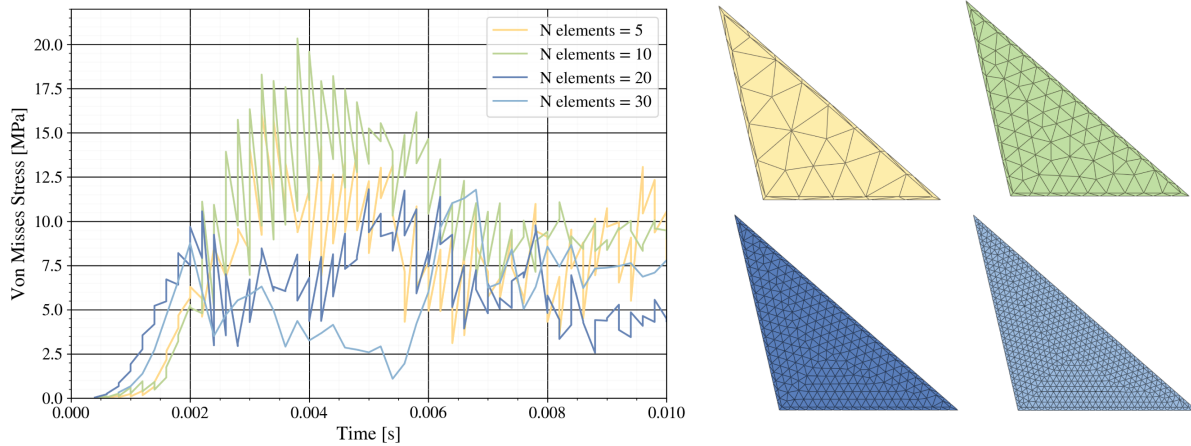


Figure 43: Von Mises evolution for different mesh sizes ( $n = 5$ ). From bigger size (10 elements per side) at upper left, to smaller size (30 elements per side) right below).

By increasing the number of elements (or reducing the element size) the results clearly improve, Fig 53. When the element size is small enough to produce at least two rows of elements in the flexible material (see blue triangle in Figure 53).

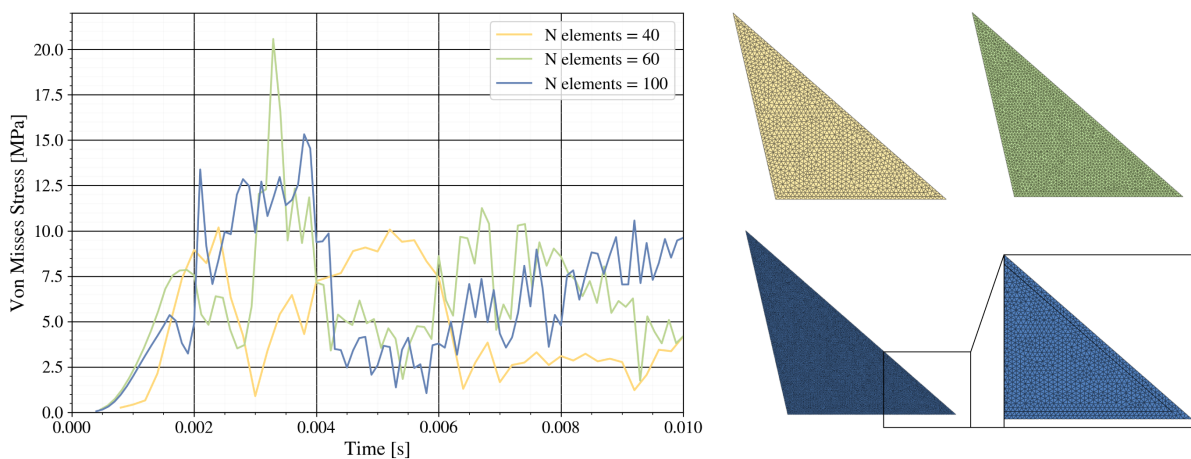


Figure 44: Von Mises evolution for different mesh sizes ( $n = 5$ ). From bigger size (40 elements per side) at upper left, to smaller size (100 elements per side) below).

Finally, by narrowing the mesh elements, an almost continuous result was gotten with 130 elements per side and 6 rows in the TPU region. As can be seen in the following figure, a previous step was made by increasing the number of rows with 100 elements, but the elements were too distorted.

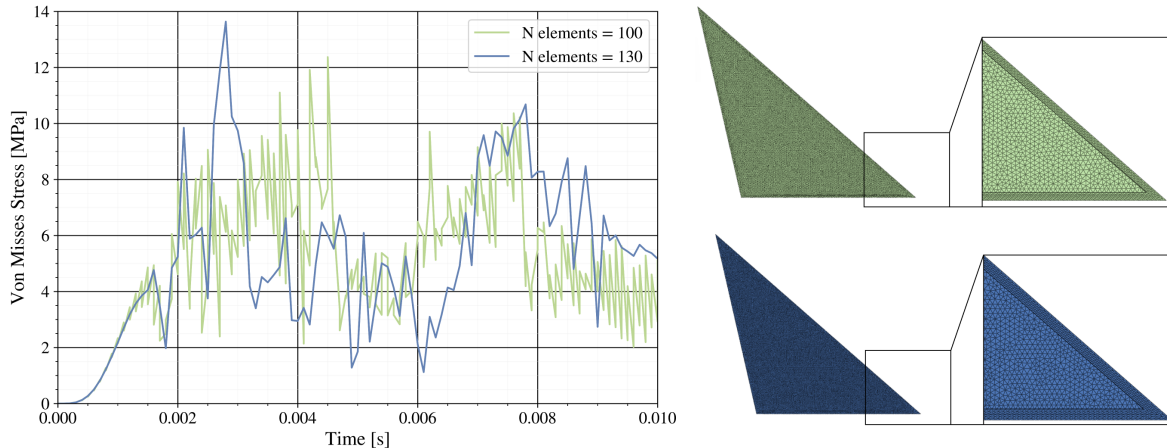


Figure 45: Von Mises evolution for different mesh sizes ( $n = 5$ ), with 6 mesh elements rows in flexible material region. From bigger size (100 elements per side) above, to smaller size (130 elements per side) below).

#### 4.3.1.2 Mesh distribution and element type

As can be seen in the mesh illustrated by now, the elements were firstly chosen as *Quads* (quadrilateral type, default Abaqus element type) and then turn into *Tri* (triangular) elements. This change was based on the numerical solver method, as it is stated, in FEM triangular elements seems to be stiffer than quadrilateral elements. This theory is founded on the smaller number of nodes used per element, involving a minus order in the polynomials solved. [30]

Nevertheless, in by simulating the *Quad* elements results better due to a minor distortion on them, making the model easier to be solver. Then, the selected element type was the *Quad-domain*, which involves *Quad* and *Tri* elements. Selection based on the triangular shape of the pattern, that offers a fittest solution using also *tri*.

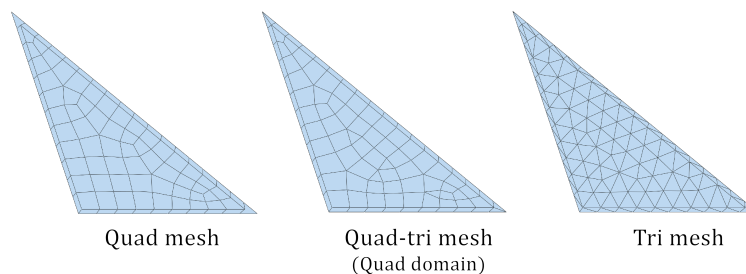


Figure 46: Illustration for three mesh types: *quad*, *quad-tri* and *tri*.

Once the mesh type was defined, the simulations shows that the mesh called for a distribution on the rigid region (internal one) and a smaller number of elements for reducing the simulating time. Therefore, another triangle was created inside the sketch previously created.

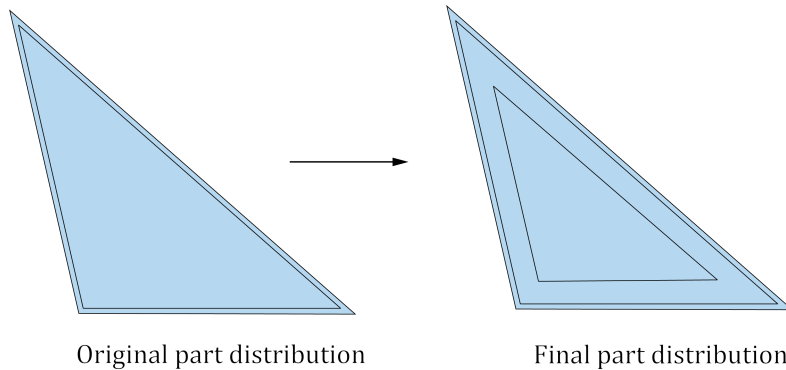


Figure 47: Final sketch implemented for the mesh distribution.

Thus, the mesh can be based on larger elements in the inner triangle and making elements smaller towards the corners. Meshing seed was based on 'Seed by edges' method, selecting each triangle and the distribution in them.

Finally, two feasible distributions were achieved by changing the distribution and the size of the elements per edge. Figure 48, shows the behaviour of both cases compared with the best case achieved.

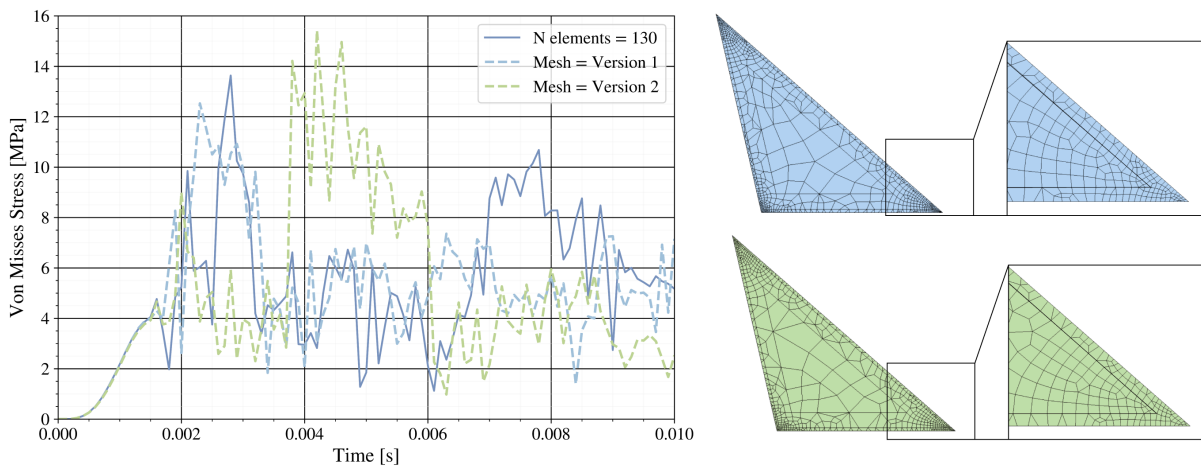


Figure 48: Von Mises evolution for distributed meshes ( $n = 5$ ). Mesh with 130 elements per side (—), distributed mesh Version 1 in blue (- -) and Version 2 in green (- -).

These three cases can be compared in number of elements per triangle, maximum mesh size and simulating time and Von Mises stress distribution. Last one illustrated in figure 48 and other showed in the following table.

Table 3: Resulting mesh comparison.

	130 elements	Version 1	Version 2
Number of elements per triangle	22 657	880	745
Maximum mesh size	a/130	a/20	a/20
Simulating time	11h	1h 20min	40 min

As can be seen in Table 3, with similar stress evolution, the finer mesh (130 elements one) and the first version differs in almost 10 hours of simulating time. Although the time is still much bigger than the expected, it means a huge improvement in the mesh analysis. Due to the optimization aim, the time should be reduced as much as possible and that is why the version 2 was chosen as the best one.

By reducing the simulation time in 10 hours and 20 minutes, the stress evolution follows the same path in the initial times and the maximum value still in the same magnitude order. Therefore, the mesh seems to be independent of the mesh. In order to ensure this fact, the energy balance shall first be checked.

Computer used for obtaining the results listed has the following processor features: Intel Core i7-9700 CPU with 8 cores at 3.00 GHz and 32.0 GB RAM.

### 4.3.2 Energy balance

Energy involved in the process shows the internal evolution of the structure. Balance during the simulation brings information about the accuracy of the model, as well as accuracy between both models to be compared. Firstly, the proposed distributed mesh (previously named as *Version 1*), is compared with the finer one in four different energy contributions.

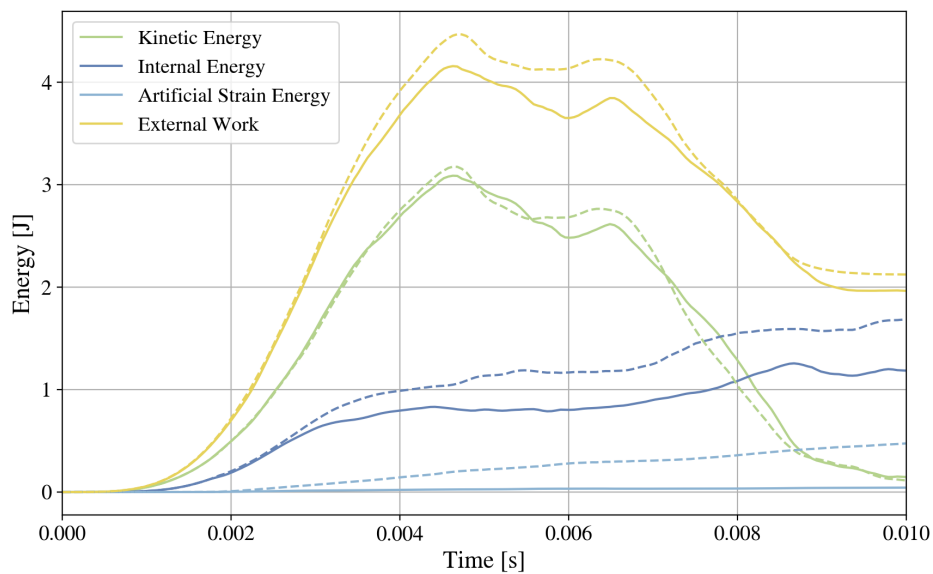


Figure 49: Energy evolution for 130 elements mesh (—) and Version 2 mesh (- -).



As the folding process is based on displacement imposition, the energy evolution shows the mayor contribution comes from this external work applied (yellow lines in Figure 49). Similar evolution is shown in the kinetic energy (green line) due to the whole displacement of the pattern. Meanwhile, internal and artificial strain energy grows with the time because the pattern folding.

Figure 49, illustrates energy from the 130 elements mesh and the Version 2. Here it can be seen that evolution and values are near for external work and kinetic energy. Appearing bigger differences for the internal energy and the artificial stain one, but they are assumed to be similar due to its initial behaviour.

Total energy, therefore, shall behave as similar as the previous energies' evolution. Resulting one is represented in Figure 50.

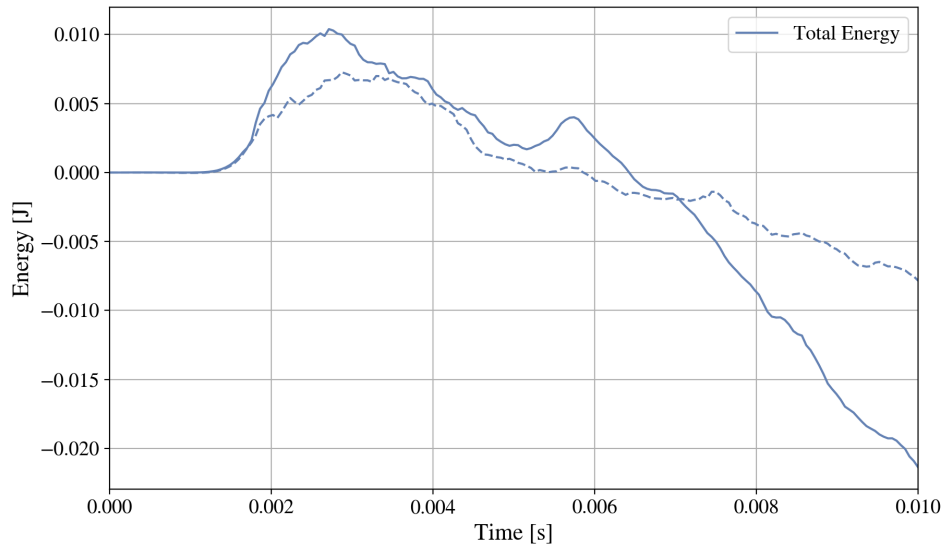


Figure 50: Total energy evolution for *130 elements* mesh (—) and *Version 2* mesh (- -).

Figure above shows the expected results, the model is much similar at folding beginning, and it starts differing from 70% of the process. Although final value might differ, overall variation is enough to assume this model as a valid one for the optimization process.

### 4.3.3 Packaging ratio

From the validated model, packaging ratio shall be defined in order to apply a feasible displacement in folding process for the optimization cases. Packaging ratio can be defined as the relation between the initial volume (deployed) and the volume height. [7]

$$\eta = \frac{V_F}{V_D} \quad (11)$$

where

$V_D \equiv$  Deployed outer volume

$V_F \equiv$  Folded outer volume

Thus, considering constant radius and cylindrical shape, this packaging ratio can be converted to:

$$\eta = \frac{h_F}{h_D} \quad (12)$$

where

$h_D \equiv$  Deployed height, equal to  $h_{3_2}$

$h_F \equiv$  Folded height

As can be notice, at this moment, the  $h_F$  is known, being needed to find the final folded height ( $h_F$ ). This value is referred to the minimum feasible height folding the pattern, i.e. height where the pattern is not deformed.

Therefore, forcing the displacement to be the total height of the structure, total energy was obtained in order to find this last minimum value. Left graph in Figure 51 shows the evolution of the total energy and final peak can be appreciated there. Then, right graph shows the evolution with minor limits in y-axis.

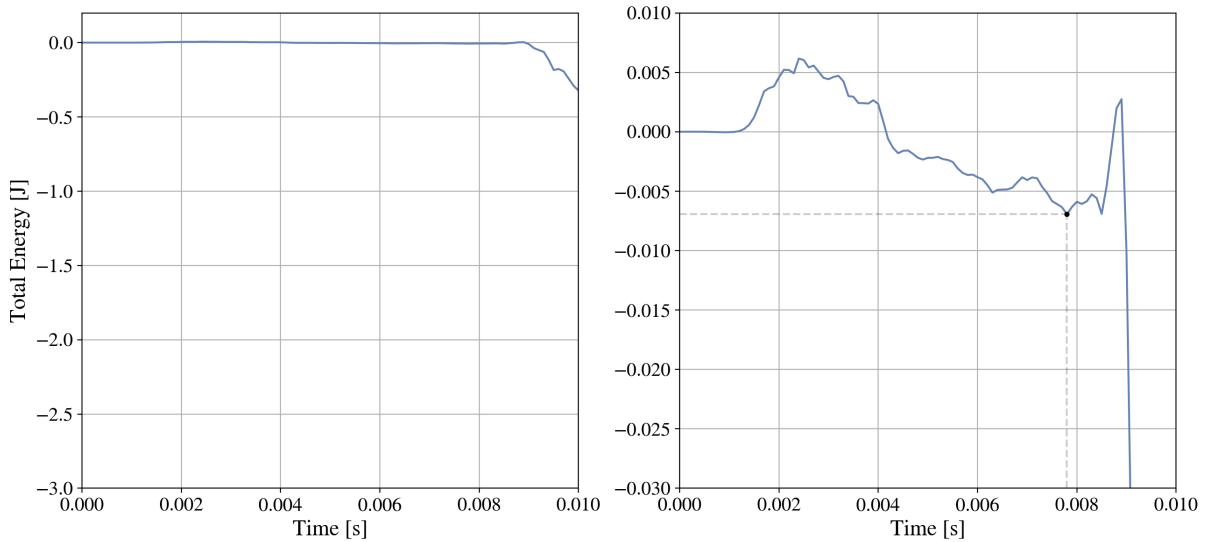


Figure 51: Total energy evolution for  $n = 5$ .

Right graph clearly shows the minimum energy value which enters in the feasible solution. After this point the energy starts to vary due to internal deformation of the material. Deformation that can be seen in Figure 52.

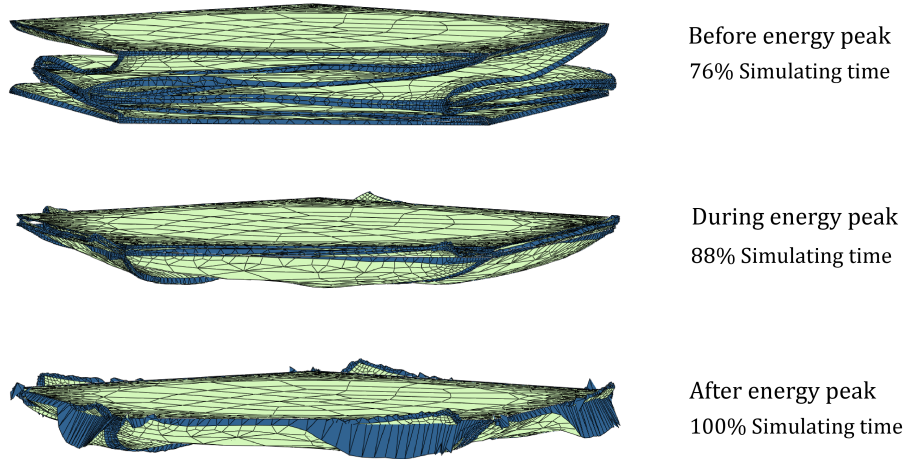


Figure 52: Deformation evolution for completed folding.

Before varying energy, the pattern was folding as the expected behaviour. However, going through the peak, deformation keeps growing until deforming most of the elements.

Minimum point seems to be in 78% of the simulation, involving in the case under study, 92.49% of the total displacement. Thus,

$$\eta = \frac{h_F}{h_D} = \frac{h_D \cdot (1 - 0.9249)}{h_D} = 0.0751 \quad (13)$$

Which means that the height of the structure can be folded and deployed a maximum of 13.316 times. Nevertheless, this value is linked to the initial model, which was based on a pentagonal structure. Therefore, it is required to find the result for oris with more number of sides.

Using different number of sides, the following graphs with total energy evolution were obtained. It can be seen the evolution for five (the previous one), six, twelve and twenty number of sided. In this last case, the simulation could not even end due to exceed of distortion in elements.

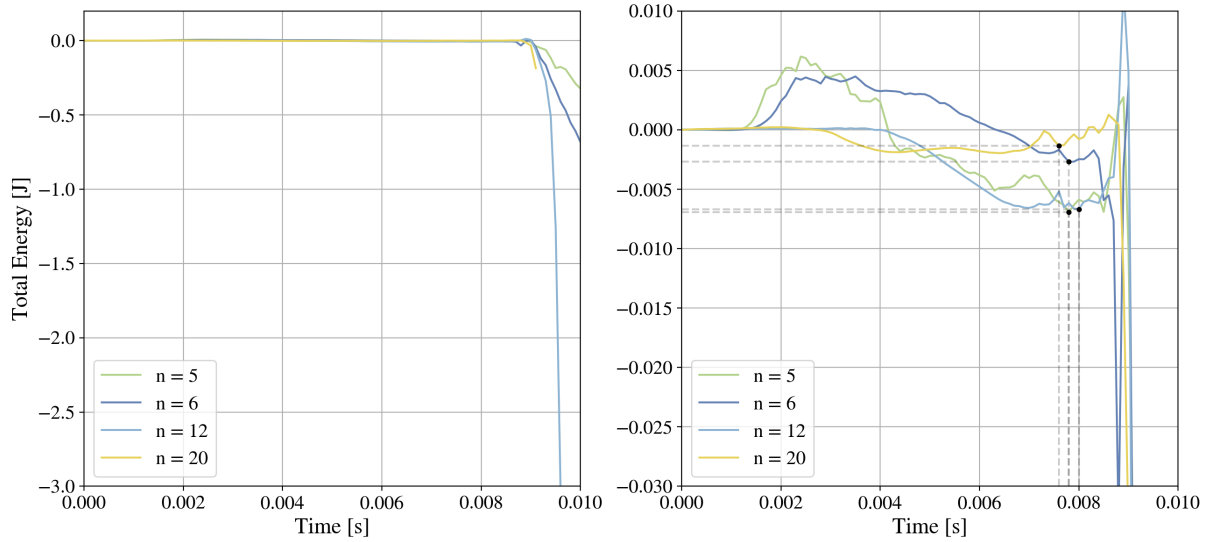


Figure 53: Total energy evolution comparison for  $n = 5$ ,  $n = 6$ ,  $n = 12$  and  $n = 20$ .

Lower value of each one is around the value obtained for the five sides (78%) for time simulation. Using the same method as the one in equation 14, the packaging ratio can be obtained for each value of  $n$ . Resulting values are summarized in the following table.

Table 4: Packaging ratio values for each number of sides.

Number of sides	5	6	12	20
Time [%]	78	78	80	76
Displacement [%]	92.49	92.58	92.52	92.36
$\eta$ [-]	0.0751	0.0742	0.0748	0.0764
$\eta^{-1}$ [-]	13.315	13.477	13.369	13.089

Which means that the package ratio is almost independent of the number of sides. Therefore, applying a safety factor around 1.2, the resulting packaging ratio is up to 0.09. Which involves that the structure **can be folded and deployed 10 times its original height**.

$$\eta = \eta_{average} \cdot 1.2 \approx 0.09 \quad \rightarrow \quad \eta^{-1} \approx 10 \quad (14)$$

However, this value is clearly linked to the thickness of the material, for the case under study, the thickness was 0.5 mm. Thus, correlating both values, **final height per ring** (considering safety factor) **is 10 times the thickness**.

$$h_F = 10 \cdot \text{thickness} \quad (15)$$

## 5 Optimization

Optimization process, as it was previously stated, is based in two phases: sampling definition and optimization model implementation. Being both selected the Latin Hypercube Sampling (LHS) and Multi-objective Genetic Algorithm (MOGA).

### 5.1 Sampling methodology

Following the LHS theory, the resulting samples are defined inside of a quadrilateral area, i.e., the region is defined as linear. Nevertheless, by try and error, a correlation was obtained calculating the second bi-stable solution: not all geometries accomplished this condition.

Thus, minimum and maximum values of flat height have been calculated for  $n$  (from 4 to 20) and the fixed value of  $R$  ( $50mm$ ). Figure 54 shows both mentioned limits and the region inside them, which involves the solution region.

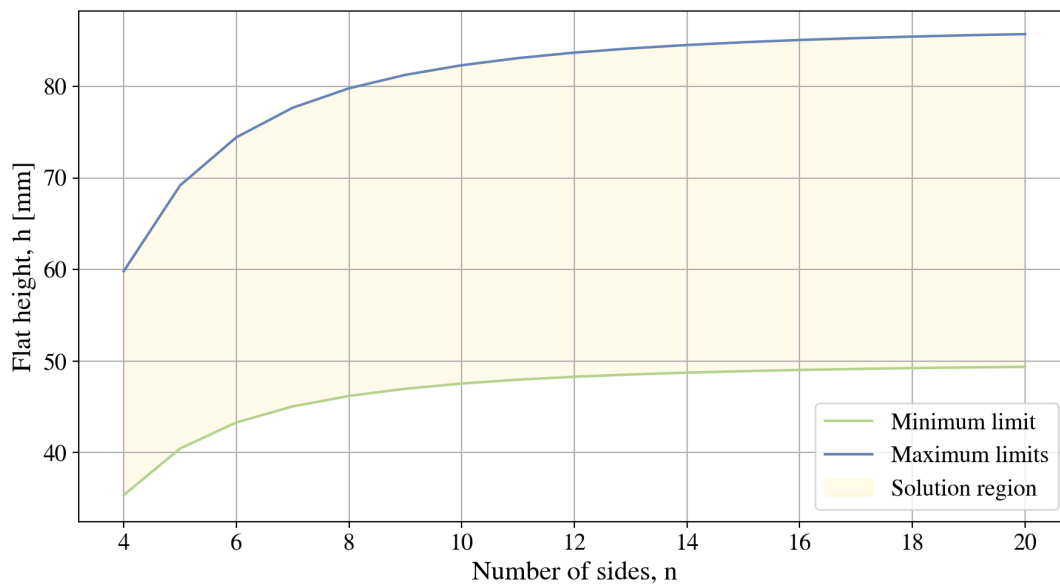


Figure 54: Maximum and minimum  $h$  values limits for feasible Kresling geometries.

As can be seen, the smaller number of sides the folding process gets harder, being smoother from almost 6 sides. However, in the manufacturing process developed in TU Delft, the larger number of sides gets harder initial folding of the pattern. Therefore, this analysis was focused on the region between 6 and 12 sides.

Applying LHS using the Python Library *SMT*, sampled data is obtained inside of a linear region between the minimum value of the minimum limits and the maximum value of the maximum limits. As result, a square with the obtained samples is represented in Figure 55.

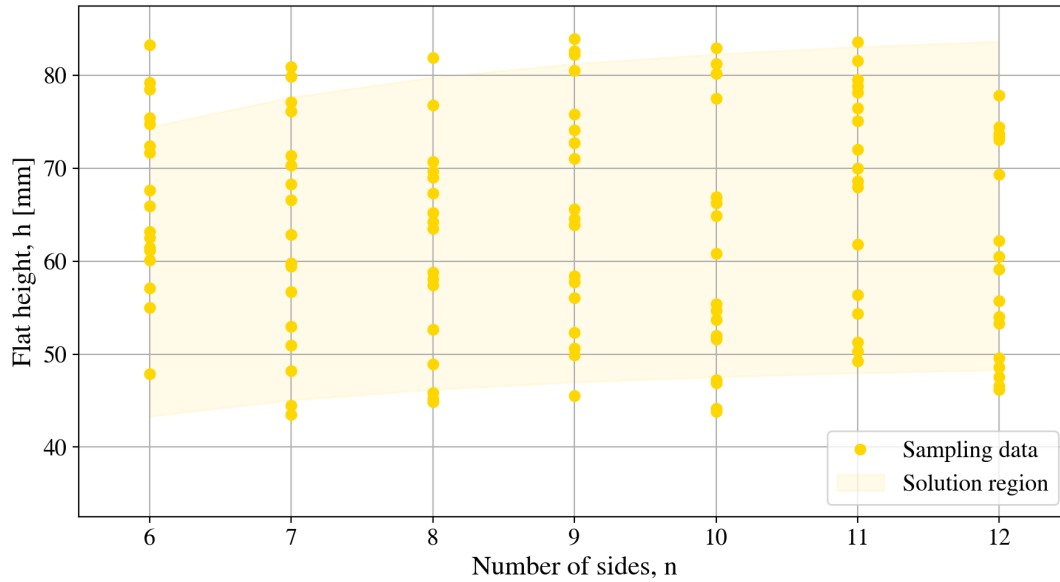


Figure 55: Sampling result with values out of bounds.

Nevertheless, it is required limiting the results to the *solution region* defined by the limits, in order to obtain feasible configurations of the pattern. Therefore, some of the samples results out of the bounds and the final sampling is represented as follows.

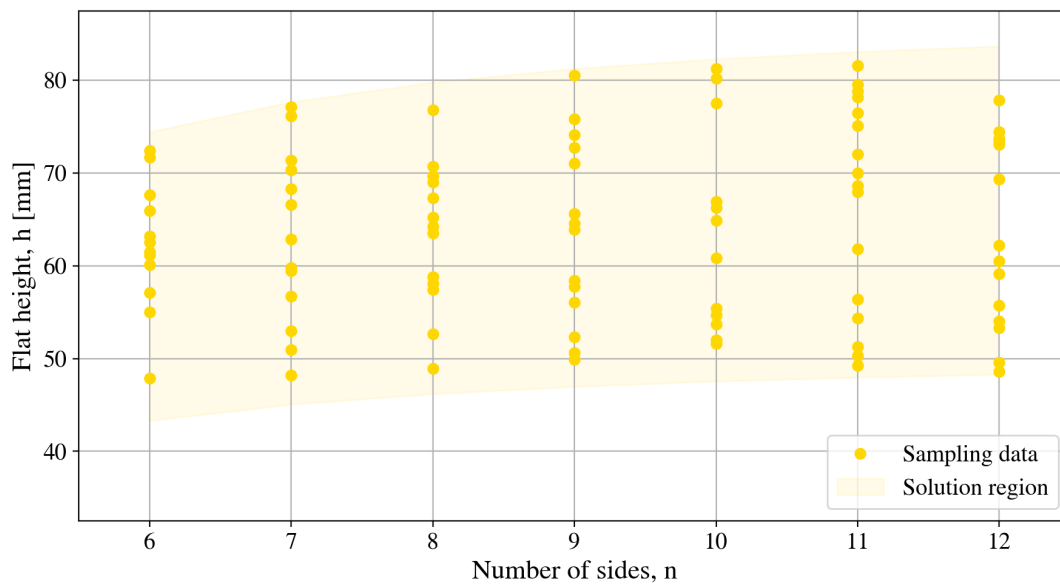


Figure 56: Corrected sampling results.

## 5.2 Design variables and model description

By the methodology described, sampled results has been obtained, see Appendix A (Table 7). As it was described on the *Simulation parameters* section (see Section 3.5), restricted inputs given for the simulation process are the *number of sides* ( $n$ ) and the *flat height* ( $h$ ). There, it can be seen the "random" distribution of the values obtained from the LHS method, which provide representative values for  $n$  and  $h$  within the *solution region* aforementioned.

Thus, the model defined for the optimization process is parameterized with the geometry values. Simulation, however, needs to specify more parameters in order to define the complete model. In this case, values used are the same as the taken in independence mesh analysis. Being them listed as follows.

- **Mesh distribution:** Version 2
  - **Minimum mesh size:** 0.2 times TPU width.
  - **Maximum mesh size:** 1/20 times  $a$  value.
- **TPU (flexible) material width:** 1 mm
- **Material thickness:** 5 mm
- **Number of rings:** 2
- **Simulating time:** 0.01 seconds
- **Number of output values:** 50 per step

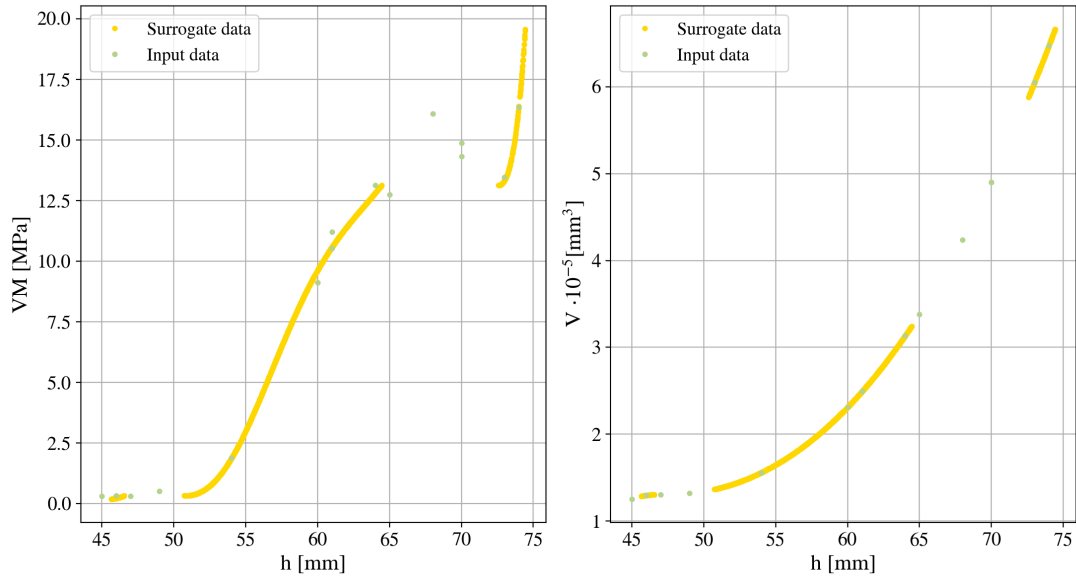
As the parameter to optimize is maximum Von Mises Stress, samples were simulated just for folding process. It shorts computing and simulating time in almost a third bringing same solution, as it was explained in *Independence mesh analysis* section (see Section 4.3.1).

## 5.3 Surrogate models

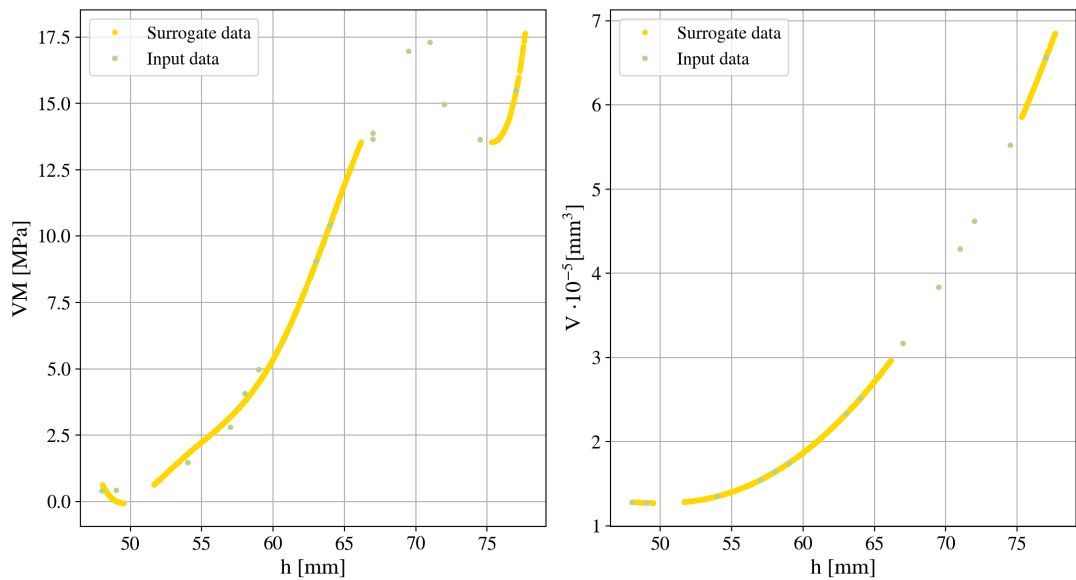
Surrogate method implemented was the based in polynomial adjustment, due to the shape of the samples taken. Firstly, surrogate model was planned to be made for all the number of sides  $n$  values sweeping the flat height  $h$ . However, non-lineal responses for  $n$  value results in an analysis for each one.

As it was not planned to generate a surrogate model for each number of sides, more simulations were run for assuring surrogate results. Obtained models were achieved with enough accuracy, as it is described for each case.

- **Six number of sides.** Surrogate evolution has been obtained by ninth degree polynomials, resulting in a coefficient of determination  $R^2$  equal to 0.9964 for stress curve and 0.9999 for volume.

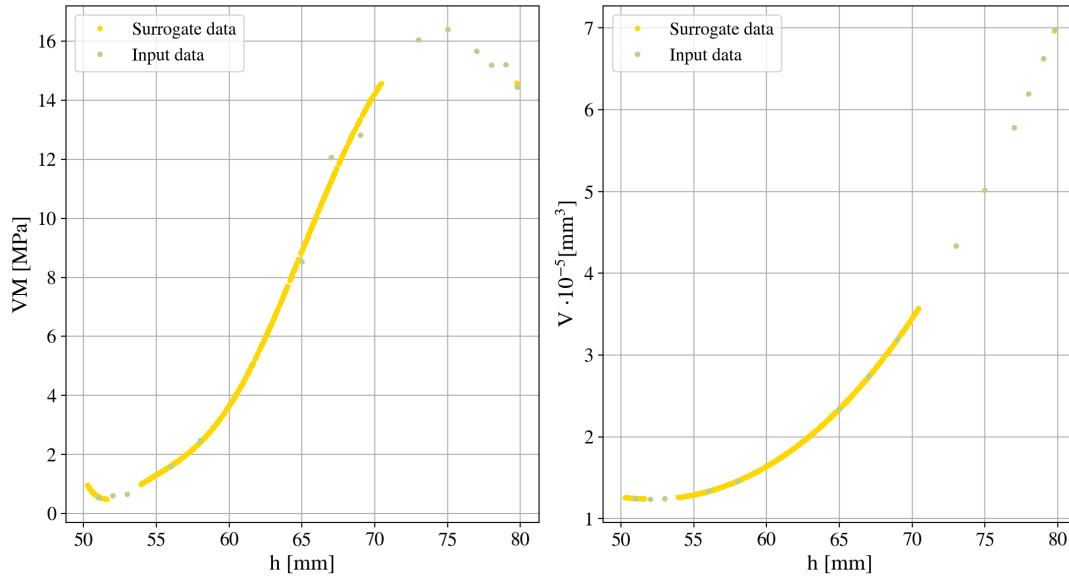
Figure 57: Surrogate model for  $n = 6$ .

- **Seven number of sides.** In this case, fitting was reached using sixth degree polynomials obtaining as  $R^2$  values as: 0.9935 for stress and 0.9999 for volume.

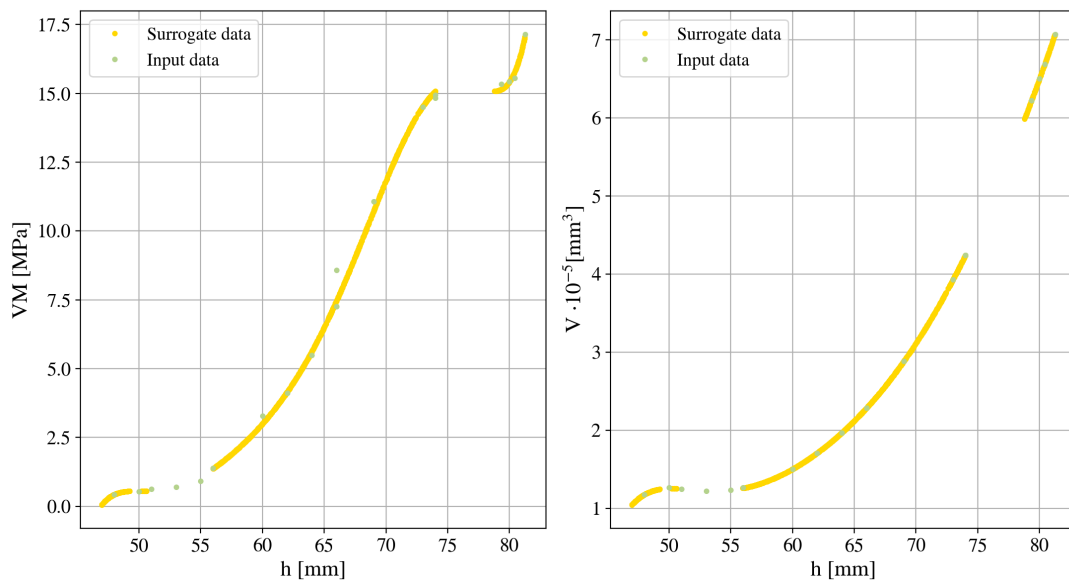
Figure 58: Surrogate model for  $n = 7$ .



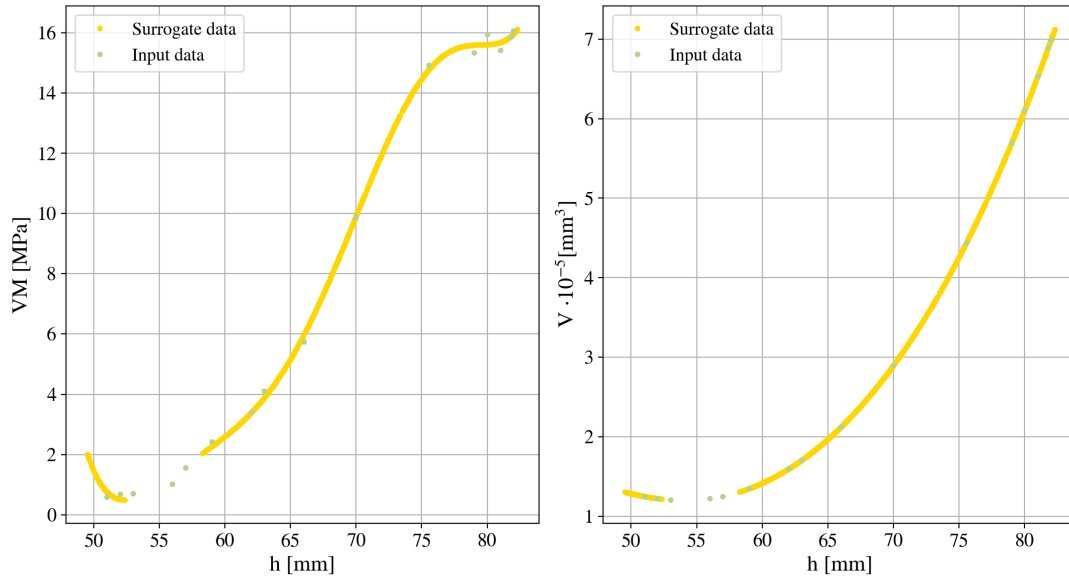
- **Eight number of sides.** For eighth case, polynomials used were of eighth degree, reaching  $R^2$  values equal to 0.9978 for Von Mises stress and 0.9999 for inner volume.

Figure 59: Surrogate model for  $n = 8$ .

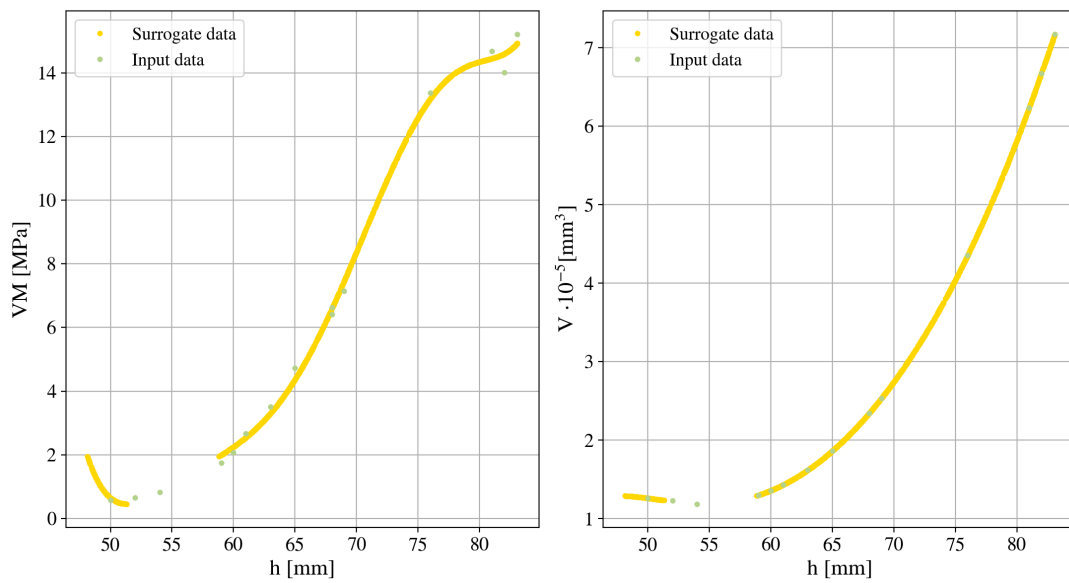
- **Nine number of sides.** Surrogate model was fitted by using seventh degree polynomials, with an  $R^2$  equal to 0.9994 and 0.9999 for stress and volume, respectively.

Figure 60: Surrogate model for  $n = 9$ .

- **Ten number of sides.** In this case, polynomial degree was six, reaching a coefficient of determination about 0.9991 for stress and 0.9999 for volume.

Figure 61: Surrogate model for  $n = 10$ .

- **Eleven number of sides.** For eleven sides, polynomial fitting was made by sixth degree ones. Von Mises stress results with an  $R^2$  equal to 0.9999 and the volume with 0.9999.

Figure 62: Surrogate model for  $n = 11$ .

- **Twelve number of sides.** Finally, twelve case was fitted with fifth degree, resulting in  $R^2$  values as: 0.9938 for stress and 0.9964 for inner volume.

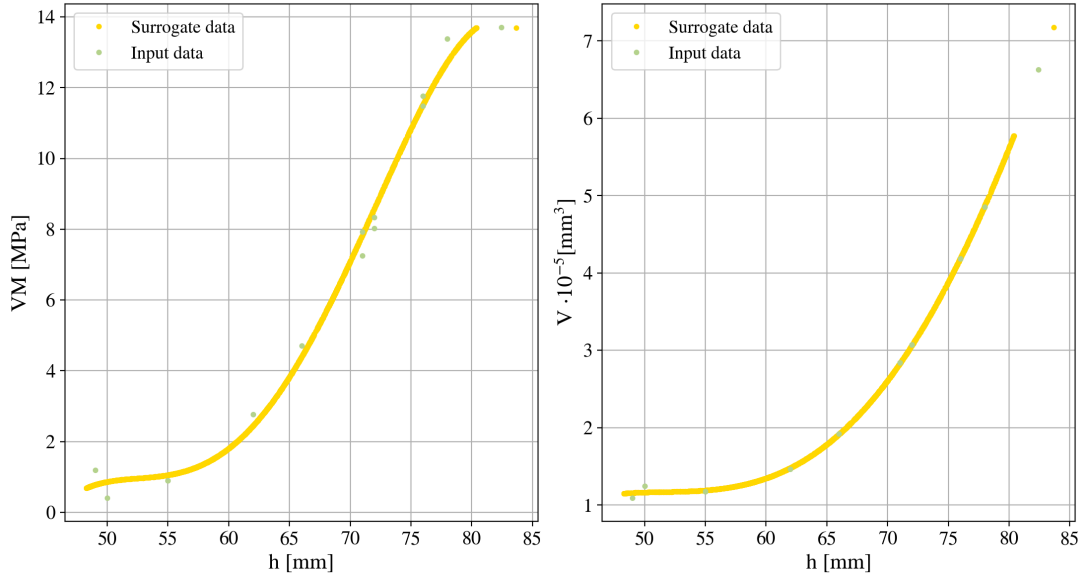


Figure 63: Surrogate model for  $n = 12$ .

As all cases has been characterized by its determination coefficient ( $R^2$ ) and the degree of the polynomial method used in surrogate model, it has been summarized in Table 5.

Table 5: Surrogate model determination coefficient comparison.

Number of sides	Polynomial degree	$R^2$ - Von Mises	$R^2$ - Inner volume
<b>6</b>	9	0.9964	0.9999
<b>7</b>	6	0.9935	0.9999
<b>8</b>	8	0.9977	0.9999
<b>9</b>	7	0.9994	0.9999
<b>10</b>	6	0.9991	0.9999
<b>11</b>	8	0.9999	0.9999
<b>12</b>	4	0.9938	0.9961

After checking the results obtained from surrogate models, Dakota obtains desired number of optimal results for each model. In this case, as seven models are considered (one per number of sides), one optimum value is request.

#### 5.4 Optimum cases analysis

From the seven cases of analysis mentioned, optimum values were obtained thanks to Dakota solver implementing MOGA, as it was mentioned in *Optimization procedure* section (see Section 3.4). By **minimizing maximum Von Mises stress** and **maximizing inner volume**, each number of sides has an involved optimum case. Thus, obtained results are grouped together in Figure 64.

Optimized results were obtained with following GA parameters: 800 as population size and 100 for number of generations.

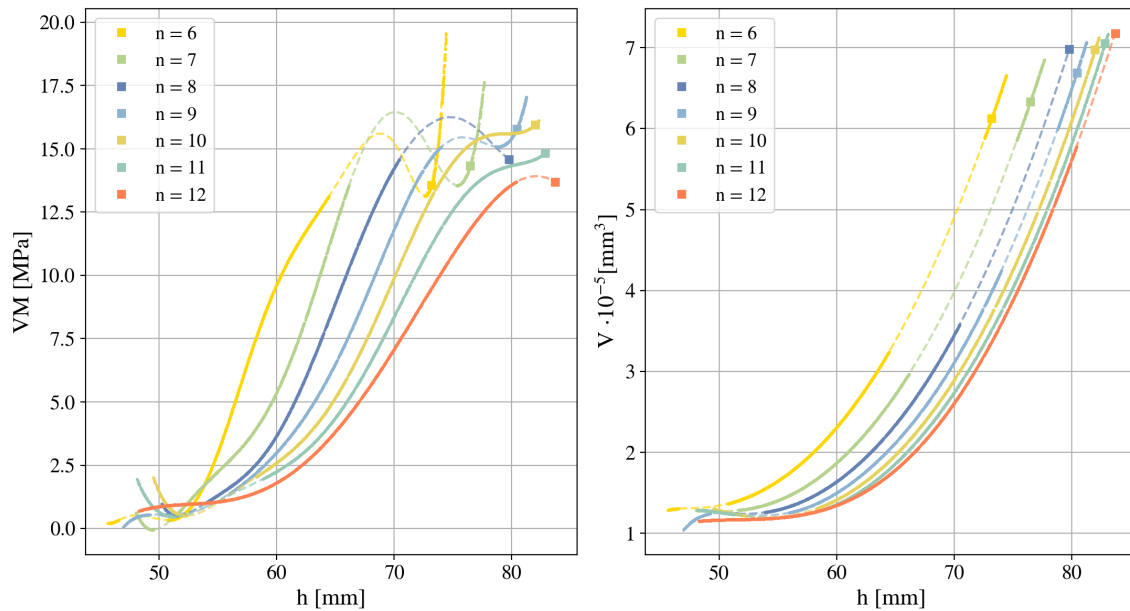


Figure 64: Optimum results evolution for the seven cases under study. Von Mises stress (left) and Inner volume (right).

Where dashed lines are not part of the surrogate model, is the polynomial approximation (according to the surrogate polynomial degree) illustrated for a better comprehension of the reader.

Therefore, in maximum stress distribution, by increasing the flat height  $h$  the results made an "S" shape behaviour, meanwhile in volume results it is half of an opened "U" response. However, by zooming in the regions near optimum solution, a valley in maximum values of Von Mises stress that shows the interest region. Obtaining, nonetheless, an almost linear evolution in the case of volume.

As the solution points there are limited by the stress, optimum behaviour is in most cases, in the point where the stress slope clearly changes. Which can be described in an optimization context, the point of interest.

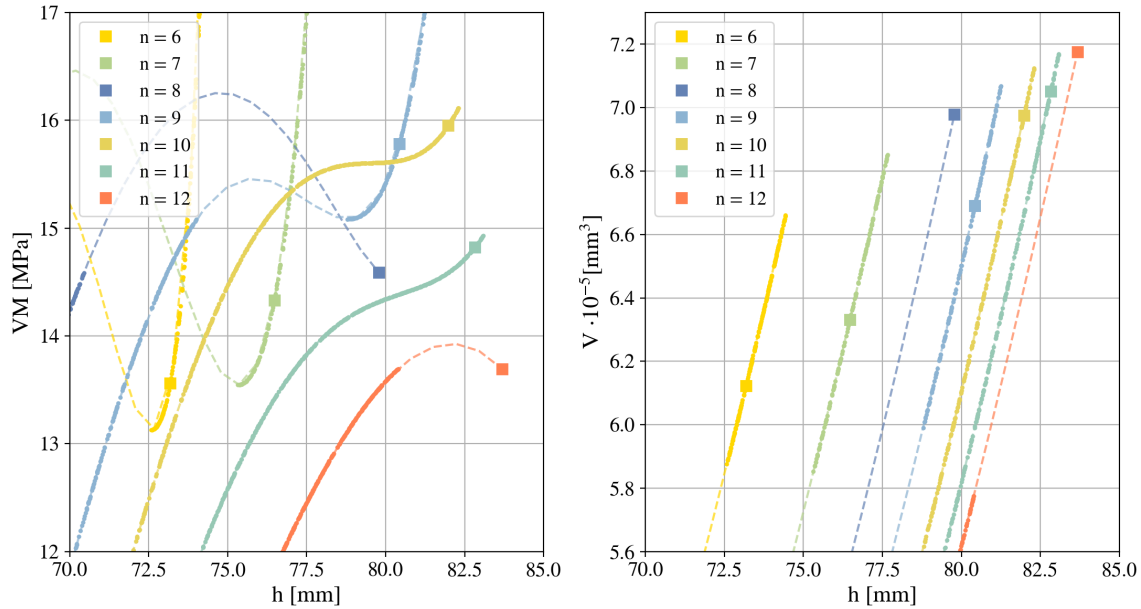


Figure 65: Zoom of optimum results evolution for the seven cases under study.

By intersecting stress and volume evolution and optimum results, following graph was obtained. Here it can be seen the correlation of optimum results and the criteria followed by Dakota in order to obtain these results.

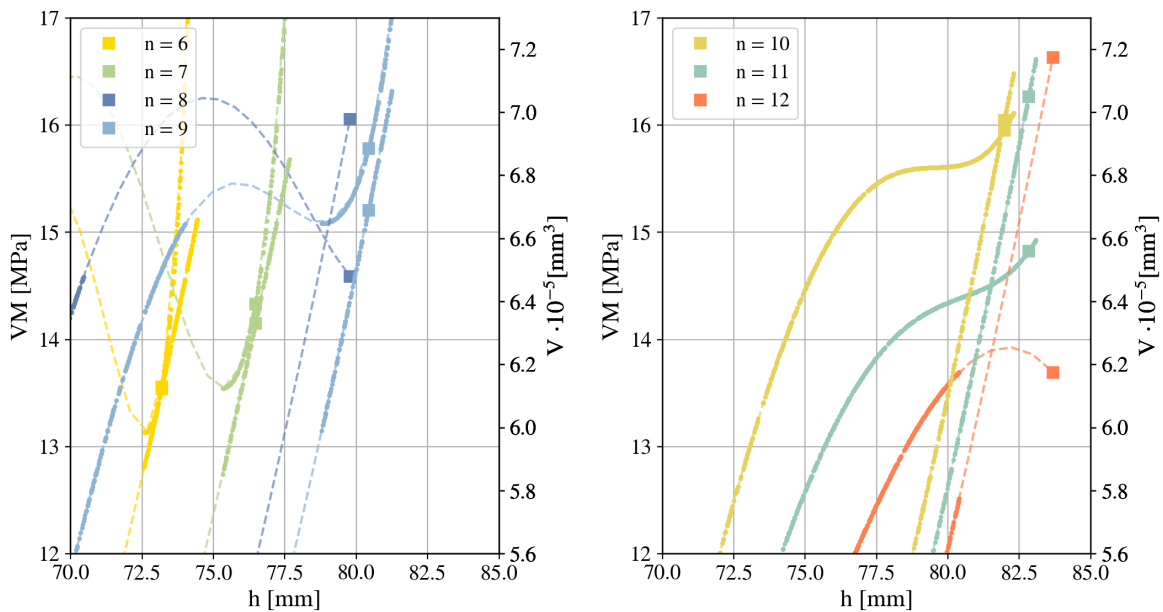


Figure 66: Optimum results represented for stress versus volume.

Overall, by representing Von Mises stress in front of Volume (Pareto Front, Figure 67), the results shows a non-dependency response due to eight sides results. Nevertheless, this value was checked with the surrogate results and, as can be seen in the figure, optimum case is much near to a real solution. Thus, this result shall be considered as well as feasible one.

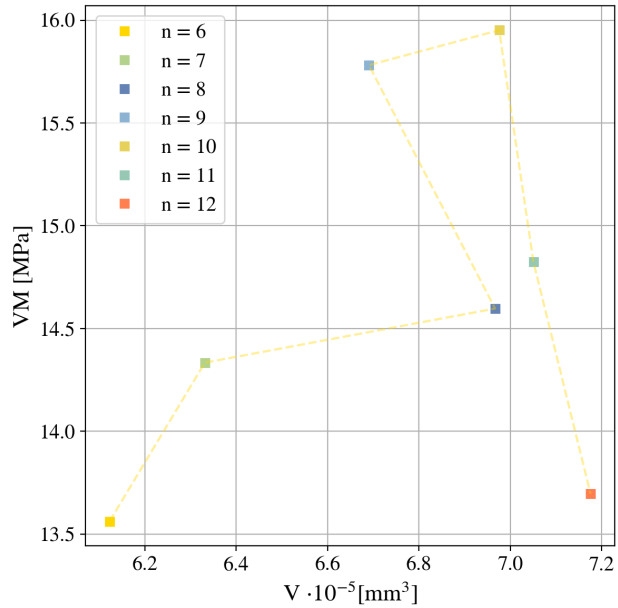


Figure 67: Pareto front. Von Mises stress in front of Inner volume for each  $n$  value.

From a Pareto Front it would be expected a curve with a tendency for results, however obtained ones shows a non-clear correlation between stress and internal volume. Because of that, results need to be validated and checked independently. Being these optimum results design variables described in following table.

Table 6: Summarized optimization results per number of sides.

Number of sides, $n$	Flat height, $h$	Von Mises stress [MPa]	Inner Volume [mm <sup>3</sup> ]
<b>6</b>	73.1808	13.5613	6.1229 e-5
<b>7</b>	76.4714	14.3336	6.33161 e-5
<b>8</b>	79.7787	14.5891	6.9786 e-5
<b>9</b>	80.4262	15.7813	6.6907 e-5
<b>10</b>	81.9779	15.9515	6.9758 e-5
<b>11</b>	82.8242	14.8237	7.0508 e-5
<b>12</b>	83.6781	13.6959	7.1757 e-5

### 5.4.1 Results for optimum cases

Results obtained for each number of sides, has being simulated in order to check its behaviour from the stress and energy evolution. This analysis of the results has been developed for folding and deployment processes.

- **Folding.** As the results were obtained with *Version 2* mesh model (see Section 4.3.1.2), stress and energy represented here are under this mesh restriction.

Firstly, Von Mises stress in the region of interest, i.e. the point where most triangles are joined (see Figure 41) shows a first peak where maximum stress for the flexible material is located.

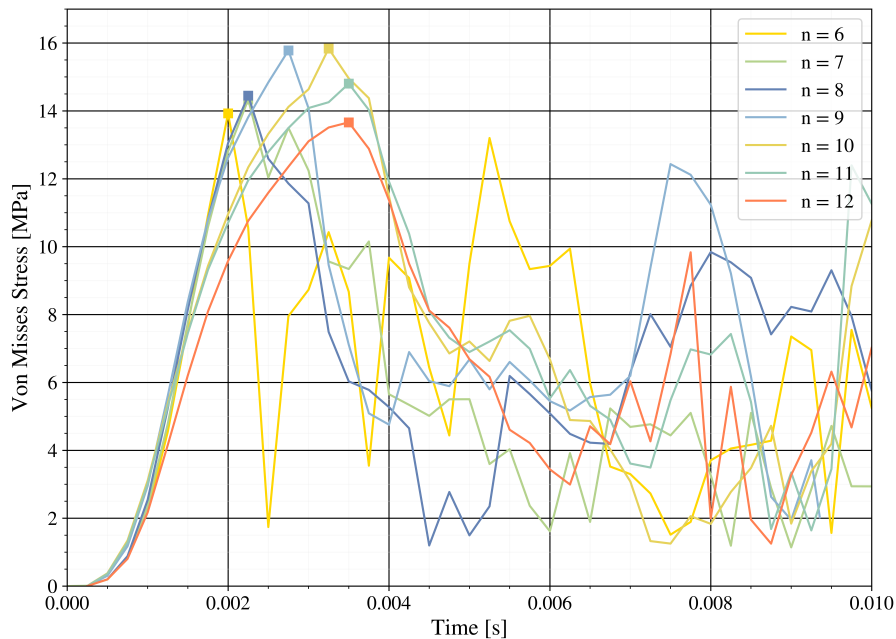


Figure 68: Von Mises stress for obtained results.

Due to the gross refinement in not interesting areas, as could be the middle of the polygon side, Von Mises stress shows bigger oscillation than can produce higher values. However, these values are not real ones due to the mesh refinement problem, being required to obtain the maximum value from the region refined.

Thus, as result, the material is not going to suffer plastic deformation being inside of its elastic limits. Being the maximum value lower than 15 MPa and tensile Module up to 26 MPa. It shall be, as well, highlighted the slope for all cases, which shows the same behaviour at the first-time steps until the peak. Comparing results from different values of  $n$ , it is seen that the width of the peak grows with the number of sides, obtaining a more stable response.

For energy results, tendency is much similar for the initial slop. By zooming in the first-time intervals, it can be seen a disruption in results, which follows three different slopes. It might be due to the mesh refinement in not all the origami pattern, generating numerical error from regions far from the point under view. This numerical error might grow as well with the number of sides, obtaining results that differ more.

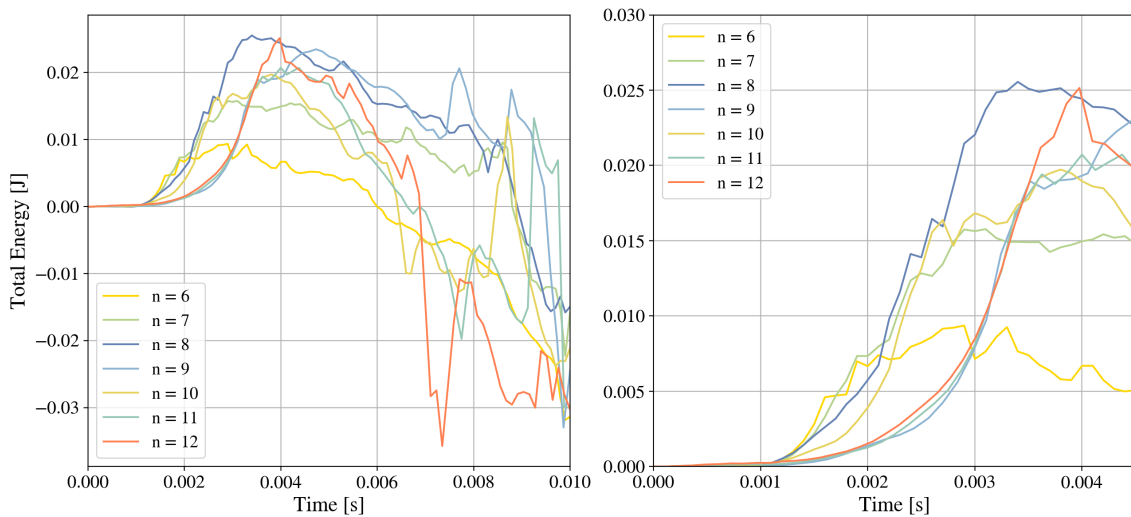


Figure 69: Total energy for obtained results.

- **Deployment.** In case of deployment, however, results have been obtained for a mesh similar to *Version 2* mesh with bigger elements. Due to computational and time limitations, simulations with higher resolution were not viable at all.

By testing inflation with different number of sides for optimum cases, it has been seen that inflation time and pressure value shall be tested and fitted. It clearly depends on the number of sides and the flat height, becoming therefore inner volume dependant.

Three stages: folding, first deployment and inflation can be seen in energy evolution (see Figure 70). This case has been modelled with same time for all procedures (10 milliseconds) and 0.01 MPa of inflation pressure. Both data were selected for achieving inflation in any case.

The seven cases under study show similar evolution at the three stages, where energy is almost flat. However, in the third stage it can be seen that, when the patten gets over inflated, energy goes crazy. This situation limits the maximum feasible inflation, giving the time to be imposed for each number of sides and flat height combination.



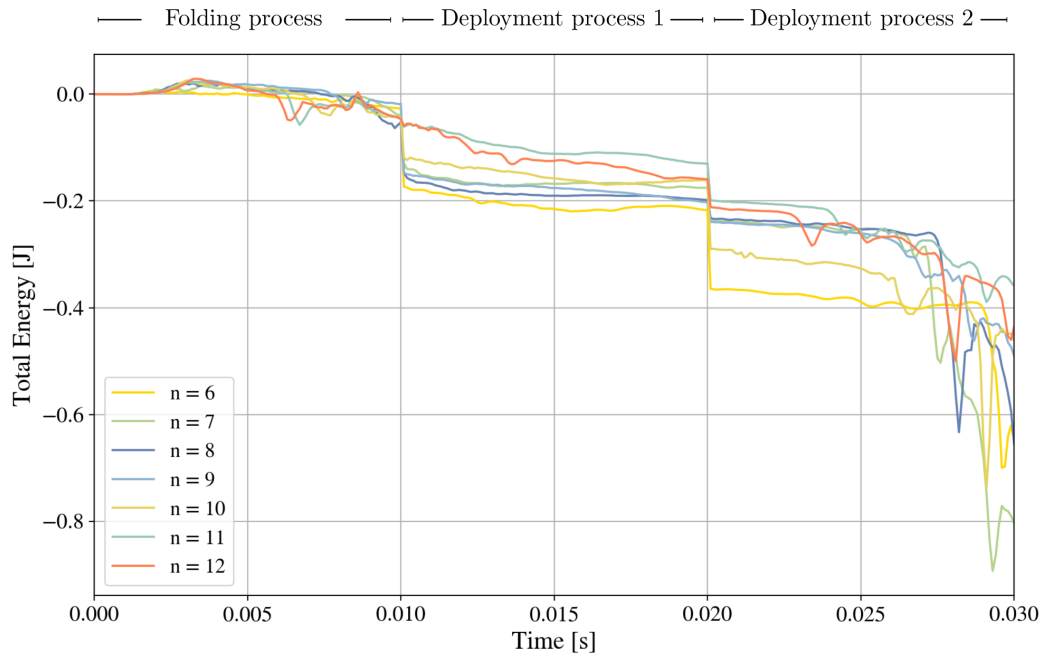


Figure 70: Total energy for obtained results at folding, free deployment and inflation.

In following figure, are represented the maximum point until the patter gets over-inflated, i.e., the maximum inflation time for the given pressure.

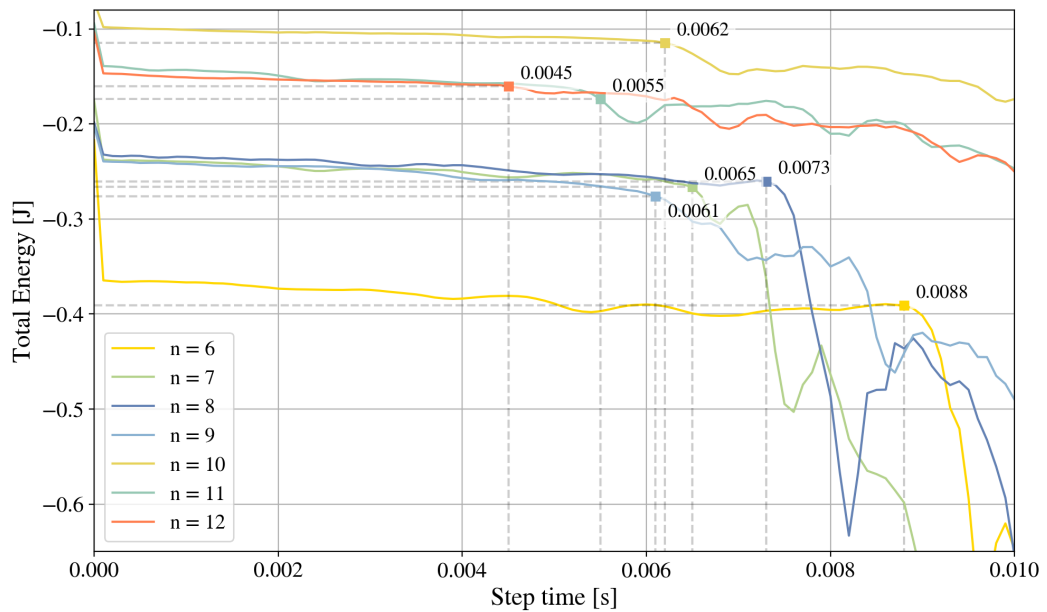


Figure 71: Total energy for obtained results zooming in second deployment. With resulting time values in seconds.

Figure 71, shows by annotations the time value where inflation was obtained for all the cases under study. Thus, for bigger number of sides, completed inflation was obtained for lower time value. As well as the energy variation was reduced by increasing the number of sides. Comparison between 6 number of sides and 12 clarify this explanation.

Over-inflation mentioned, can be seen in the following figure, where stages are indicated for the six number of sides case. Here it is seen the evolution from initial state to folding and free deployment (above) and then inflation (below). Three inflation states are illustrated: first which is the almost completely deployed origami, second seems to become over-inflated and the final result with an over-inflated one.

Between first and second pattern of the row below shall be the inflated one without getting over. Being this solution the same as the represented in Figure 71.

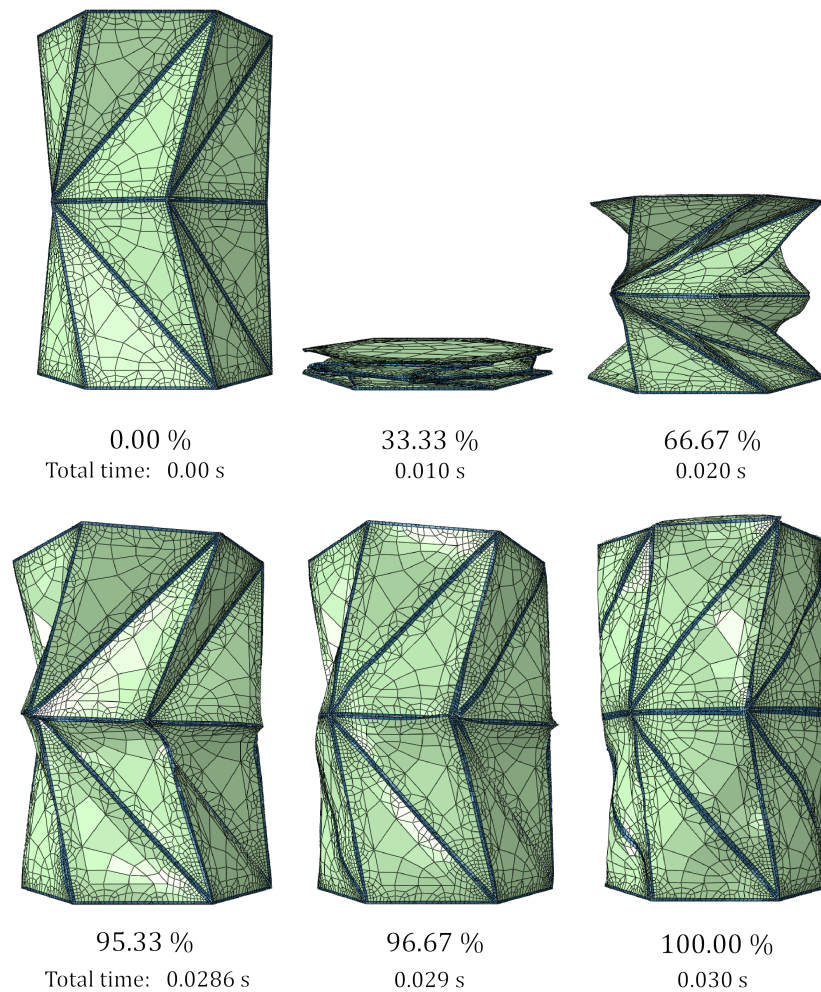


Figure 72: Illustration about structure evolution during the whole process.

### 5.4.2 N rings results

Considering the packaging ratio obtained in section 4.3.3, the final origami patten shall suit in the 12U satellite. Thus, using a maximum folded height of 150 mm due to satellite restrictions [7], maximum number of rings will be given by the thickness implemented.

In this case, the thickness used was 0.5 mm, which means that maximum number of rings is given by

$$N_{max} = \frac{\text{Max height}}{\text{Thickness} \cdot 10} = \frac{150}{0.5 \cdot 10} = 30 \quad (16)$$

Nevertheless, due to computational and time restrictions, simulation has been made for 10 rings, instead of 30. This case is expected to be scalable and comparable with the desired case. For folding process, evolution resulted is represented in Figure 74.

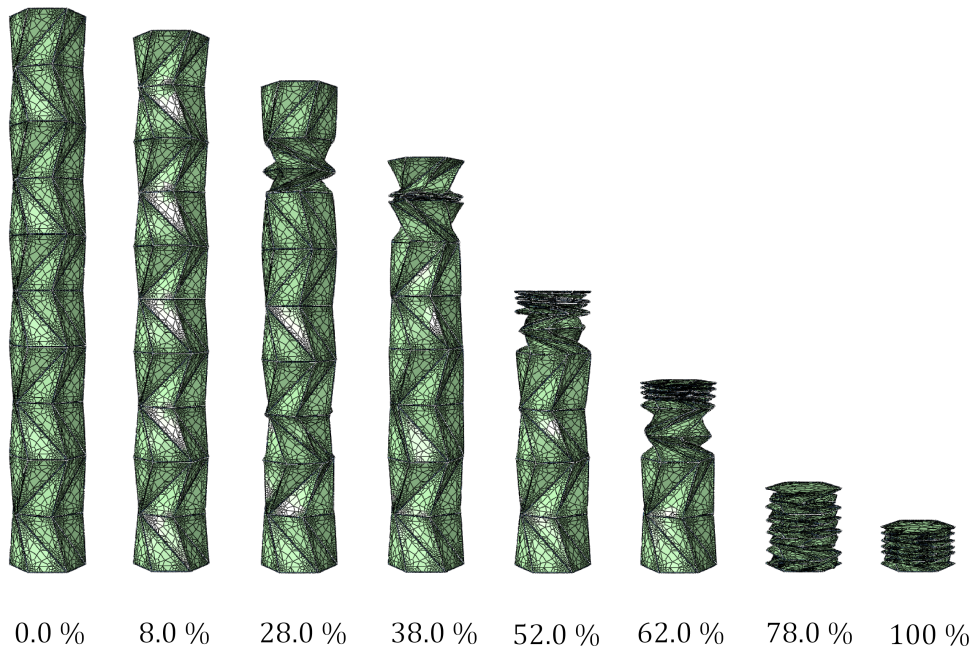


Figure 73: Folding evolution for  $N = 10$ .

Evolution obtained shows a particular behaviour by folding the rings by pairs. It is shown that energy goes through the whole structure and then starts folding second and third rings (starting from above) as pairs. This behaviour might be produced due to the bigger rigidity produced in both bounds by the constraints imposed.

For deployment process, free and inflation one, results has been obtained for completed free one and half of inflation one. This evolution is shown in Figure 74.

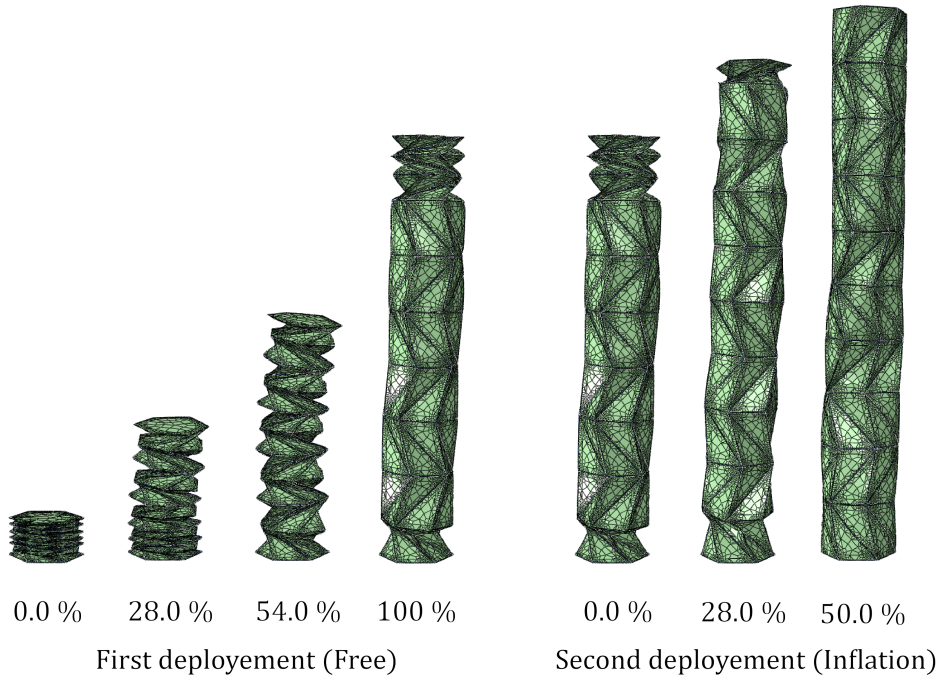


Figure 74: Deployment evolution (first and second) for  $N = 10$ .

Here can be seen that free deployment produce almost completed deployment, and it might be produced at all with more time. This behaviour occurs due to stress inside of the material when folding, storing stress until free deploy. Resulting in a completed deployed state with just half of the inflation process.

Therefore, it is possible to regard deployment process a not scalable problem, which might require a deeper study in future work. Being almost deployed liberating the structure with just 10 rings, structure desired with 30 rings could reach completed deploy state with just first deployment process.

## 6 Conclusion and future works

### 6.1 Conclusions

Aiming for analyze and optimize large pressurized structures as could be habitats or fuel tanks, parameterized simulation models has been developed by Python scripting. Coding generated includes desired innovative use and modelling of printable materials and its refined mesh. Therefore, a whole process from mathematical implementation for geometry definition, going thought FEM model, to optimization analysis has been developed in this thesis.

Regarding the 5 aims introduced in this document, following conclusions has been obtained.

- Assembly process for Kresling geometry was be made for it second bi-stable behaviour in order to obtain a feasible solution in any configuration case. By trying different cases, it was a probability of non-feasible assembling for the obtained height for the first bi-stable mode. Therefore, the developed tool check this behaviour and assembly a mathematical feasible model.
- Due to computational limitations (1 CPU with 8 cores at 3GHz and 32 RAM) compromise the results obtained. All results presented here seems to be feasible and at least continuous, offering an enough good solution for the dual material implementation. Therefore, *Version 2* mesh model with distributed configuration offers a quick and representative solution. Nevertheless, mesh refinement shall be improved with finer elements near the corners of the Kresling triangles.
- Inner volume calculus shows a non linear behaviour from flat height value due to Kresling geometry characterization. Moreover, these calculus has been made without considering the error produced by the thickness and the printable material errors. Solutions obtained are well compared due to its own correlation.
- Stress evolution for different number of sides, follows a similar "S" behaviour, offering a valley region with great interest. Moreover, optimum results for stress (compromised by the inner volume) were obtained in the region were the "S" changes its slope in aforementioned valley region.
- Best surrogate model fitting was reached with polynomial approach, with a determination coefficient over 0.99. Correlation for optimum results in function of the number of sides was not achieved, due to non-linear behaviour. However, Pareto front was obtained in order to show its major trend.
- Increasing the number of sides (restricted by manufacturing constraints) makes easier its folding process, due to a more stable response in stress and energy evolution. As well as for deployment and folding process. Where it was obtained that the higher number of sides, the less the time required for inflation process. Seeming the structure more stable in the three stages for higher number of sides.

- Using large number of rings produce a better deployment response for the whole structure. Internal stress of the material produce a better behaviour in free deployment, producing an almost deployed state.

All in all, the five aims planned to achieve were almost reach or at least study. Obtaining a completed analysis and optimization for origami-inspired structure based on Kresling geometry pattern.

## 6.2 Future works

Throughout this thesis, results have been considered as model response accuracy correspond with real origami behaviour. Nevertheless, there is a long way to go until achieve accurate results for such complex geometries. Future works are based on points out of this thesis reach, since the development time were not enough for them.

The author would like to continue them working with URJC and TU Delft. Some of the expected future works in the project are listed a summarized as follows.

- **Mesh refinement for more accurate results.** As the thesis timeline was restricted, the mesh refined was compromised. Although depending on the computational capacity available, simulation cost is clearly influenced by the number of elements in the model and simulation time indeed.

It would affect to optimization process, by refinement the curves generated by the surrogate model. Therefore, higher regions (near to obtained optimum values) shall be deeper analyzed.

- **Deeper analysis in inflation process.** Being inflation process the limiting one, inflation after first deployment process has been not study at all. There is a clear requirement for time and pressure adjustment depending on the inner volume of the pattern.
- **Manufacturing validation.** After manufacturing process developed in TU Delft, validation of the model generated is required. This validation is, overall, based in the following aims.
  - **Packaging ratio validation.** Simulation analysis shows a packaging ratio up to 10, while real pattern might not achieve at all this statement. It shall be tested by folding different configurations of the pattern.
  - **Strain validation by DIC (Digital Image Correlation).** Implementing DIC technology, which is a non-contact full-field strain measurement technique [31], allows to correlate the values from simulation to the real results.
  - **Optimization process validation.** Optimal results might not be as accurate as is expected and they need to be validated in experimental measurement process.

## Appendices

### A Sampled design variables

Design variables obtained thanks to Latin Hypercube Sampling (LHS), which describe the pattern geometry, summarized in the following table. Radius in any case was 50 mm, following the constraints in *Statement of the problem* section (see Section 3).

Table 7: Design variables from LHS.

	Number of sides (n)	Flat patter height (h) [mm]
<b>Sample 1</b>	9	69.40
<b>Sample 2</b>	11	81.30
<b>Sample 3</b>	9	66.10
<b>Sample 4</b>	6	69.70
<b>Sample 5</b>	12	71.90
<b>Sample 6</b>	9	56.20
<b>Sample 7</b>	9	60.30
<b>Sample 8</b>	6	70.00
<b>Sample 9</b>	9	63.60
<b>Sample 10</b>	10	55.50
<b>Sample 11</b>	6	45.20
<b>Sample 12</b>	6	53.60
<b>Sample 13</b>	8	52.60
<b>Sample 14</b>	9	72.90
<b>Sample 15</b>	9	53.30
<b>Sample 16</b>	11	53.90
<b>Sample 17</b>	8	68.70
<b>Sample 18</b>	6	60.00
<b>Sample 19</b>	10	51.30
<b>Sample 20</b>	8	75.20
<b>Sample 21</b>	6	49.40
<b>Sample 22</b>	12	76.50
<b>Sample 23</b>	11	50.40
<b>Sample 24</b>	8	74.50
<b>Sample 25</b>	12	54.90
<b>Sample 26</b>	8	75.50

---

<b>Sample 27</b>	9	48.40
<b>Sample 28</b>	10	57.50
<b>Sample 29</b>	9	62.00
<b>Sample 30</b>	8	78.40
<b>Sample 31</b>	12	77.70
<b>Sample 32</b>	11	56.80
<b>Sample 33</b>	9	79.70
<b>Sample 34</b>	8	78.70
<b>Sample 35</b>	7	58.40
<b>Sample 36</b>	7	59.40
<b>Sample 37</b>	12	71.00
<b>Sample 38</b>	7	67.10
<b>Sample 39</b>	10	81.90
<b>Sample 40</b>	6	68.10
<b>Sample 41</b>	6	46.50
<b>Sample 42</b>	9	65.80
<b>Sample 43</b>	10	70.30
<b>Sample 44</b>	10	59.10
<b>Sample 45</b>	6	60.70
<b>Sample 46</b>	9	73.60
<b>Sample 47</b>	12	70.70
<b>Sample 48</b>	11	59.70
<b>Sample 49</b>	11	58.70
<b>Sample 50</b>	12	71.60
<b>Sample 51</b>	7	57.10
<b>Sample 52</b>	9	73.90
<b>Sample 53</b>	7	66.80
<b>Sample 54</b>	7	72.30
<b>Sample 55</b>	12	66.50
<b>Sample 56</b>	8	50.70
<b>Sample 57</b>	10	61.60
<b>Sample 58</b>	8	57.80
<b>Sample 59</b>	7	49.10
<b>Sample 60</b>	6	74.20
<b>Sample 61</b>	11	62.90



---

<b>Sample 62</b>	11	69.00
<b>Sample 63</b>	10	80.60
<b>Sample 64</b>	10	52.90
<b>Sample 65</b>	11	81.60
<b>Sample 66</b>	6	64.50
<b>Sample 67</b>	7	77.40
<b>Sample 68</b>	9	54.60
<b>Sample 69</b>	9	50.00
<b>Sample 70</b>	8	52.00
<b>Sample 71</b>	11	75.80
<b>Sample 72</b>	12	76.10
<b>Sample 73</b>	7	48.10
<b>Sample 74</b>	8	73.20
<b>Sample 75</b>	11	68.40
<b>Sample 76</b>	6	63.90
<b>Sample 77</b>	8	76.80
<b>Sample 78</b>	10	62.60
<b>Sample 79</b>	12	49.70
<b>Sample 80</b>	11	67.80
<b>Sample 81</b>	8	74.80
<b>Sample 82</b>	7	64.20
<b>Sample 83</b>	6	47.10
<b>Sample 84</b>	8	64.90
<b>Sample 85</b>	7	63.20
<b>Sample 86</b>	11	65.20
<b>Sample 87</b>	9	51.00
<b>Sample 88</b>	10	80.00
<b>Sample 89</b>	10	79.40
<b>Sample 90</b>	11	61.30
<b>Sample 91</b>	12	48.80
<b>Sample 92</b>	10	65.50
<b>Sample 93</b>	12	62.30
<b>Sample 94</b>	8	55.80
<b>Sample 95</b>	12	55.20
<b>Sample 96</b>	7	71.30

<b>Sample 97</b>	11	51.70
<b>Sample 98</b>	6	61.00
<b>Sample 99</b>	12	58.10
<b>Sample 100</b>	12	56.50
<b>Sample 101</b>	7	54.20
<b>Sample 102</b>	8	67.40
<b>Sample 103</b>	6	72.60
<b>Sample 104</b>	10	52.30

---

**Part II**  
**SPECIFICATION SHEET**



## II Specification Sheet

This document bases the minimum requirements for carrying out this project and what is described throughout the Report, its Annexes and Budget. Likewise, this Specification Sheet defines the way to execute the project taking into account the technical, economic, regulatory, labour and administrative conditions.

Because of the nature of the project, all the specifications described are linked to software conditions. Thus, the minimum required standards are indicated for each tool or software used.

### 1 Software Conditions

As the implemented tool has been mentioned in the introduction (see Section 1.5), required conditions for each implements software are listed as follows.

#### 1.1 Python 3.11

Python is described as "an interpreted, object-oriented, high-level programming language with dynamic semantics". Most famous advantage of this language are the amount of free interpreter and standard library available for almost any purpose. [35]

Newest major release of the Python programming language, Python 3.11, was the version implemented in this thesis. It was launched in early 2023 (the year this thesis has been elaborated) and developers assure to be 10-60% faster than Python 3.10. [36, 37]

Thus, requirements given in order to run this Python release are resumed as follows.

- **Operative system:** Linux such Ubuntu 20.04 or above or Windows 7 to 10 or above.
- **Memory:** At least 4GB of RAM.

#### 1.2 Abaqus CAE 2022

As Abaqus CAE is a FEM solver, it offers "a complete solution for realistic structural simulation covering both routine and advanced workflows across the range of industrial applications". The version used in this thesis is the last one, as it was given by TU Delft. [11]

Being the last realise of Abaqus, this software has been tested for many configurations per platform. Therefore, the device has accomplished at least [34]:

- **Operative system:** Linux such RHEL 7.9 (Ubuntu 22.04) or above or Windows 10 or above.
- **Memory:** At least 8GB of RAM for Windows and Linux computer or 4GB for Windows laptop.

### 1.3 Dakota Sandia

As Dakota is the optimization tool implemented in this thesis, it does not require any license, by being project developed by Sandia National Laboratories. Device requirements given by the developers are [13]:

- **Operative system:** Linux such RHEL 7.8 (Ubuntu 22.04) or above, Mac OS 11 (Mac OS X 10.9-10.12) or above or Windows 10 or above.
- **Memory:** At least 2GB computer memory available.

### 1.4 Adobe Illustrator and Adobe Photoshop 2023

Adobe software for images editing and designing (Photoshop) and for illustration and vector graphics (Illustrator) are available due to the ETSID licenses. The version used in this thesis is the 2023 for both software, being required for the device achieve at least: [33]

- **Operative system:** Mac OS 11 or above or Windows 10 or above.
- **Processor:** 6th Generation or newer.
- **Memory:** At least 6GB computer memory available and 8GB of RAM.

## 2 Tools Conditions

Additional tools related to software mentioned were also implemented during this thesis. In this case, two specific Python Libraries were used: *abqpy* and *SMT*, both requirements are described below.

### 2.1 abqpy Library

Library developed in Python 3, although the Python interpreter in Abaqus is Python 2. Therefore, code shall be wrote in a compatible way for Python 2 and 3. This library is made for Abaqus 2022, if the Abaqus version used is the 2021, the developer has another Library version, *pyabaqus*. [12]

### 2.2 SMT Library

As surrogate Modelling Toolbox (SMT) is an open-source Python package, it has been adapted to run in any Python 3 version. [32]

### 3 Hardware Requirements

All in all, the software conditions are the ones that limits the hardware requirements. By taking the most restrictive one from the categories: *Operative system*, *Processor* and *Memory*, the following requirements were considered:

<b>Operative System</b>	Windows 10 or above
<b>Processor</b>	6th generation
<b>Computer memory available</b>	>16 GB
<b>RAM</b>	8GB

Table 8: Hardware requirements for the project development.

The operative system which achieve all the requirements is just *Windows*. However, excluding the post-processing tools, i.e., Photoshop and Illustrator, requirements are summarized in the following table for each OS.

	<b>Windows</b>	<b>Linux</b>
<b>Operative System</b>	10 or above	RHEL 7.8/Ubuntu 22.04 or above
<b>Processor</b>	6th generation	6th generation
<b>Computer memory available</b>	>16 GB	>16 GB
<b>RAM</b>	8GB	4 GB

Table 9: Hardware requirements (without post-processing) for the project development.





---

**Part III**

**Sustainable Development Goals (SDG)**



### III Sustainable Development Goals

Seventeen goals were selected by United Nations for being the Sustainable Development Goals for achieving them until 2030. These goals are proposed in a global partnership with the aim of providing a shared blueprint for peace and prosperity for people and the planet, now and into the future. [42]

#### 1 Project contribution

In this thesis, the focus is on space and analyse an in orbit technology demonstrator. Thus, most of the goals are out of the aim of the project and might not proceed. Nevertheless, their contribution is represented in the following table.

Sustainable Development Goals	High	Mid	Low	Not proceed
<b>ODS 1. No poverty</b>				X
<b>ODS 2. Zero hunger</b>				X
<b>ODS 3. Good health and well-being</b>				X
<b>ODS 4. Quality education</b>				X
<b>ODS 5. Gender equality</b>			X	
<b>ODS 6. Clean water and sanitation</b>				X
<b>ODS 7. Affordable and clean energy</b>				X
<b>ODS 8. Decent work and economic growth</b>				X
<b>ODS 9. Industry, innovation and infrastructure</b>		X		
<b>ODS 10. Reduced inequalities</b>				X
<b>ODS 11. Sustainable cities and communities</b>				X
<b>ODS 12. Responsible consumption and production</b>				X
<b>ODS 13. Climate action</b>				X
<b>ODS 14. Life below water</b>				X
<b>ODS 15. Life on land</b>				X
<b>ODS 16. Peace, justice and strong institutions</b>				X
<b>ODS 17. Partnerships for the goals</b>				X

Table 10: Degree of compliance with the sustainable development goals.

## 2 Each goal compliance explanation

As contribution was made just for "*Gender equality*" and "*Industry, innovation and infrastructure*", explanation about both contributions are described as follows.

### 2.1 Gender equality

Being the fifth goal, *Gender Equality* follows to achieve "gender equality and empower all women and girls". This project, as it was described in the *Framework* Section (see Section 1.2), is under develop by a group made of 3 women (including the author) and 1 man. Being this group of women majority not the usual distribution in aerospace research groups, results in something to be highlighted.

Women representation in STEM (Science, Technology, Engineering and Math) areas is 28%, whereas engineering and architecture occupation is just 16.5%. Whereas this project women participation is about the 75%. By promoting projects where women can develop their ideas and build scientific referents for future girls interested in STEM fields, gender equality is clearly under the field of view.

### 2.2 Industry, innovation and infrastructure

Increasing aerospace industry produce a consequently increased amount of rocket launch per year. As it is studied by scientists from NOAA and The Aerospace Corp, it is expected to obtain an elevation of 0.5-2° Celsius in the stratosphere due to rocket launches, which would change global circulation patterns by slowing the subtropical jet streams as much as 3.5%, and weakening the stratospheric overturning circulation. [43]

Therefore, developing new technologies that allows to send large structure in a single rocket, not requiring more than one launch, will severally reduce this rocket contribution to climate change. Nowadays International State Station is made by pieces launched and renovated periodically (excepting the main module) and this technology will allow to send a whole station structure or modules with a single rocket. Thus, this project aims for promoting "sustainable industrialization", as it is called by United Nations, for future space industry.

---

**Part IV**  
**BUDGET**



## IV Project budget

Whole project budget can be divided into three great contributions: hardware required, software used and qualified personal involved. Last two ones' contributions depend on the hours expended on the project. Therefore, first the time distribution is resumed and then the budget breakdown is obtained.

### 1 Time distribution

This thesis has been developed under twenty weeks, as it is indicated in the Project Organization section (see Section 1.3). Nevertheless, report writing is not included in the initial organization, and one extra week were introduced in the planned made. Thus, the time dedicated from the author is calculated as 8 hours per day during these 21 weeks (from Monday to Friday), therefore:

$$8 \frac{\text{hours}}{\text{day}} \cdot 5 \frac{\text{days}}{\text{week}} \cdot 21 \text{ weeks} = 840 \text{ hours} \quad (17)$$

Being these weeks the dedicated by the student, that can be divided into: project meetings, supervisor meetings, meetings with qualified personal in specific areas, report disposition, programming, simulating and post-processing time. Thus, meetings and project development are as well divided and explained as follows:

- **Meetings.** As no one of the personal involved in this thesis were working on their area of expertise, many contributors were involved.

- **Project meetings.** Biweekly meetings with the project personal in TU Delft were the project meetings. Thus,

$$2 \frac{\text{hours}}{\text{week}} \cdot 10 \text{ weeks} = 20 \text{ hours} \quad (18)$$

- **Supervisor meetings.** As this thesis is made as an external collaboration with the URJC in Madrid, all the supervisor meeting has been made with the external supervisor. Thus, the time involved by the supervisor were 4 hours per week, including project meetings.

$$4 \frac{\text{hours}}{\text{week}} \cdot 20 \text{ weeks} - 20 \text{ hours} = 60 \text{ hours} \quad (19)$$

- **Meetings with qualified personal in specific areas.** These meetings were made with experts in Abaqus (Marta Moure Cuadrado) and in Optimization process (Javier Paz Méndez). It was required because URJC and TU Delft supervisor did not have enough knowledge about both areas.

Both were URJC personal, and their involvement in the project was overall around an hour per week.

$$1 \frac{\text{hours}}{\text{week}} \cdot 20 \text{ weeks} = 20 \text{ hours} \quad (20)$$

- **Project development** The resulting 740 hours were expended on the development of the project, in areas as the aforementioned. Distribution time of each great area was made as follows.

- **Report disposition.** This area involve writing, generating the required diagrams and the figures made before results ones. Made using Overleaf (free online tool) for writing and Adobe Illustrator and Photoshop. Time dedicated in Overleaf were around 50 hours and in Adobe software around 40. Thus,

$$50 \text{ hours} + 40 \text{ hours} = 90 \text{ hours} \quad (21)$$

- **Programming.** The time expended on understood the library and Abaqus scripting from Python, parameterization of the pattern and its development. It takes the author 245 hours.
- **Simulating time.** This time is divided into two parts: first, supervised simulations, which requires the active supervision of the author and simulations running it own.

For the first part, it takes at least 3 hours per day:

$$3 \frac{\text{hours}}{\text{day}} \cdot 5 \frac{\text{days}}{\text{week}} \cdot 20 \text{ weeks} = 300 \text{ hours} \quad (22)$$

Apart from the total of 840 hours dedicated, simulations expend running just optimization samples 5 completed days. Moreover, previous simulations were as well launched during the night for mesh analysis and other. All in all, extra simulation time can be computed as

$$24 \frac{\text{hours}}{\text{day}} \cdot 5 \frac{\text{days}}{\text{week}} + 8 \frac{\text{hours}}{\text{day}} \cdot 20 \frac{\text{days}}{\text{week}} \text{ hours} = 280 \text{ hours} \quad (23)$$

- **Post-processing time.** Time expended in optimization and post-processing of the results obtained from the simulation. This part takes most of the time of the last three weeks of study. Therefore,

$$7 \frac{\text{hours}}{\text{day}} \cdot 5 \frac{\text{days}}{\text{week}} \cdot 3 \text{ weeks} = 105 \text{ hours} \quad (24)$$

Finally, time distribution can be summarized as it is in the following table.



	Meeting time	Project development	Extra time
<b>Project meetings</b>	20 h	-	-
<b>Supervisor meetings</b>	60 h	-	-
<b>Qualified personal meeting</b>	20 h	-	-
<b>Report disposition</b>	-	90 h	-
<b>Programming</b>	-	245 h	-
<b>Supervised simulations</b>	-	300 h	-
<b>Un-supervised simulations</b>	-		280 h
<b>Post-processing</b>		105 h	-
<b>Total</b>	100 h	740 h	280 h

Table 11: Project time distribution in hours.

## 2 Budget breakdown

As time division is obtained, budget breakdown can be calculated. Following the areas mentioned in section above, budget contribution is based on: meetings, by the cost of each one of the personal involved per hours and software contribution per hour used.

### 2.1 Salary cost

As the project is based as research developed by two different universities, salary corresponding to each participant person in the project is based on the university quantities. Each cost, therefore, is calculated as the contribution made per hour following Table 11. As salary is commonly indicated per month or year, it is required to convert it per hour. Thus,

$$5 \frac{\text{days}}{\text{week}} \cdot 4 \frac{\text{weeks}}{\text{month}} \cdot 8 \frac{\text{hours}}{\text{days}} = 160 \frac{\text{hours}}{\text{month}} \quad (25)$$

Eight hours were considered like working-day as it is regulated by law in Spain. For URJC salary, quantities were obtained thanks to its *Transparency Portal*, where salaries are distributed per category [39].

- **Supervisor.** In this case, supervisor was under *Profesor Visitante Lector no doctor*, which involves 1,547.66 € per month, which means in this case:

$$1,547.66 \frac{\text{€}}{\text{month}} / 160 \frac{\text{hours}}{\text{month}} \cdot 60 \text{ hours} = 580.38 \text{ €} \quad (26)$$

- **Qualified personal.** Qualified personal were hired as *Contratado doctor*, which means 2,432.62 € per month for both qualified people involved.

$$2,432.62 \frac{\text{€}}{\text{month}} / 160 \frac{\text{hours}}{\text{month}} \cdot 60 \text{ hours} = 304.08 \text{ €} \quad (27)$$

- **Research assistance.** The author was not retrieved due to the work made during this thesis, however in order to simulate the cost for this work it was considered the category as *Personal Investigador*. Category selected based on the work developed by the author and its education level. Thus, salary per month should be 1,466.00 €.

$$1,466.00 \frac{\text{€}}{\text{month}} / 160 \frac{\text{hours}}{\text{month}} \cdot 840 \text{ hours} = 7,696.50 \text{ €} \quad (28)$$

On the other hand, TU Delft contribution (**Project meetings**) was based on one extra supervisor hired as *Assistance professor*, meaning a salary from 3,974 € to 6,181 € [40]. For minimum case, contribution would be:

$$3,974.00 \frac{\text{€}}{\text{month}} / 160 \frac{\text{hours}}{\text{month}} \cdot 20 \text{ hours} = 496.75 \text{ €} \quad (29)$$

Nevertheless, regarding the maximum salary:

$$6,181.00 \frac{\text{€}}{\text{month}} / 160 \frac{\text{hours}}{\text{month}} \cdot 20 \text{ hours} = 772.63 \text{ €} \quad (30)$$

Taking a mid-value between both, in order to obtain a midway order of magnitude, TU Delft contribution, was around 634.69 €.

## 2.2 Software cost

- **Abaqus CAE.** The cost for Abaqus CAE has been estimated with the data given by Principia [38], which generated a budget for this type of Licence, destined for Academic and Research purposes. Its cost were about 16,900.00 € per year, including creation of the license and maintenance. As the calculus has been made for hours, it has been converted into cost per hour as

$$16,900.00 \frac{\text{€}}{\text{year}} / 365 \frac{\text{days}}{\text{year}} / 24 \frac{\text{hours}}{\text{days}} = 1.93 \frac{\text{€}}{\text{hour}} \quad (31)$$

Regards simulating time, its total cost was:

$$1.93 \frac{\text{€}}{\text{hour}} \cdot (300 + 280) \text{ hours} = 1,119.40 \text{ €} \quad (32)$$

- **Adobe Licenses.** Creative Cloud, which includes all apps for Adobe use, is the license selected by the ETSID. It commonly cost 62.99 € per month [41]. As the project has been developed in 5

months, it means:

$$62.99 \frac{\text{€}}{\text{month}} / 5 \text{ month} = 314.95 \text{ €} \quad (33)$$

### 2.3 Hardware cost

By the hardware restrictions given, the price of the computer differs in function of its use. Nevertheless, in this thesis, the computer used for running the simulations was custom defined and updated with the years, being its cost not clear at all. By the specifications defined, it would be around 1.

Moreover, for post-processing and report elaboration one laptop was used in order to let the main computer running the simulations. Computer was bought on 2021 and its current cost has been obtained from the vendor price for second hand similar product, with an estimated devaluation of 100 € per year.

$$2,200.00 \text{ €} + 1,800.00 \text{ €} - 100.00 \text{ €} \cdot 2 \text{ years} = 3,800.00 \text{ €} \quad (34)$$

### 2.4 Budget summary

All in all, whole budget expended in the current thesis can be summarized as it is in the following table. However, it is required to highlight that this budget is an orienting value for the reader and might not be exactly the required one.

		Cost per month [€]	Cost per hour [€]	Total cost [€]
Salary cost	Supervisor	1,547.66	9.67	580.38
	Qualified personal	2,432.62	15.20	304.08
	Project personal	3,974.00 - 6,181.00	24.83 - 38.63	634.69
	Research assistance	1,466.00	9.16	7,696.50
Software cost	Abaqus CAE	1,408.33	1.93	1,119.40
	Adobe Creative Cloud	62.99	-	314.95
Hardware cost	Customizad computer	-	-	2,200.00
	MSI Personal laptop	-	-	1,600.00
			<b>TOTAL</b>	<b>13,869.62</b>

Table 12: Budget summary.

Thus, total budget for developing this thesis was:

**THIRTEEN THOUSANDS EIGHT HUNDRED SIXTY NINE EUROS SIXTY TWO CENT  
(13,869.62€)**



---

## References

- [1] Jaxa, “Small solar power sail demonstrator "IKAROS",” 2003, [Online]. Available: [https://global.jaxa.jp/countdown/f17/overview/ikaros\\_e.html](https://global.jaxa.jp/countdown/f17/overview/ikaros_e.html) (Last visited: 27/02/2023).
- [2] N. Kidambi and K. W. Wang, “Dynamics of kresling origami deployment,” *Physical Review E*, vol. 101, no. 6, jun 2020, = <https://doi.org/10.1103/PhysRevE.101.063003> (Last visited: 03/03/2023).
- [3] S. W. Grey, “Embedded actuation of reconfigurable origami,” Ph.D. dissertation, University of Bristol, January 2021.
- [4] J. Fulton and H. Schaub, “Deployment dynamics analysis of an origami-folded spacecraft structure with elastic hinges,” *Journal of Spacecraft and Rockets*, vol. 59, no. 2, pp. 401–420, 2022, [Online]. Available: <https://doi.org/10.2514/1.A349388> (Last visited: 03/03/2023).
- [5] E. A. Peraza Hernandez, D. J. Hartl, E. Akleman, and D. C. Lagoudas, “Modeling and analysis of origami structures with smooth folds,” *Computer-Aided Design*, vol. 78, pp. 93–106, 2016, sPM 2016. [Online]. Available: <https://www.sciencedirect.com/science/article/pii/S0010448516300306>
- [6] F. Bre and V. Fachinotti, “A computational multi-objective optimization method to improve energy efficiency and thermal comfort in dwellings,” *Energy and Buildings*, vol. 154, 08 2017.
- [7] I. Uriol and P. Solano-López, “Preliminary study of an origami-inspired deployable structure for a small-scale demonstrator,” 73rd International Astronautical Congress (IAC), Paris, France, September 2022.
- [8] J. Berre, F. Geiskopf, L. Rubbert, and P. Renaud, “Toward the design of kresling tower origami as a compliant building block,” *Journal of Mechanisms and Robotics*, vol. 14, pp. 1–12, 12 2021, [Online]. Available: [https://www.researchgate.net/publication/357311947\\_Towards\\_the\\_design\\_of\\_Kresling\\_tower\\_origami\\_as\\_a\\_compliant\\_building\\_block](https://www.researchgate.net/publication/357311947_Towards_the_design_of_Kresling_tower_origami_as_a_compliant_building_block) (Last visited: 13/05/2023).
- [9] J. Paz Méndez, “Crashworthiness analysis and design optimization of hybrid energy absorption devices: application to aircraft structures,” Ph.D. dissertation, Universidade da Coruña, 2018, available: <http://hdl.handle.net/2183/21137> (Last visited: 05/03/2023).
- [10] Xometry Europe GmbH. (2023) 3D Printing Materials. [Online]. Available: <https://xometry.eu/en/ms/3d-printing/> (Last visited: 10/05/2023).
- [11] *ABAQUS Online Documentation: Version 6.6-1, Build ID: 2006\_03\_01-08.54.35 22833*, ABAQUS, Inc., [Online]. Available: <https://classes.engineering.wustl.edu/2009/spring/mase5513/abaqus/docs/v6.6/index.html> (Last visited: 12/06/2023).
- [12] W. Hailin, *abqpy Documentation*, [Online]. Available: <https://abqpy.com> (Last visited: 26/06/2023).

- 
- [13] B. Adams et al., *Dakota, A Multilevel Parallel Object-Oriented Framework for Design Optimization, Parameter Estimation, Uncertainty Quantification, and Sensitivity Analysis: Version 6.15 User's Manual*, Sandia Technical Report SAND2020-12495, [Online]. Available: <https://dakota.sandia.gov/> (Last visited: 20/06/2023).
- [14] M. Meloni et al., "Engineering origami: A comprehensive review of recent applications, design methods, and tools," *Advanced Science*, May 2021, [Online]. Available: <https://onlinelibrary.wiley.com/doi/10.1002/advs.202000636> (Last visited: 25/02/2023).
- [15] T. Tachi, "Geometric considerations for the design of rigid origami structures," *Proceedings of the International Association for Shell and Spatial Structures (IASS) Symposium*, January 2010, [Online]. Available: [https://origami.c.u-tokyo.ac.jp/~tachi/cg/DesignOfRigidOrigamiStructures\\_tachi\\_IASS2010.pdf](https://origami.c.u-tokyo.ac.jp/~tachi/cg/DesignOfRigidOrigamiStructures_tachi_IASS2010.pdf) (Last visited: 25/02/2023).
- [16] K. Miura and T. D. U. K. Kenkyūjo, *Proposition of Pseudo-cylindrical Concave Polyhedral Shells*, ser. Report (Tōkyō Daigaku. Uchū Kōkū Kenkyūjo). Institute of Space and Aeronautical Science, University of Tokyo, 1969.
- [17] K. Miura, "Triangles and quadrangles in space," Symposium of the International Association for Shell and Spatial Structures, Valencia, 2009, [Online]. Available: <http://hdl.handle.net/10251/6461> (Last visited: 25/02/2023). ISBN: 978-84-8363-461-5.
- [18] L. Dudte, E. Vouga, T. Tachi, and L. Mahadevan, "Programming curvature using origami tessellations," *Nature Materials*, vol. 15, January 2016.
- [19] A. Lebé, "From folds to structures, a review," *International Journal of Space Structures*, vol. 30, pp. 55–74, June 2015.
- [20] K. Yang, S. Xu, S. Zhou, and Y. M. Xie, "Multi-objective optimization of multi-cell tubes with origami patterns for energy absorption," *Thin-Walled Structures*, vol. 123, pp. 100–113, 2018, [Online]. Available: <https://www.sciencedirect.com/science/article/pii/S0263823117309643> (Last visited: 05/03/2023).
- [21] L. Sarabia and M. Ortiz, "1.12 - response surface methodology," in *Comprehensive Chemometrics*, S. D. Brown, R. Tauler, and B. Walczak, Eds. Oxford: Elsevier, 2009, pp. 345–390, [Online]. Available: <https://www.sciencedirect.com/science/article/pii/B9780444527011000831> (Last visited: 05/03/2023).
- [22] R. Mohanty, S. Suman, and S. K. Das, "Chapter 16 - modeling the axial capacity of bored piles using multi-objective feature selection, functional network and multivariate adaptive regression spline," in *Handbook of Neural Computation*, P. Samui, S. Sekhar, and V. E. Balas, Eds. Academic

- 
- Press, 2017, pp. 295–309, [Online]. Available: <https://www.sciencedirect.com/science/article/pii/B9780128113189000168> (Last visited: 05/03/2023).
- [23] G. W. Hunt and I. Ario, “Twist buckling and the foldable cylinder: an exercise in origami,” *International Journal of Non-Linear Mechanics*, vol. 40, no. 6, pp. 833–843, 2005, [Online]. Available: <https://www.sciencedirect.com/science/article/pii/S0020746204001581> (Last visited: 15/05/2023).
- [24] M. Collinson, M. Bower, T. J. Swait, C. Atkins, S. Hayes, and B. Nuhiji, “Novel composite curing methods for sustainable manufacture: A review,” *Composites Part C: Open Access*, vol. 9, p. 100293, 2022, [Online] Available: <https://www.sciencedirect.com/science/article/pii/S2666682022000573> (Last visited: 19/05/2023).
- [25] E. Brancewicz-Steinmetz, J. Sawicki, and P. Byczkowska, “The influence of 3d printing parameters on adhesion between polylactic acid (pla) and thermoplastic polyurethane (tpu),” *Materials*, vol. 14, p. 6464, 10 2021.
- [26] R. B. Rector, “Generalized differential calculus and applications to optimization,” Ph.D. dissertation, Portland State University. Department of Mathematics and Statistics. Dissertations and Theses. Paper 3627, 2017, available: <https://doi.org/10.15760/etd.5519> (Last visited: 16/06/2023).
- [27] F. Glover, *Future paths for integer programming and links to artificial intelligence*, ser. In Computer and Operations Research (1986), vol. 13, pp. 533–549.
- [28] J. P. Walser, *Integer Optimization by Local Search*, ser. Lecture Notes in Artificial Intelligence. Springer, 1999, iSBN: 3-540-66367-3.
- [29] M. D. McKay, R. J. Beckman, and W. J. Conover, “A Comparison of Three Methods for Selecting Values of Input Variables in the Analysis of Output from a Computer Code,” 2023, [Online]. Available: <http://www.jstor.org/stable/1271432> (Last visited: 16/06/2023).
- [30] E. Oñate Ibáñez de Navarra, P. Díez, J. F. Zárate Araiza, and A. Larese De Tetto, *Introduction to the finite element method*. Universitat Politècnica de Catalunya, 2008, [Online]. Available: <http://hdl.handle.net/2117/184007> (Last visited: 18/06/2023).
- [31] W. Broughton, “6 - testing the mechanical, thermal and chemical properties of adhesives for marine environments,” in *Adhesives in Marine Engineering*, ser. Woodhead Publishing Series in Welding and Other Joining Technologies, J. R. Weitzenböck, Ed. Woodhead Publishing, 2012, pp. 99–154. [Online]. Available: <https://www.sciencedirect.com/science/article/pii/B9781845694524500060>
- [32] P. Saves, R. Lafage, N. Bartoli, Y. Diouane, J. H. Bussemaker, T. Lefebvre, J. T. Hwang, J. Morlier, and J. R. R. A. Martins, “SMT 2.0: A surrogate modeling toolbox with a focus on hierarchical and mixed variables gaussian processes,” *ArXiv preprint*, 2023.

- 
- [33] Adobe. (2023) System Requirements. [Online]. Available: <https://www.3ds.com/support/hardware-and-software/simulia-system-information/abaqus-2022/> (Last visited: 20/06/2023).
- [34] Dassault Systèmes. (2022) 2022 Graphics Devices. [Online]. Available: <https://www.3ds.com/support/hardware-and-software/simulia-system-information/abaqus-2022/> (Last visited: 20/06/2023).
- [35] Python Software Foundation. (2023) What is Python? Executive Summary. [Online]. Available: <https://www.python.org/doc/essays/blurb/> (Last visited: 20/06/2023).
- [36] Python Software Foundation. (2022) Python 3.11.0. [Online]. Available: <https://www.python.org/downloads/release/python-3110/> (Last visited: 19/06/2023).
- [37] Python Software Foundation. (2022) What's New In Python 3.11. [Online]. Available: <https://docs.python.org/3/whatsnew/3.11.html> (Last visited: 19/06/2023).
- [38] Principia. (2022) Principia 3DExperience - Abaqus. [Online]. Available: <https://principia.es/plataforma-3dexperience/simulia/abaqus/> (Last visited: 27/06/2023).
- [39] Universidad Rey Juan Carlos (URJC). (2023) Portal de transparencia. [Online]. Available: <https://transparencia.urjc.es/cifras/personal-pdi.php> (Last visited: 27/06/2023).
- [40] Delft University of Technology (TU Delft). (2023) More about the Delft Technology Fellowship. [Online]. Available: <https://www.tudelft.nl/over-tu-delft/werken-bij-tu-delft/campagnes/delft-technology-fellowship/more-about-the-delft-technology-fellowship> (Last visited: 27/06/2023).
- [41] Adobe. (2023) Planes y precios de las aplicaciones de Creative Cloud y mucho más. [Online]. Available: <https://www.adobe.com/es/creativecloud/plans.html> (Last visited: 27/06/2023).
- [42] United Nations. Department of Economic and Social Affairs Sustainable Development. (2023) THE 17 GOALS. [Online]. Available: <https://sdgs.un.org/goals> (Last visited: 25/06/2023).
- [43] NOAA Research. (2022) Projected Increase In Space Travel May Damage Ozone Layer. [Online]. Available: <https://research.noaa.gov/2022/06/21/projected-increase-in-space-travel-may-damage-ozone-layer/> (Last visited: 25/06/2023).
- [44] NOAA Research. (2022) Projected Increase In Space Travel May Damage Ozone Layer. [Online]. Available: <https://www.aauw.org/resources/research/the-stem-gap/> (Last visited: 25/06/2023).
- [45] PcComponentes. (2023) MSI Prestige 15 A10SC-060XES Intel Core i7-10710U/16GB/1TB SSD/GTX 1650/15.6". [Online]. Available: <https://www.pccomponentes.com/msi-prestige-15-a10sc-060xes-intel-core-i7-10710u-16gb-1tb-ssd-gtx-1650-156?refurbished> (Last visited: 17/06/2023).